TECHNISCHE UNIVERSITÄT WIEN

VIENNA UNIVERSITY OF TECHNOLOGY

DIPLOMARBEIT

Transport and Thermoelectric Performance of Ba$_8$-based Clathrates

Ausgeführt am
Institut für Festkörperphysik
der Technischen Universität Wien

unter der Anleitung von
Ao.Univ.Prof. Dipl.-Ing. Dr.techn. Ernst Bauer

durch

Friedrich Röhrbacher
Grinzinger Straße 137/1/15
1190 Wien

Februar 2007

_____
Unterschrift

Contents

Acknowledgments

Chapter 1

Introduction

Thermoelectric materials have the ability to convert thermal energy into electrical energy. This offers the opportunity to use waste heat from engines for conversion into electricity. This reduces energy losses and improve their efficiency.

In 1821 Thomas Johann Seebeck discovered that a temperature difference between the two ends of a metal rod causes an electric voltage [1]. This was the first time that heat could be converted into electricity. The voltage U, depending on the difference in temperature ΔT, is then defined by the Seebeck coefficient (also called thermopower) and is derived by $S = \frac{U}{\Delta T}$. The magnitude of S is solely a property of the material to which the temperature gradient is applied. However, the efficiency of thermoelectric conversion is not only determined by S but also by the thermal conductivity (λ) and the electrical resistivity (ρ) of this material. Therefore, the "figure of merit" Z needs to be investigated to get useful information about the suitability of the material for converting heat into electrical energy [2]. It is expressed by the formula $Z = \frac{S^2}{\lambda \cdot \rho}$ [3]. Consequently, when searching for materials with large S-values, (λ) and (ρ) should be as small as possible.

As shown by the formula above, promising materials need to have a large Seebeck coefficient but low thermal conductivity and low electrical resistivity to be effective. Nature, however, does not favour such a combination since large thermopower requires usually materials with low charge carrier concentration.

In order to improve the thermoelectric performance of clathrates, substitution and doping is a promising method. Clathrates are compositions of elements that form large cages in their crystal structure in which other elements are caught as in a trap. The interaction of this trapped element with the crystal lattice influences the transport coefficients (λ, ρ, S) of the material. As the elements in the samples are changed, the transport properties

are, of course, changed as well. This might then lead to an improvement of the figure of merit.

Consequently, the change of elements and their concentrations in clathrates by substitution and doping can improve the efficiency of thermoelectric processes and therefore increase the figure of merit.

This diploma thesis focuses on the investigation of Ba_8-based clathrates with copper, zinc and cadmium as variable elements. Furthermore, the concentration of cadmium is altered. As the results of the measurements will show, some of these compositions offer an outstanding figure of merit and, thus, promise to have useful applications in technical processes.

Chapter 2

Theoretical Aspects

This chapter is mainly based on the book *Thermoelectrics - Basic Principles and New Materials Developments* by *G.S.Nolas, J.Sharp* and *H.J.Goldsmid* published by *Springer-Verlag* as well as on the scripts of the lectures *Highly Correlated Electron Systems* and *Metallphysik Praktikum - Transportphänomene in Festkörpern* given by *E. Bauer* and S. Bühler-Paschen at the *Vienna University of Technology* in 2006.

2.1 Transport Phenomena

Transport phenomena describe the ability of a material to transport energy and electrical charge in consequence of external electric and magnetic fields as well as temperature gradients. While the external fields and the temperature gradient act as driving forces, various scattering processes finally lead to a state of equilibrium. This combination of driving forces and scattering processes provide transport coefficients such as

- Electric Resistivity (ρ)

- Thermal Conductivity (λ)

- Seebeck Coefficient (S)

- Peltier Coefficient (Π)

- Magneto Resistance

- Hall Coefficient

which are characteristic for each material. Consequently, the measurement of these physical values is important in the investigation of thermoelectric

materials. For this thesis the first three transport coefficients (ρ, λ, S) are investigated and explained in detail in this chapter. Since the transport of energy and the scattering processes consist partly of two contributions, namely that of the lattice and that of the electrons, these two are described first.

2.1.1 Electronic Contribution

To explain the behaviour of electrons it turned out that their distribution described by the *Maxwell-Boltzmann distribution function*

$$f_0(E) = \frac{1}{e^{\frac{E-E_F}{k_B T}}} \tag{2.1}$$

in the theory of a free electron gas failed in the description of most processes in solid state physics like for example the electronic contribution to specific heat. *Enrico Fermi* and *Paul Dirac* developed an alternative model that combines the Maxwell-Boltzmann distribution function with quantum mechanics. This led to the *Fermi-Dirac distribution function*

$$f_0(E) = \frac{1}{e^{\frac{E-E_F}{k_B T}} + 1} \tag{2.2}$$

where $k_B = 1.38 \times 10^{-23}$ J/K is the Boltzmann constant and E_F the Fermi energy for free electrons, given by

$$E_F = \frac{h^2}{2m_e}\left(3n\pi^2\right)^{\frac{2}{3}}. \tag{2.3}$$

E_F is the energy at $T = 0$ K below that all states are occupied by electrons while above none of the states are occupied and m$_e$ is the electron mass. n is the number of free electrons per unit volume, derived by

$$n = \frac{1}{V}\int_0^\infty f_0(E)g(E)dE. \tag{2.4}$$

The Fermi-Dirac distribution function (2.2) represents the probability that a state is occupied by an electron. The number of states within the energy range $(E, E + dE)$ is given by

$$g(E)dE = \frac{V(2m_e^*)^{\frac{3}{2}}\sqrt{|E|}}{4\pi^2 h^3}d|E| \tag{2.5}$$

with m_e^* as effective mass of an electron given by

$$\frac{1}{m_e^*} = \frac{1}{\hbar^2} \cdot \frac{d^2E}{dk^2}.$$ (2.6)

The increase of energy an electron aquires due to thermal excitation can only be of the order of k_BT. Since for metals at ordinary temperatures k_BT is always much smaller than the Fermi energy E_F only very few electrons can be excited from a state below E_F to a state above E_F and therefore contribute to transport properties of materials. However, for semi-metals and semiconductors k_BT might be in the same order of magnitude as E_F or even higher. As Equation (2.3) shows E_F is proportional to the number of free electrons. Since n is much smaller for semi-metals and semiconductors than for metals k_BT can become larger than E_F for such materials. Then it is possible to obtain the condition $k_BT \gg E_F$ at room temperature and the Fermi-distribution can be replaced by the Maxwell-Boltzmann-distribution. In this case the electron gas is said to be non degenerate whereas when n is large enough so that $k_BT \ll E_F$ a degenerated electron gas is responsible for the electronic contribution to the transport properties.

Additionally to the free electron gas theory the band theory of solids needed to be developed in order to explain their transport properties. Each electron in crystalline solids is exposed to a periodical potential caused by the nuclei. It furthermore undergoes the field determined by all other electrons. Thus the electron's movement is strongly influenced by these two forces. The periodic boundary conditions and the translation symmetry lead to discrete solutions of the wave function. These solutions are always within bands of energies that are separated from one another by forbidden areas, so called energy gaps.

The relation between energy and wave number of an electron is given by

$$E(k) = \frac{h^2k^2}{8\pi^2 m_e^*}$$ (2.7)

which is the same as for the free electron gas except that in this case the electron mass m_e is replaced by its effective mass m_e^*. However, this relation is only correct for small values of E and k, that is, next to the center of the *first Brillouin zone*. The second derivation d^2E/dk^2 is of special interest because if it is negative the charge carriers seem to be negative with negative mass. However, it is convenient to regard it as positive carrier of positive mass. In this case, the energy E must be measured downward from the band edge and $f_0(E)$ is the probability that a state is unoccupied by an electron,

that is, occupied by a hole. Hence, equation (2.4) needs to be separated into an electronic part and a part representing the density of holes:

$$n_n = \int_{E_F}^{\infty} f_0(E)N(E)dE, \qquad (2.8)$$

$$n_p = \int_{-\infty}^{E_F} \big(1 - f_0(E)\big)N(E)dE. \qquad (2.9)$$

Now the electric behaviour of conductors, semiconductors and insulators could be explained. If the Fermi energy lies within an energy band the electrons can be excited easily and the material is a conductor. In case the Fermi energy lies within a band gap the material is an insulator since the excitation of the electrons requires an energy of the order of E_g - the difference between the valence and the conduction band. The situation for semiconductors is similar, however, in this case E_g is small enough so that electrons can be excited from the valence band into the conduction band. Such materials are called *intrinsic semiconductors*. In case conduction and valence band overlap one another the material is a semi-metal. Its transport properties are similar to that of narrow-gap semiconductors.

On the other hand one can change the electric properties of a material by adding impurities. Such materials are called *extrinsic semiconductors*. If the impurity consists of atoms with one more valence electron than the original semiconductor has an additional energy level (*donor level*) for electrons right below the conduction band edge is created. The electrons of this level can therefore be excited easily into the conduction band. In contrast, if the added atoms have one electron less than the original semiconductor an additional energy level for holes (*acceptor level*) is created right above the band edge of the valence band. Consequently, the excitation of holes into the valence band requires only a small amount of energy. Due to the major charge carriers the first one is called *n-type semiconductor* whereas the latter one is said to be a *p-type semiconductor*.

Electron Scattering Processes

The electronic contribution to transport properties and their coefficients are determined by their scattering processes. An electron can be scattered by

- lattice imperfections (impurities, crystal defects)

- thermal vibrations of the lattice (phonons)

- magnetic moments of the lattice atoms

- ionised atoms (*piezoelectric scattering*)

- other electrons.

The transport coefficients can be derived from the *linearised Boltzmann equation*[1]

$$\left(\frac{\partial}{\partial t} + \dot{\vec{r}}\nabla_r + \dot{\vec{k}}\nabla_k\right)f_\gamma = \left(\frac{\partial f_\gamma(E)}{\partial t}\right)_{coll} \tag{2.10}$$

in which $\gamma = (\vec{k}, \vec{r})$, $\vec{k}$ is the wave vector, $\vec{r}$ the position vector, $\vec{v}$ the velocity and $f_\gamma(E)$ the Fermi-Dirac distribution function of an electron. The left term (=field term) represents the driving forces due to external fields and temperature gradient while the right term represents scattering processes. A common way to solve this equation is the *relaxation time approximation*. If the *Fermi-Dirac distribution function* is distributed from its equilibrium f_γ^0 because of external fields and $|f_\gamma - f_\gamma^0| \ll f_\gamma^0$ as well as the velocity at which f_γ returns to f_γ^0 is proportional to $|f_\gamma - f_\gamma^0|$ the system relaxes according to

$$\left(\frac{\partial f_\gamma(E)}{\partial t}\right)_{coll} = \frac{f_\gamma(E) - f_\gamma^0(E)}{\tau_\gamma} \tag{2.11}$$

in which τ is the time the system needs for this relaxation process and $f_\gamma(E)$ and $f_\gamma^0(E)$ are the perturbed and unperturbed distribution functions, respectively. According to *Matthiessen's rule* the scattering processes can be regarded as independent from each other in a first approximation, thus

$$\frac{1}{\tau_e} = \sum_i \frac{1}{\tau_{e,i}} \tag{2.12}$$

where i is the index of the various scattering processes. In order to obtain $f_\gamma(E) - f_\gamma^0(E)$ in terms of the electric field and the temperature gradient the Boltzmann equation can be solved with the help of the relaxation time approximation:

$$\frac{f_\gamma(E) - f_\gamma^0(E)}{\tau_\gamma} = -\dot{\vec{k}}\frac{\partial f_\gamma(E)}{\partial \vec{k}} - \dot{\vec{r}}\frac{\partial f_\gamma(E)}{\partial \vec{r}} \tag{2.13}$$

Since $|f_\gamma(E) - f_\gamma^0(E)| \ll f_\gamma^0(E)$ (only small displacements of $f_\gamma(E)$) $f_\gamma(E)$ can be replaced on the right-hand side of equation (2.13) by f_γ^0. Because the displacement of $f_\gamma(E)$ is caused by the temperature gradient and the external electric field equation (2.13) can be written like

$$\frac{f_\gamma(E) - f_\gamma^0(E)}{\tau_\gamma} = u\frac{\partial f_\gamma^0(E)}{\partial E}\left(\frac{\partial E_F}{\partial x} + \frac{E - E_F}{T}\frac{\partial T}{\partial x}\right) \tag{2.14}$$

---

[1]To simplify the work all calculations are only in x-direction

where u is the velocity of the charge carriers in x-direction. The electric current density j is given by

$$j = \mp \int_0^\infty e u f_\gamma(E) g(E) dE \qquad (2.15)$$

with - for electrons and + for holes as charge carriers. The density of the rate of heat flow is

$$q = \int_0^\infty u(E - E_F) f_\gamma(E) g(E) dE \qquad (2.16)$$

where $E - E_F$ represents the total energy transported by each carrier. Again the approximation of small displacements is used and $f_\gamma(E)$ in Equation (2.15) and (2.16) can be replaced by $f_\gamma(E) - f_\gamma^0(E)$. Since we only consider one direction and because all movements are equally distributed over all directions (i.e. one third for each direction) the velocity of the charge carriers may be set as

$$u = \sqrt{\frac{2E}{3m_e^*}}. \qquad (2.17)$$

Thus i and w can be calculated as follows:

$$j = \mp \frac{2e}{3m_e^*} \int_0^\infty g(E) E \tau_e \frac{\partial f_\gamma^0(E)}{\partial E} \left(\frac{\partial E_F}{\partial x} + \frac{E - E_F}{T} \frac{\partial T}{\partial x} \right) dE \qquad (2.18)$$

and

$$q = \pm \frac{E_F}{e} j + \frac{2}{3m_e^*} \int_0^\infty g(E) E^2 \tau_e \frac{\partial f_\gamma^0(E)}{\partial E} \left(\frac{\partial E_F}{\partial x} + \frac{E - E_F}{T} \frac{\partial T}{\partial x} \right) dE. \qquad (2.19)$$

To derive the electrical conductivity σ the temperature gradient can be set to zero since it does not influence the conductivity. Since the electric field is given by

$$\vec{E} = \frac{1}{e} \frac{\partial E_F}{\partial x}$$

the electrical conductivity is

$$\sigma = \frac{j}{\vec{E}} = \frac{2e^2}{3m_e^*} \int_0^\infty g(E) E \tau_e \frac{\partial f_\gamma^0(E)}{\partial E} dE. \qquad (2.20)$$

According to the same consideration as above the electric current can be set equal to zero in order to find a formula for the Seebeck coefficient. Hence, equation (2.18) may be written as

$$\frac{\partial E_F}{\partial x} \int_0^\infty g(E) E \tau_e \frac{\partial f_\gamma^0(E)}{\partial E} dE = \pm \frac{1}{T} \frac{\partial T}{\partial x} \int_0^\infty g(E) E \tau_e (E - E_F) \frac{\partial f_\gamma^0(E)}{\partial E} dE.$$

$$(2.21)$$

Since the Seebeck coefficient S is the relation of a resulting voltage due to an applied temperature gradient it is given by

$$S = \frac{\Delta U}{\Delta T} = \frac{1}{e} \frac{\frac{\partial E_F}{\partial x}}{\frac{\partial T}{\partial x}}. \tag{2.22}$$

In combination with equation (2.21) S can be expressed as

$$S = \pm \frac{1}{eT} \left(E_F - \frac{\int_0^\infty g(E) E^2 \tau_e \frac{\partial f_\gamma^0(E)}{\partial E} dE}{\int_0^\infty g(E) E \tau_e \frac{\partial f_\gamma^0(E)}{\partial E} dE} \right) \tag{2.23}$$

where S is negative if the charge carriers are electrons and positive if they are holes. In order to get an expression for the electronic contribution to thermal conductivity the same consideration as for the Seebeck coefficient can be used. Thus, the electrical current i can be set again equal to zero. The thermal conductivity λ_e is basically given by

$$q = -\lambda_e \frac{\partial T}{\partial x} \tag{2.24}$$

and therefore calculated as follows:

$$\lambda_e = \frac{2}{3m_e^* T} \left[\frac{\left(\int_0^\infty g(E) \tau_e E^2 \frac{\partial f_\gamma^0(E)}{\partial E} dE \right)^2}{\int_0^\infty g(E) \tau_e E \frac{\partial f_\gamma^0(E)}{\partial E} dE} - \int_0^\infty g(E) \tau_e E^3 \frac{\partial f_\gamma^0(E)}{\partial E} dE \right]. \tag{2.25}$$

To simplify the formulas for the transport coefficients their integrals can be replaced by so called *transport integrals* K_n given by

$$K_n = -\frac{2T}{3m_e^*} \int_0^\infty g(E) \tau_e E^{n+1} \frac{f_\gamma^0(E)}{\partial E} dE. \tag{2.26}$$

Thus, the transport coefficients can be simplified to

$$\sigma = \frac{e^2}{T} K_0 \tag{2.27}$$

$$S = \pm \frac{1}{eT} \left(E_F - \frac{K_1}{K_0} \right) \tag{2.28}$$

$$\lambda_e = \frac{1}{T^2} \left(K_2 - \frac{K_1^2}{K_0} \right) \tag{2.29}$$

For the calculation of these transport coefficients it is necessary to use numerical methods. Otherwise, equation (2.27) to (2.29) together with appropriate measurement results can be used to find out important parameters of the investigated materials such as Fermi energy, effective mass, relaxation time and lattice conductivity.

2.1.2   Lattice Contribution to the thermal conductivity

In contrast to electrons the lattice contributes only to the thermal conductivity (except for the phonon-drag that contributes to the thermopower). The atoms in a solid do not vibrate independently. The vibrational energy of one atom is transfered to its neighbours due to inter atomic forces. Thus, the energy moves through the solid in waves called phonons which are responsible for heat conduction by the lattice. One way to describe the thermal conductivity is based on the kinetic theory of gases leading to

$$\lambda_l = \frac{1}{3} c_v \nu l_t \tag{2.30}$$

where c_v is the specific heat, ν the speed of sound and l_t the mean free path length. According to *Debye's model* [4] the specific heat is given by

$$c_v = 9 N k_B \left(\frac{T}{\theta_D}\right)^3 \int_0^{\frac{\theta_D}{T}} \frac{x^4 e^x}{(e^x - 1)^2} dx. \tag{2.31}$$

θ_D is the Debye temperature and N is the number of atoms per unit volume.

Scattering Processes

In order to explain physical properties like for example thermal resistivity various scattering processes have to be taken into account. Phonons can be scattered by

- other phonons (normal- and Umklapp-processes),

- lattice imperfections (impurities, crystal defects),

- electrons and

- grain boundaries

Phonon-Phonon Scattering, Umklapp-Processes: In many materials the thermal conductivity shows a 1/T-dependence as long as their temperature is not much less than θ_D. This rule is based on observations by *Eucken* [5]. In order to explain Eucken's 1/T-law Peierls [6] introduced the concept of the quantisation of the lattice vibrations called phonons. In pure crystals at high temperatures, phonons are scattered predominantly by other phonons. This interaction process between two phonons with wave vector $\vec{q_1}$ and $\vec{q_2}$ results in a third one with wave vector $\vec{q_3}$:

$$\vec{q_1} + \vec{q_2} = \vec{q_3}.$$

If $\vec{q}_3$ lies within the first Brillouin zone $|\vec{q}|$ and therefore momentum is conserved (*Normal-processes*). Thus heat is transported without resistivity of the crystal lattice. However, in case $\vec{q}_3$ points outside the first Brillouin zone it is backscattered due to Bragg reflexion. This can be described if $\vec{q}_3$ is reduced to the first Brillouin zone by subtracting the reciprocal lattice vector (*Umklapp-processes*). Since the absolute value of the wave vector is proportional to the temperature, Bragg reflexion is the common process at higher temperatures. Hence, thermal conductivity decreases with increasing temperature.

Scattering of Phonons by Defects, Normal-Processes: In addition to scattering of phonons by other phonons, scattering of phonons by defects occur frequently in real crystals. Such defects can be foreign impurities, vacancies, density variations or dislocations, for example. The probability of scattering processes of waves on point-like defects are usually proportional to the fourth power of the frequency. Thus, we would expect for the scattering time

$$\tau \propto \frac{1}{\nu^4}. \tag{2.32}$$

Since the probability for Umklapp-processes also decrease with temperature an exceedingly large thermal conductivity at lowest temperatures would be the consequence. However, this is not the case because of the redistribution of phonons by Normal-processes into modes for which the scattering is stronger.

The model developed by *Callaway* [7, 8, 9] includes such Normal-processes. The model furthermore uses the relaxation time τ instead of the mean free path length l_t. Since Umklapp-processes do not conserve momentum the perturbed phonons relax toward an equilibrium distribution while the momentum conserving Normal-processes cause them to relax towards a non equilibrium distribution. If only Umklapp-processes occur (as it is the case at higher temperatures) the total relaxation time is given by

$$\frac{1}{\tau_l} = \frac{1}{\tau_U} + \frac{1}{\tau_{l,0}} + \frac{1}{\tau_{l,e}} + \frac{1}{\tau_{l,b}}, \tag{2.33}$$

where τ_U is the relaxation time for non-momentum-conserving processes (Umklapp-processes), τ_0, τ_e and τ_b are the relaxation times corresponding to scattering on lattice imperfections, electrons and boundaries, respectively. In order to take Normal-processes into consideration Callaway obtained an additional factor β which is calculated by

$$\beta = \frac{\int_0^{\frac{\theta_D}{T}} \frac{\tau_l}{\tau_n} \frac{x^4 e^x}{(e^x-1)^2} dx}{\int_0^{\frac{\theta_D}{T}} \frac{1}{\tau_{l,n}} \left(1 - \frac{\tau_l}{\tau_{l,n}}\right) \frac{x^4 e^x}{(e^x-1)^2} dx}. \tag{2.34}$$

Thus, the lattice contribution to thermal conductivity is obtained by

$$\lambda_l = \frac{k_B^4 T^3}{2\pi^2 v_s \hbar} \int_0^{\frac{\theta_D}{T}} \left[\tau_l \frac{x^4 e^x}{(e^x - 1)^2} + \beta \right] dx \qquad (2.35)$$

where $v_s = \frac{k_B \theta_D}{\hbar (6\pi^2 n)^{1/3}}$ is the speed of sound, $x = \frac{\hbar\omega}{k_B T}$ and θ_D the Debye-temperature.

2.1.3 Electrical Resistivity

The electric resistivity is determined by the scattering of electrons as described in Section 2.1.1. The average time for an electron between two scattering processes is the relaxation time τ_e that is determined by the electron velocity and the mean free path length. Although all scattering processes as described in Section 2.1.1 contribute to the electrical resistivity only those due to lattice imperfections and phonons are important for simple metals without magnetic moments. According to *Matthiessens's rule* the relaxation times of both processes can be considered as independent from each other. Subsequently, for simple metals without magnetic moments τ_e can be calculated to

$$\frac{1}{\tau_e} = \frac{1}{\tau_{e,0}} + \frac{1}{\tau_{e,ph}}. \qquad (2.36)$$

$\tau_{e,0}$ is the time between two electron-imperfection scattering processes and $\tau_{e,ph}$ the time between two electron-phonon scattering processes. The relation between the relaxation time and the electrical resistivity is given by the *Drude formula*

$$\rho = \frac{m_e}{ne^2\tau}. \qquad (2.37)$$

It is the relaxation time that is responsible for the magnitude and temperature dependence of the electrical resistivity of a material. Since interactions between electrons and lattice imperfections are independent of temperature it follows that

$$\rho(T) = \rho_0 + \rho_{ph}(T) \qquad (2.38)$$

where ρ_0 and $\rho_{ph}(T)$ are the resistivities due to scattering processes on crystal defects and phonons, respectively. While the first term can be determined only by measurements the second one can also be calculated by the *Bloch-Grünseisen formula* [10] which is derived from the linearised Boltzmann equation:

$$\rho_{ph} = \mathcal{R} \left(\frac{T}{\theta_D} \right)^5 \int_0^{\frac{\theta_D}{T}} \frac{z^5}{(e^z - 1)(1 - e^{-z})} dz. \qquad (2.39)$$

where $\mathcal{R}$ represents the interaction strength between conduction electrons and phonons and contains the ionic mass, Fermi velocity, etc. For high temperatures the electrical resistivity shows approximately a linear behaviour

$$\rho_{ph}(T) \approx \frac{\mathcal{R}}{4}T \ldots T \gg \theta_D \tag{2.40}$$

whereas for low temperatures $\rho_{ph}(T)$ shows T^5 dependence given by

$$\rho_{ph}(T) \approx \frac{\mathcal{R}}{\theta_D}\left(\frac{T}{\theta_D}\right)^5 \ldots T \ll \theta_D \tag{2.41}$$

In order to calculate θ_D and $\mathcal{R}$ in practice these two values are used as fit parameters to approximate $\rho_{ph}(T)$ to actual measurement curves.

Depending on the elements the investigated material consists of, electron scattering on magnetic moments might occur. This is the case when the lattice atoms have a resulting magnetic moment (e.g. the 4f moments of the rare earth elements). Thus, equation (2.38) has to be completed by adding $\rho_{mag}(T)$:

$$\rho(T) = \rho_0 + \rho_{ph}(T) + \rho_{mag}(T). \tag{2.42}$$

The contribution of $\rho_{mag}(T)$ to the total electric resistivity depends on the temperature. If the temperature is low enough so that all magnetic moments of the lattice atoms are aligned parallel (i.e. $T < T_C \rightarrow$ ferromagnetic state) one obtains

$$\rho_{mag}(T) = AT^2, \tag{2.43}$$

where A is a constant. Consequently, the contribution of the magnetic moments is zero at 0 K. This behaviour can be explained if the conduction electrons are regarded as waves. At 0 K without any phonons and perfect magnetic order the electrons move as *Bloch-waves*, hence, they do not suffer scattering processes. However, as soon as the temperature is above that of magnetic order (*Currie temperature T_C*) the contribution of magnetic moments becomes temperature independent:

$$\rho_{mag} = \frac{3\pi N m_e^*}{2e^2\hbar E_F}|J|^2(g-1)^2 j(j+1) \tag{2.44}$$

where $(g-1)^2 j(j+1)$ is the *deGennes-factor*, g the *Landé-factor*, J the coupling constant between the spin of the conduction electron and the spin total angular momentum of the magnetic ion and j the total angular momentum of the magnetic ion.

Figure 2.1 shows the temperature dependence of each contribution and of the total electric resistivity. From the explanations above it follows that the electric resistivity of a perfect crystal (no defects at all) next to 0 K is zero.
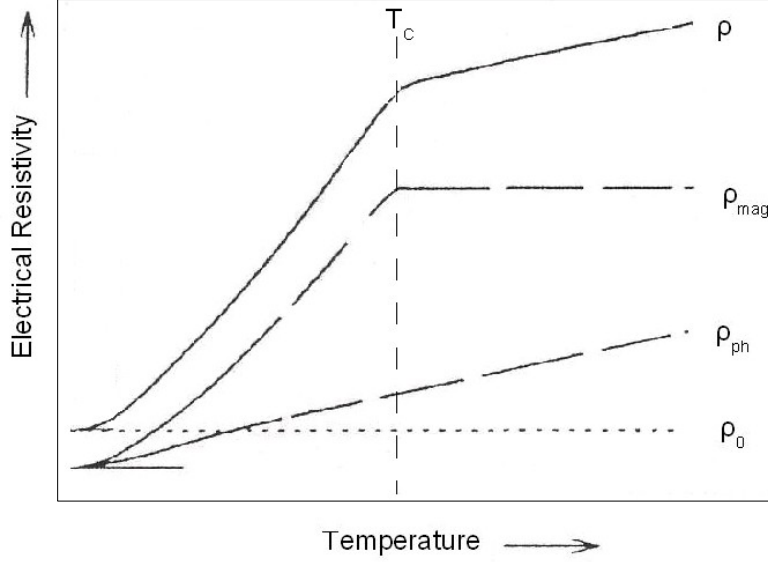
Figure 2.1: Example of temperature dependent resistivity behaviour of magnetically ordered rare earth compounds. Diagram taken from [11].

2.1.4   Thermopower

The thermopower of a material, represented by its *Seebeck coefficient*, is a consequence of the movement of the charge carriers due to a temperature gradient. The resulting displacement of electrons and holes causes an electric voltage. The relation between this voltage and the temperature gradient is then the Seebeck coefficient. Hence, the Seebeck coefficient S_x of a material x is given by

$$U = S_x \nabla T \tag{2.45}$$

For homogeneous materials ∇T can be replaced by ΔT.

For metals, the contributions to their thermopower is given by

$$S = S_e + S_{ph} + S_m \tag{2.46}$$

where S_e is the diffusion term, resulting from the movements of the electrons due to the temperature gradient. S_{ph} and S_m are the drag terms representing the phonon-electron drag (caused from electron drag due to phonons) and the magnon-electron drag (caused from electron drag due to magnons), respectively. However, due to their small contribution the drag terms are usually neglected. Since the kinetic energy of the electrons correspond to their temperature the average movement of the electrons is from the warmer

to the colder part of the material (figure 2.2). The one-dimensional average velocity due to the temperature gradient can be derived to

$$v_{diff} = \frac{v_1 + v_2}{2} = \frac{v(x - v\tau) - v(x + v\tau)}{2}, \tag{2.47}$$

which can be developed in first order to

$$v_{diff} = -\frac{\tau}{2}\frac{dv^2}{dT}\frac{dT}{dx}. \tag{2.48}$$

For three dimensions v can be replaced by $\frac{1}{3}v^2$ leading to

$$v_{diff} = -\frac{\tau}{6}\frac{dv^2}{dT}\nabla T. \tag{2.49}$$

The electron velocity due to the electric field is given by

$$v_{drift} = -\frac{e\tau}{m}\vec{E}. \tag{2.50}$$

Since in equilibrium both contributions compensate each other so that the resulting current is zero one obtains

$$\frac{1}{3}\frac{d}{dT}\left(\frac{mv^2}{2}\right)\nabla T + e\vec{E} = 0. \tag{2.51}$$

Together with $\frac{d}{dT}\left(\frac{mv^2}{2}\right) = \frac{c_V}{n}$ [2] and (2.45) the Seebeck coefficient is given by

$$S_e = -\frac{\pi^2 k_B^2 T}{6eE_F}. \tag{2.52}$$

In contrast to electric resistivity and thermal conductivity Matthiessen's rule cannot be used in this case. In order to split the contributions to S_e the *Kohler rule* is used instead.

$$S_e W_e = S_{e,0} W_{e,0} + S_{e,ph} W_{e,ph} + S_{e,mag} W_{e,mag} \tag{2.53}$$

W_e represents the thermal resistivity for electrons. Since it is difficult to derive this value from thermal conductivity measurements the *Wiedemann-Franz law* (see section 2.1.6) is used so that

$$S_e \rho = S_{e,0}\rho_0 + S_{e,ph}\rho_{ph} + S_{e,mag}\rho_{mag}. \tag{2.54}$$

---

[2]In a first approximation the inner energy U is given by the kinetic energy: $U \approx k_B T \approx \frac{mv^2}{2}$. The specific heat is the change of U with respect to temperature: $c_V = \frac{dU}{dT}$
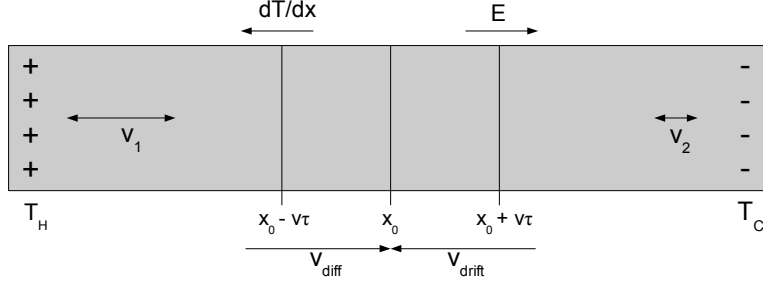
Figure 2.2: The temperature gradient causes the electrons to move from the warmer end at T_H to the colder end at T_C. The resulting field takes an opposite effect on the electrons. In equilibrium the currents compensates each other.

An analytical expression for S can be derived via the *Peltier coefficient*

$$\Pi = T \cdot S \tag{2.55}$$

with

$$\Pi = \frac{\sum_i h_i v_i}{e \sum_i v_i}. \tag{2.56}$$

v_i is the velocity of the ith electron and h_i its thermal energy. The latter one is the difference between the energy of the ith electron and the Fermi-energy

$$h_i = E_i - E_F. \tag{2.57}$$

Hence, the nominator in equation (2.56) represents the total amount of transported thermal energy while the denominator stands for the electric current. If follows that

$$S = \frac{1}{eT} \frac{\sum_i (E_i - E_F) v_i(x)}{j_x} \tag{2.58}$$

If only the contribution of the energy interval $(E, E + dE)$ is considered we obtain

$$S = \frac{1}{eT} \frac{\int (E - E_F) j_x(E) dE}{\int j_x dE}. \tag{2.59}$$

The current can be derived from the linear Boltzmann equation and the relaxation time approximation to

$$j_x = -\frac{e^2 \vec{E}_x}{4\pi^3 \hbar} \int \int \tau \frac{v_x^2}{v} dA \frac{df_0}{dE} dE, \tag{2.60}$$

where $\int dA$ is a surface integral. The electrical conductivity σ can be expressed as follows

$$\sigma_x = \frac{e^2}{4\pi^3\hbar} \int \tau \frac{v_x^2}{v} dA \tag{2.61}$$

Thus, the electric current in x-direction is given by

$$j_x = -\vec{E}_x \int \sigma_x(E) \frac{df_0}{dE} dE. \tag{2.62}$$

The general expression for the thermopower is therefore given by

$$S = \frac{1}{eT} \frac{\int \sigma_x(E)(E - E_F)\frac{df_0}{dE} dE}{\int \sigma_x(E)\frac{df_0}{dE} dE}. \tag{2.63}$$

As equation (2.63) shows the Seebeck coefficient is correlated to the electrical conductivity and its energy dependence. Thus, $S = 0$ if $\sigma(E)$ is constant over a range of energy $E \in (-k_BT, +k_BT)$ for which $\frac{df_0}{dE} \neq 0$. Further assumptions such as df_0/dE has only in the range k_BT above E_F appreciable large values and $E = E_F$ finally lead to

$$S = \frac{(\pi k_B)^2}{3e} T \left(\frac{\partial}{\partial E} \ln \sigma(E) \right) \tag{2.64}$$

The complete derivation of equation (2.64) was made under the assumption that only elastic scattering processes occur and that all transport processes are independent of direction (no anisotropic effects).

2.1.5 Thermal Conductivity

The thermal conductivity of a material is described by the coefficient λ which is the relation between an applied temperature gradient ∇T and the resulting heat flow $\vec{q}$ expressed by *Fourier's law*:

$$\vec{q} = -\lambda \nabla T \tag{2.65}$$

As explained in Section 2.1 electrons as well as phonons contribute to thermal conductivity, thus

$$\lambda = \lambda_e + \lambda_l. \tag{2.66}$$

Contribution of Electrons

Concerning the electronic part, *Matthiessen's rule* can be used to describe the different scattering processes. For simple metals the electronic contribution can be split into interaction processes between electrons and crystal defects and that between electrons and phonons.

$$\frac{1}{\lambda_e} \equiv W_e = W_{e,0} + W_{e,ph} \tag{2.67}$$

Analogue to the electrical resistivity, model calculations have been developed based on the linearised Boltzmann equation and the relaxation time approximation. The thermal resistivity W_e at low temperatures is mainly determined by interaction processes of electrons and crystal defects:

$$W_{e,0} = \frac{\alpha}{T}. \tag{2.68}$$

At higher temperatures electron-phonon interaction processes become dominant. These are described by the *Wilson equation,* which is similar to the Bloch-Grüneisen formula:

$$W_{e,ph} = \frac{4R}{L_0 T}\left(\frac{T}{\theta_D}\right)^5\left[\left(1 + \frac{3}{4\pi^2}\left(\frac{\theta_D}{T}\right)\right)J_5(z) - \frac{1}{2\pi^2}J_7(z)\right] \tag{2.69}$$

where $J_n(z)$ are Debye-integrals given by

$$J_n(z) = \int_0^{\frac{\theta_D}{T}} \frac{z^n}{\left(e^z - 1\right)\left(1 - e^{-z}\right)}dz. \tag{2.70}$$

L_0 is the *Lorenz number* (see Section 2.1.6) and R is a constant depending on electronic properties and on the strength of the electron-phonon interaction. For low temperatures ($T \ll \theta_D$) the thermal resistivity can be approximated by

$$W_{e,ph} \approx const \cdot \left(\frac{124.4}{\theta_D}\right)^3 T^2 \dots T \ll \theta_D, \tag{2.71}$$

whereas for high temperatures ($T \gg \theta_D$) the thermal resistivity is temperature independent:

$$W_{e,ph} \approx \frac{R}{L_0\theta_D} \dots T \gg \theta_D \tag{2.72}$$

Thus, concerning thermal conductivity, the contribution of electrons cause a T^2-dependence at low temperatures but remains constant as the temperature increases.

As for the electric resistivity, additional scattering processes have to be considered if the material contains atoms with permanent magnetic moments. This increases the thermal resistivity due to interactions between electrons and the magnetic moments leading to

$$\frac{1}{\lambda_e} \equiv W_e = W_{e,0} + W_{e,ph} + W_{e,mag}. \tag{2.73}$$

Naturally, scattering processes of electrons on magnetic moments depend on their structure. For a magnetically disordered range ($T > T_C$, paramagnetic state) the thermal resistivity is approximately given by

$$W_{e,mag} \cdot T = \mathrm{D}|J|^2 (g-1)^2 j(j+1) \tag{2.74}$$

where D is a constant. For the ferromagnetic state ($T < T_C$) no analytical expression has been derived so far. However, from experiments we know that below the Curie-temperature $W_{e,mag} \cdot T$ increases with temperature.

Lattice Contribution

Thermal resistivity due to phonon scattering results from interaction between phonons and crystal defects, phonon-phonon processes and scattering of phonons by conduction electrons and boundaries. Analog to λ_e the contributions of the lattice thermal conductivity can be added up leading to

$$\frac{1}{\lambda_l} \equiv W_l = W_{l,0} + W_{l,ph} + W_{l,e} + W_{l,B}. \tag{2.75}$$

Based on the relaxation time approximation *Callaway* developed a model assuming that these different scattering processes can be regarded as independent from each other. According to Matthiesen's rule, the total relaxation time is given by

$$\frac{1}{\tau_l} = \frac{1}{\tau_{l,0}} + \frac{1}{\tau_U} + \frac{1}{\tau_N} + \frac{1}{\tau_{l,e}} + \frac{1}{\tau_{l,b}} \tag{2.76}$$

The corresponding relaxation times for phonon-phonon interactions are τ_N for Normal-processes and τ_U for Umklapp-processes. $\tau_{l,0}$ denotes for scattering on crystal defects, $\tau_{l,b}$ for scattering on boundaries and $\tau_{l,e}$ for phonon-electron interaction processes. The contribution of each single process to the

total relaxation time is given by

$$\frac{1}{\tau_{l,0}} = Ax^4T^4, \tag{2.77}$$

$$\frac{1}{\tau_U} = BT^3x^2e^{\frac{-\theta_D}{3T}}, \tag{2.78}$$

$$\frac{1}{\tau_{l,b}} = C, \tag{2.79}$$

$$\frac{1}{\tau_{l,e}} = DTx \tag{2.80}$$

$$\tag{2.81}$$

where $x = \left(\frac{\hbar\omega}{k_BT}\right)$. Normal processes are represented by equation (2.34). The lattice thermal conductivity is then given by equation 2.35. Due to their small contribution Normal processes are usually neglected.

The temperature dependence is at low temperatures mainly determined by interactions between phonons and conduction electrons, yielding $\lambda_{l,e} \propto T^2$. As the temperature increases Umklapp-processes become dominant leading to a $\lambda_l \propto \frac{1}{T}$. Figure 2.3 gives an overview about the influence of the scattering processes to thermal conductivity and resistivity. At lowest temperatures boundary and point defect scattering are the most important interactions while Umklapp processes become dominant as the temperature increases.

Both Contributions

The separation of both contributions (λ_l and λ_e) is difficult and is only possible under certain circumstances. For example, in metals and inter-metallic compounds with excellent conductivity at low temperatures λ can be approximated as follows:

$$\lambda = \lambda_e + \lambda_l = \frac{1}{W_{e,0} + W_{e,ph}} + \lambda_{l,e} = \frac{1}{\frac{\alpha}{T} + \gamma T^2} + \delta T^2 \tag{2.82}$$
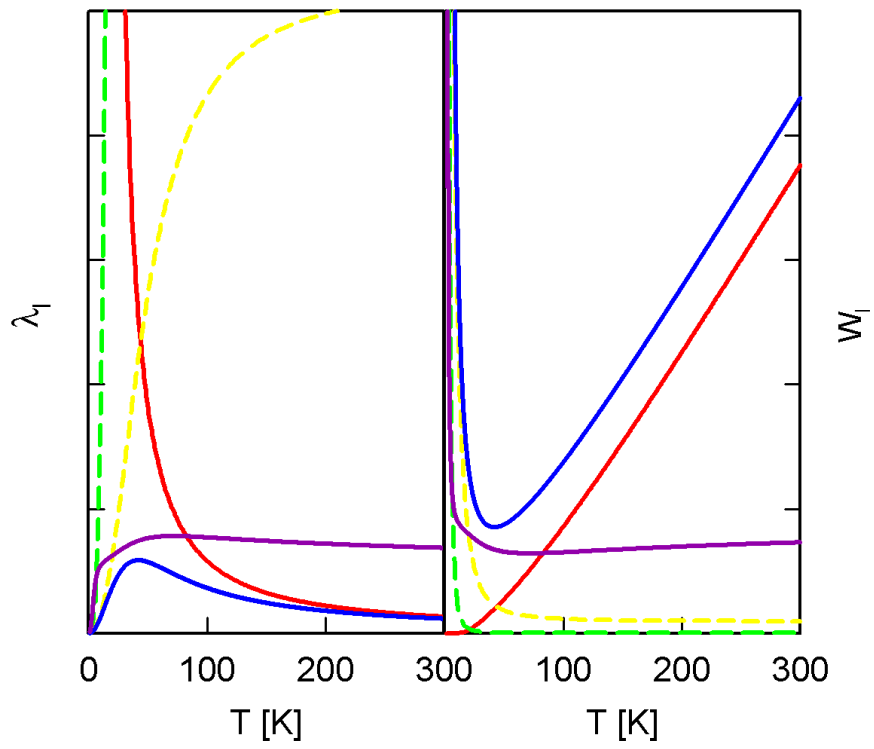
Figure 2.3: On the left side of this figure the lattice thermal conductivities are displayed as they would look like if only one of the scattering processes occure. In contrast, the contributions to thermal resistivity for phonons are plotted on the right side.

2.1.6 The Lorenz Number

The descriptions of thermal and electrical conductivity have shown a lot of similarities. The relation between both coefficients was already discovered in 1853 by *Wiedemann* and *Franz* [12].

In the model of a classical electron gas the electronic part of the thermal conductivity can be expressed as

$$\lambda_e = \frac{1}{3}nc_ev_el_e, \tag{2.83}$$

where c_e is the electronic heat capacity per electron, n the number of conduction electrons per unit volume, v_e the electron velocity and l_e the electron free path length. Since for a free electron gas one can set $v_e = v_F$, $c_e = \pi^2 k_B^2 T / m v_F^2$ and $l = v_F\tau$ the thermal conductivity becomes

$$\lambda_e = \frac{\pi^2 n k_B^2 T \tau}{3m}. \tag{2.84}$$

If this is compared with the Drude formula (2.37) one obtains

$$\frac{\lambda_e}{\sigma} = \frac{\pi^2 k_B^2}{3e^2}T = L_0 T, \tag{2.85}$$

in which $L_0 = 2.45 \cdot 10^{-8} W\Omega K^{-2}$ is the *Lorenz number* for a free electron model. For this calculation the mean life time τ is assumed to be the same for thermal and electrical transport processes. The Lorenz number can be defined for real metals as follows:

$$L_e = \frac{\lambda_e \rho}{T}. \tag{2.86}$$

Since L_e is temperature dependent it can significantly differ from L_0. In order to calculate L_e one has to subtract λ_e from λ. However, since λ_l is difficult to calculate the expression

$$L(T) = \frac{\lambda \rho}{T} \tag{2.87}$$

is mostly used. For metals where the thermal conductivity is mainly determined by the electronic contribution the situation can be simplified by setting $L(T) \approx L_e \approx L_0$

2.2 Efficiency of Thermoelectric Systems: Figure of Merit

Thermoelectric processes based on the *Seebeck-* and *Peltier-effect* can be used in order to generate electrical energy from a temperature gradient (Seebeck) or to pump heat via electricity (Peltier). However, in all applications of thermoelectric processes their efficiency and performance have to be considered. As described above thermoelectric processes are not independent, rather they influence each other, mostly in a negative way. Thus, for example, materials with large thermopower S also offer large values of the Peltier-coefficient Π (see equation (2.55)). Consequently, the temperature gradient is reduced which lowers the performance for electric power generation.

In order to calculate the efficiency of a thermoelectric system the *Figure of Merit Z* has to be derived. Figure 2.4 shows a sketch of an idealised thermo-couple consisting of two branches (one p-type and one n-type). They are of different length and cross section and arranged in an electric (serial) and thermal (parallel) assembly. An external electric voltage is applied at the end of each branch causing an electrical current that works as a heat pump due to the Peltier effect. Additionally, the upper endings of the branches are connected to a heat source with constant temperature T_H while the lower endings are connected to a heat sink with constant temperature T_C. This temperature gradient generates a heat flow and, because of the Seebeck effect, an electrical current. Both currents lead to an increase of the temperature of the branches.

For this consideration all losses due to radiation are neglected. Furthermore, electrical and thermal resistances at the junctions are assumed to be zero. The coefficients S, λ and ρ should not vary with temperature and the only way to exchange heat between source and sink are the thermo-couples. Because of the major charge carriers S is positive in the p-type branch and negative in the n-type. Based on equation (2.55) and (2.56) the total heat flow within each branch is

$$q_p = S_p I T - \lambda_p A_p \frac{dT}{dx} \quad \text{and} \quad q_n = -S_n I T - \lambda_n A_n \frac{dT}{dx} \tag{2.88}$$

The first terms in these equations represent the heat flow due to the current (Peltier-effect) while the second one stands for the heat flow resulting from the temperature gradient. Since S_n is negative the Peltier heat flow is positive in both branches. The rate of heat generation within each branch due to the Joule-effect is given by

$$\frac{dq}{dx} = I^2 \frac{\rho}{A}. \tag{2.89}$$
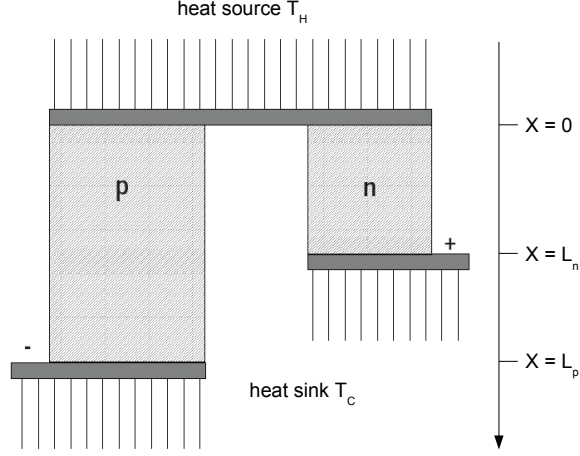
Figure 2.4: Principle design of a thermo-couple for electric power generation or heat pumping. (Scetch taken from [3].)

This causes a non constant thermal gradient:

$$-\lambda_{p,n} A_{p,n} \frac{d^2 T}{dx^2} = \frac{I^2 \rho_{p,n}}{A_{p,n}} \tag{2.90}$$

Since $T = T_H$ at $x = 0$ and $T = T_C$ at $x = L_{p,n}$ it follows

$$\lambda_{p,n} A_{p,n} \frac{dT}{dx} = -\frac{I^2 \rho_{p,n}(x - \frac{L_{p,n}}{2})}{A_{p,n}} + \frac{\lambda_{p,n} A_{p,n} \Delta T}{L_{p,n}} \tag{2.91}$$

with $\Delta T = T_H - T_C$. Since the rate at which heat is removed from the source is $q_C = (q_p + q_n)|_{x=0}$ the net heat pumping rate is given by

$$q_C = (S_p - S_n) I T_C - K \Delta T - \frac{I^2 R}{2} \tag{2.92}$$

with the total thermal conductance

$$K = \frac{\lambda_p A_p}{L_p} + \frac{\lambda_n A_n}{L_n} \tag{2.93}$$

and the total electrical resistance

$$R = \frac{L_p \rho_p}{A_p} + \frac{L_n \rho_n}{A_n}. \tag{2.94}$$

The current at which the maximum cooling power is reached is calculated by $\frac{dq_C}{dI} = 0$:

$$I_{max} = \frac{(S_p - S_n)T_C}{R}. \tag{2.95}$$

If follows that

$$q_{C,max} = \frac{(S_p - S_n)^2 T_C^2}{2R} - K\Delta T. \tag{2.96}$$

A positive cooling effect only can be obtained if $Q_{C,max} \geq 0$. Introducing the definition for the *figure of merit*

$$Z = \frac{(S_p - S_n)^2}{KR} \tag{2.97}$$

the maximum achieveable temperature gradient is given by

$$\Delta T_{max} = (T_H - T_C) = \frac{1}{2}ZT^2 \tag{2.98}$$

From equations (2.97), (2.93) and (2.94) it follows that Z depends on length and cross section of the branches. However, for material sciences the geometry of the investigated material should not be of importance. To maximise Z the factor KR has to be minimised. This is the case if

$$\frac{L_n A_p}{L_p A_n} = \left(\frac{\rho_p \lambda_n}{\rho_n \lambda_p}\right)^{1/2}. \tag{2.99}$$

This leads to an independent formula for the figure of merit:

$$Z = \frac{(S_p - S_n)^2}{[(\lambda_p \rho_p)^{1/2} + (\lambda_n \rho_n)^{1/2}]^2} \tag{2.100}$$

This definition is of convenience for combined thermoelectric devices. In order to characterise a single material the figure of merit is defined as

$$Z_{p,n} = \frac{S_{p,n}^2}{\rho_{p,n}\lambda_{p,n}}. \tag{2.101}$$

An optimum thermoelectric performance of a material is therefore given by a large Seebeck coefficient. However, due to irreversible thermoelectric effects (heat conduction and Joule heating) the values for thermal conductivity and electrical resistivity should be small. Since the overall unit of the fraction on the right side of (2.101) would be 1/K it is more convenient to use ZT instead of Z.

2.3   Clathrates

Glen Slack announced 1995 his idea of the *PLEC-concept (Phonon Lattice and Electron Crystal)* that combines the properties of a crystal with that of a glass [13]. This combination offers a rigid structure, responsible for good electrical conductivity, and heavy atoms rattling in cages of this structure leading to a lower thermal conductivity due to additional scattering of phonons. Clathrates are compounds with such properties. The framework, usually realised with germanium or silicon atoms, provides large cages filled by heavy electropositive elements like for example barium, caesium, strontium, europium or rubidium. In order to stabilise the framework and for a proper adjustment of the electronic structure p and d elements like cadmium, zinc or copper are added to the compound. For this diploma thesis the ternary clathrate phases $Ba_8Cd_xGe_{43-\frac{5}{8}x}\square_{3-\frac{3}{8}x}$ were investigated, with x = 2.4, 4.7, 6.5 and 7.6. The number of vacancies $\square$ decreases almost linearly with increasing cadmium content. Additional measurements were taken on $Ba_8Cu_5Ge_{41}$ and $Ba_8Zn_{7.7}Ge_{38.3}$ in order to get a better understanding about how the included elements influence the thermoelectric properties.

The electronic structure of clathrates can be understood in terms of the *Zintl concept*. Although this model simplifies the real situation, it provides a good description of their thermoelectric behaviour. According to this concept, the electronic structure of binary clathrates, like for example $Ba_8Ge_{43}\square_3$ with three framework defects, can be formulated as $[Ba^{+2}]_8[Ge^0]_{43}[\square^{-4}]_3$ [14, 15]. This leads to a deficiency of four electrons and, thus, to an improved electrical conductivity. Substitution and doping is a fruitful way in order to tune the charge carrier concentration and therefore to optimise the thermoelectric performance of a material. Figure 2.5 shows the crystal structure of two compounds, namely $Ba_8Cd_{2.4}Ge_{41.1}\square_{2.2}$ and $Ba_8Cd_{7.6}Ge_{38.4}$ and how the cadmium content is changed.
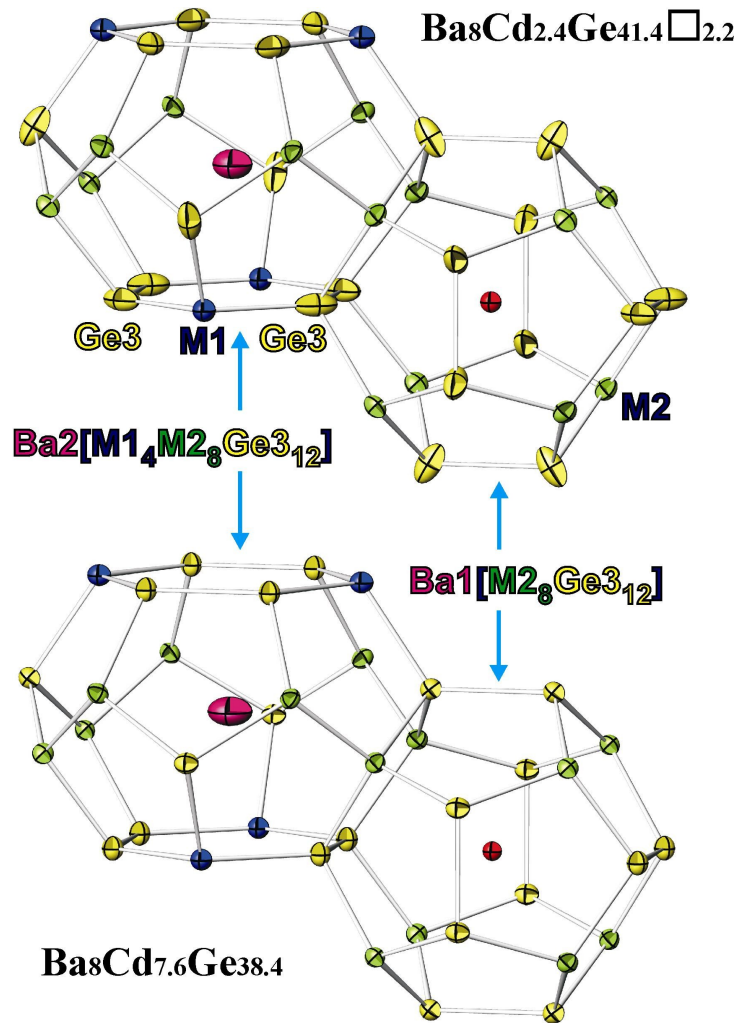
Figure 2.5: Crystal structure of $Ba_8Cd_x(Ge_{43-\frac{5}{8}x}\square_{3-\frac{3}{8}x})$ clathrates and how their cadmium content is changed [16].

Chapter 3

Experimental Design

This chapter describes the setup of the experiments and some necessary details about materials and devices. Except of the thermal conductivity the thermoelectric factors (ρ and S) were measured at two different temperature ranges[1]. From 4.2 K up to 300 K, in the following named as *low temperature*, and from 300 K up to 700 K named as *high temperature*. Furthermore, in all cases the measurement is from lower to higher temperatures in order to get more stable conditions. Finally, measurement values (S, ρ and λ) and the respective temperatures are displayed graphically on the screen and stored in a text file.

Although furnace and sample holders would provide even higher temperatures none of the measurements are above 700 K since the clathrates might then melt and the results become more inaccurate. For all measurements at low temperatures liquid helium was used as cooling medium.

The procedure is similar for each measurement. First the sample needs to be contacted with the sample holder. Afterwards the sample holder is inserted either into a cryostat (in case of low temperature measurement) or into the furnace (for measurements at high temperatures). The next step is then to plug the sample holder to the devices and to start the program that controls the measurement.

Clathrates show very interesting behaviour concerning their transport properties. However, it is one of the clathrates feature to break into pieces as soon as they are touched not absolutely smoothly. Contacting the sample can therefore be a tough challenge.

---

[1]As it will be explained later on no samples for λ-measurements at high temperatures were left (see Section 3.3).

3.1 Electrical Resistivity

For both temperature ranges a 4-terminal system is used to contact the sample in which a current is applied via two contacts at its ends and the resulting voltage drop along the sample is detected via two more contacts in between them. Figures 3.1 and 3.3 show sketches of both sample holders. The result is then the absolute resistivity R of the sample given by Ohm's law

$$R = \frac{U}{I}.$$

Since R still includes the sample's geometry (length l and cross section A) the parameters l and A need to be known in advance. Based on the equation

$$\rho = R\frac{A}{l}$$

the specific resistivity ρ is finally calculated by

$$\rho = \frac{U}{I}\frac{A}{l}. \tag{3.1}$$

The SI-unit for ρ is then Ωm.

3.1.1 Low Temperatures

Measurement Setup

As explained above the sample is contacted via four terminals, two outer ones to apply the current and two inner ones to measure the resulting voltage drop. In case of low temperatures these terminals are implemented by gold pins that are supported elastically and pushed towards the sample by small springs at their base. The samples should be bar-shaped, between 5 and 12 mm long and have a cross section of about 1 mm². Figure 3.1 shows a sketch how the sample holders are constructed.

The list of devices for this measurement is pretty short. Only a PC and the *Lakeshore Resistance Bridge 370AC* are necessary. The measurement is controlled by the PC while the resistance bridge applies the current and measures voltage and temperature. The data are then sent to the PC where the specific resistivity ρ is calculated via equation (3.1). Its results against temperature are displayed graphically and, furthermore, stored in a text file. An overview of the measurement station is given by Figure 3.2.
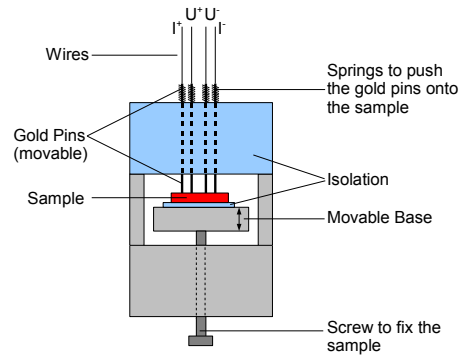
Figure 3.1: Sample holder for resistivity measurements at low temperatures. The current is applied via the two outer pins while the voltage is detected between the inner pins. The resistivity is finally calculated by equation (3.1)

Work Flow

After the sample is mounted to the sample holder that is inserted into the cryostat it is cooled down to 4.2 K by pumping liquid helium from a can into the sample chamber of the cryostat. The setup offers even lower temperatures of about 1.5 K if the pressure in the sample chamber is reduced by pumping the helium from the cryostat back into the recirculation system. As soon as the desired temperature is reached the measurement can be started via PC.
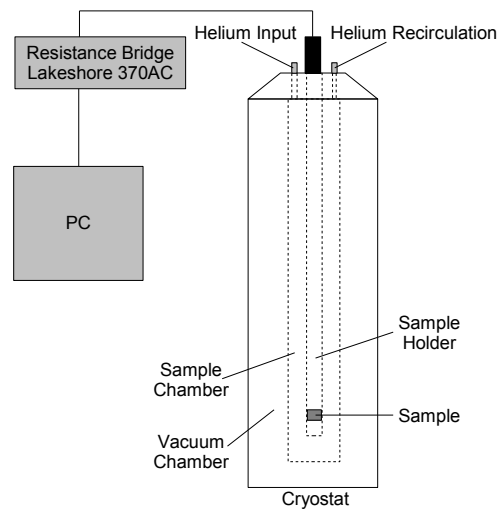
Figure 3.2: Measurement station for resistivity measurements at low temperatures

3.1.2   High Temperatures

Measurement Setup

The concept of this measurement is similar to the previous one, however, instead of gold pins copper wires are used to contact the sample. This is more useful for high temperatures measurements since the fragile springs of the gold pins would loose their tension as the temperature increases. This might then lead to worse contacts to the sample and therefore to wrong results. Usually it is no problem to fix copper wires onto the sample by spot-welding. However, in the case of clathrates this method does not work since either the electrical performance would not be sufficient to melt the copper or the sample would be destroyed because of the point like heat caused by the current. Instead of spot-welding conduction silver was used for the contact between copper wire and clathrate. This of course influences the result twofold: The cross section as well as the tap length diverge from that of the sample and the specific resistivity is influenced by silver. The first error occurs due to the silver contacts which are much larger and more imprecise than the contacts of the welded copper or the gold pins would be. The second one arises from the diffusion of silver into the sample as the temperature increases. While the first problem can be solved easily by multiplying the result with the ratio $\frac{\rho_{HT}}{\rho_{LT}}$ (= geometrical correction factor)[2] the second one is impossible to be solved. However, since the high-temperature measurement curves of all samples fit quite well to that at low-temperatures (concerning value and slope at room temperature) the error due to the diffusion can be neglected in a first approximation.

As Figure 3.3 shows, the sample holder offers two measurement places where the samples are fixed between two small mica dies. Each mica die is mounted by two screws onto a ceramic plate. To contact the copper wires of the sample with the measurement wires of the sample holder both are spooled around a screw that has to be tightened before the measurement starts. The temperature is detected via a Ni-NiCr thermocouple and a thermo flask filled with ice water as reference.

Like for the low temperature measurement a constant current is sent through the sample via the outer contacts and the voltage drop due to its resistivity is measured via the inner contacts. However, in this case it is not a resistance bridge that applies the current and measures voltage and temperature but two different devices: A constant DC-Calibrator (*Knick J152*),

---

[2]Comparison measurements using two samples of NBS-steel, one contacted by spot-welding and one with conduction silver, have shown that this kind of correction works fine.

controlled by the PC, supplies the current and a nanovoltmeter (*Keithley 181*) measures the voltages of the samples as well as of the thermocouple. In order to compensate thermo voltages the voltage drop along the sample is measured twice with opposite direction of the current. The voltage drop used to calculate ρ is then the arithmetic average of both values. Since the nanovoltmeter has only one line-in a multi-plexer with gold coated mechanical contacts (*Burster 1630*) is used to switch between the different signals. The data are subsequently sent to the PC where the voltage of the thermocouple is converted into temperature while the voltage drop along the sample together with equation (3.1) is used to calculate the specific resistivity ρ. Figure 3.4 shows what the whole measurement station looks like. More detailed information are given in the Appendix where a schematic diagram is displayed.

Work Flow

First four copper wires of appropriate length (approx. 10 cm) are spooled around the sample. The wires are then fixed onto the sample by conduction silver. After both samples are clamped between the mica dies the copper wires are spooled around the screws that need to be tightened to provide good electrical contact between the copper wires from the sample and the measurement wires of the sample holder. Furthermore, the sample holder is inserted into the steel pipe (= sample chamber) of the furnace (*Naber R70/9*) and connected to the devices via two plugs. To prevent the sample and the sample holder from oxidation the steel pipe needs to be evacuated before the heating starts. After program and furnace are started the measurement is controlled automatically by the PC that displays ρ against temperature on the screen and stores the data in a text-file.
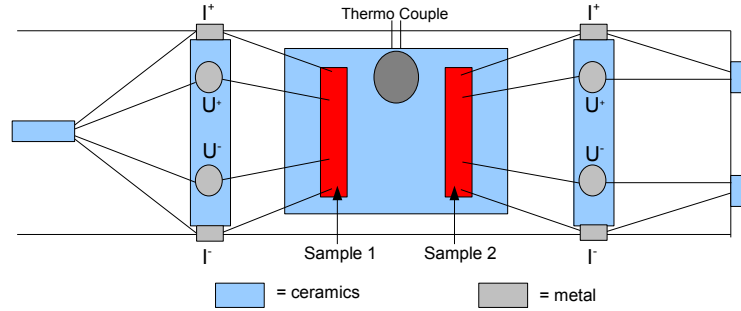
Figure 3.3: Sample holder for resistivity measurements at high temperatures. In order to geht rid of thermo–voltages the direction of the current is switched in each measurement step. Thus, I^+ and I^- as well as U^+ and U^- are exchanged during one step.
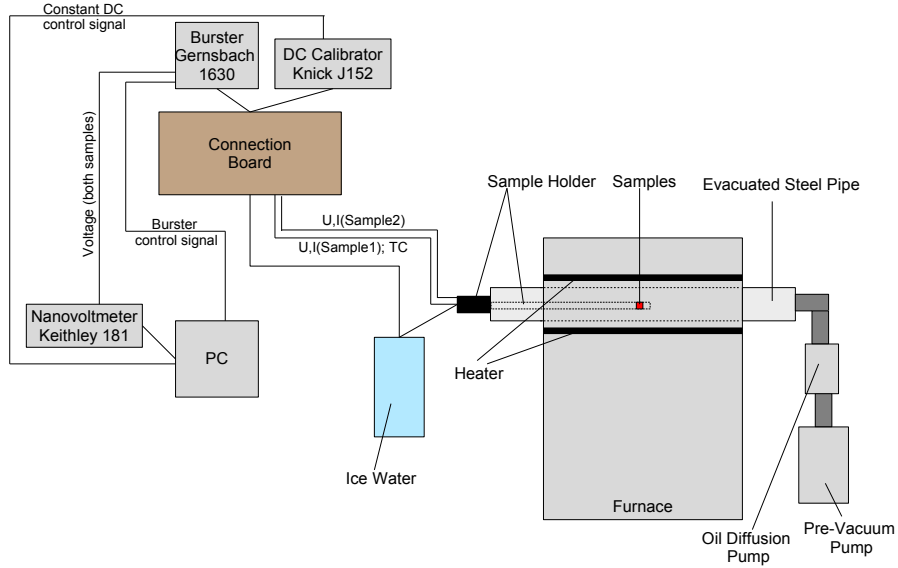
Figure 3.4: Measurement station for resistivity measurements at high temperatures

3.2   Thermopower

As described in Section 2.1.4 the measurement of the Seebeck coefficient
of a material requires the measurement of the resulting voltage due to the
applied temperature gradient. The temperature gradient is measured by two
thermocouples one at each end of the sample. The voltage drop at the sample
is then measured by detecting the voltage at the two ends of the unalloyed
wires. The thermal voltage inside the wires cancel out each other except of
the voltage that rises from the additional temperature at the warmer end
of the sample. The temperatures at each end of the sample are measured
with thermocouples[3]. The measurement principle is illustrated in figure 3.5
where a sample is contacted between two thermocouples. Each thermocouple
consists of two thermo-wires of material A and B, respectively. Based on
equation (2.45) the Seebeck coefficient of a sample is calculated as follows:

$$U_{meas} = \int_{T_{meas}}^{T_1} S_A(T)dT + \int_{T_1}^{T_2} S_{sample}(T)dT + \int_{T_2}^{T_{meas}} S_A(T)dT \qquad (3.2)$$

Since the relations of the temperatures are ($T_2 > T_1 > T_{meas}$) the last integral
can be split. Thus, we obtain

$$U_{meas} = \int_{T_{meas}}^{T_1} S_A(T)dT + \int_{T_1}^{T_2} S_{sample}(T)dT + \int_{T_2}^{T_1} S_A(T)dT + \int_{T_1}^{T_{meas}} S_A(T)dT$$
$$(3.3)$$

The first and the last integral sum up to zero. It follows, that

$$U_{meas} = \int_{T_1}^{T_2} \big(S_{sample}(T) - S_A(T)\big)dT \qquad (3.4)$$

Assuming that $\frac{dS}{dT}$ is constant for small ΔT [4] we finally get

$$U_{meas} = \big(S_{sample}(T_m) - S_A(T_m)\big)\Delta T \qquad (3.5)$$

Hence, the Seebeck coefficient is derived by

$$S_{Sample} = S_A - \frac{U_{meas}}{\Delta T}. \qquad (3.6)$$

Consequently, the SI-unit of S is $\frac{V}{K}$.

   The principles of the experimental design of the high and low temperature
measurements are the same. The sample is fixed between two plates of noble

---

[3]See Appendix for details

[4]This allows to replace the integral by a difference and set $T_m = \frac{T_2 - T_1}{2}$
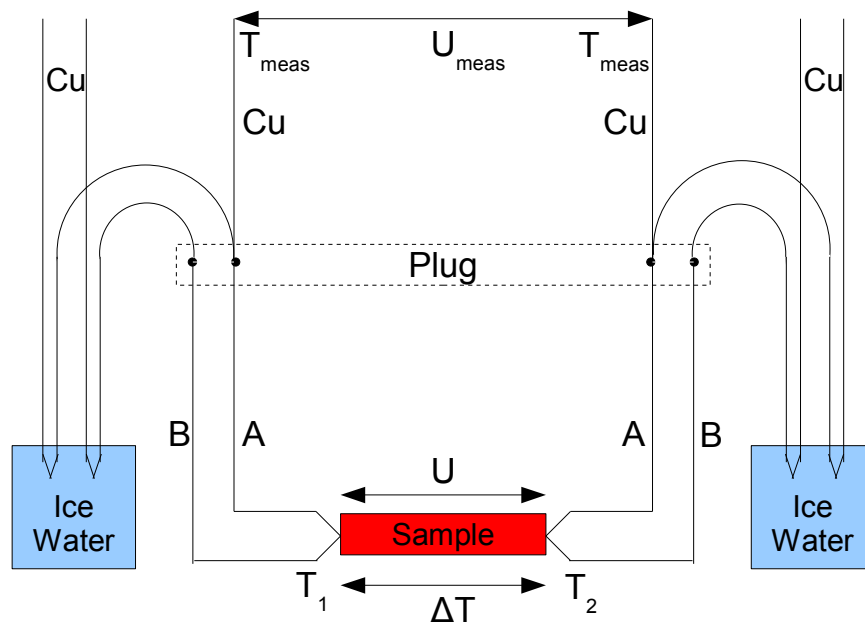
Figure 3.5: Measurement principle of thermopower measurements. The temperatures at each end of the sample are detected via the thermo couples (AB) ($\Delta T = T_2 - T_1$) while the voltage drop along the sample is measured at the ends of the copper wires.

metal that are connected to the thermocouples at their back side to measure temperature gradient and voltage. A thermocoax-wire is spooled next to the lower plate to apply the temperature gradient. An electrical current heats up the wire that, in turn, heats up the plate and therefore the sample. The average sample temperature is then the arithmetic temperature average of the upper and lower thermocouple.

Furthermore, both sample holders are flexible concerning the size and shape of the sample as long as the opposite conduction surfaces are parallel to each other. The length can be from a few millimeters up to approximately 1.5 cm.

3.2.1 Low Temperatures

Measurement Setup

The equipment used in our laboratory offers a temperature range from approximately 4 K up to room temperature (< 300 K). The cooling is provided by liquid helium that surrounds the evacuated tube where the sample holder is placed. The temperatures at both ends of the sample are measured by Pb-Au0.07%Fe thermocouples for the range from 4 K up to 15 K and by Pb-Chromel[5] for 15 K up to 300 K. The splitting is necessary due to the better accuracy of Pb-Au0.07%Fe thermocouples at temperatures below 15 K, whereas Pb-Chromel is more accurate above.

The sample is placed between two small plates of gold which offers a good thermal and electrical contact. Each plate has a socket at its backside where the connected thermocouples are fixed with tin-solder. Due to the good conductivity of gold temperature and voltage at the thermocouples are assumed to be the same as at the sample. Below the lower plate the thermocoax wire is spooled around the isolated thermo-wires. As soon as the electrical current is sent through it, the wire heats up the lower gold plate and therefore applies the temperature gradient to the sample. The temperature of a copper pod, installed approximately 20 cm above the upper gold plate, is the reference for the thermocouples. Inside this pod the thermo-wires are connected to wires made of copper that finally lead to the measurement devices. This setup allows to reduce the costs since less thermo-wire is needed. To determine the temperature of the pod two temperature sensors (one Pt- and one Ge-sensor) are installed inside it. For the range up to 40 K the Ge-sensor is used while the Pt-Sensor is for the range from 40 K up to 300 K.

The measurement temperature of the sample is determined by the average temperature of its both ends measured by upper and lower thermocouple while the temperature gradient is the difference between them. The voltage drop at the sample is measured via the Lead wires. Figure 3.6 shows a sketch of the the sample holder and how the sample is contacted. The lower part of the sample holder (right side of the picture) is equipped with two springs to push the lower gold plate (including the heater and the thermo-wires) upwards. Samples of different size and shapes can then be fixed between the two parallel gold plates. According to equation (3.6) and to the thermocouples used in this setup the equation for this measurement is

$$S_{Sample} = S_{Pb} - \frac{U}{\Delta T} \tag{3.7}$$

---

[5]Chromel is an alloy of 90% Nickel and 10% Chromium

The measurement station furthermore consists of a multiplexer with gold coated mechanical contacts (*Burster 1630*) to switch between the signals of the thermocouples and the temperature sensors, a temperature controller (*Lakeshore 91C*) to convert the signals from these sensors into temperature and to stabilise the absolute temperature as well as of a nanovoltmeter (*Keithley 2182*) to detect the voltages of the thermocouples. Two constant-DC supplies (*Knick J152*) provide the Pt- and Ge-sensor as well as the heater with electrical current. Due to the isolation of this setup it would take quite a long time to heat the sample up to room temperature only by means of the gradient heater. Thus, another heater is installed inside the cryostat. It consists of a thermo coax wire that is spooled around the outer side of the sample chamber and controlled by the *Lakeshore Temperature Controller 91CA*. All devices are connected to a PC that controls the whole measurement. Figure 3.7 gives a rough overview about how the measurement station looks like.

Work Flow

After the sample is mounted between the two gold plates the sample holder is inserted into the sample chamber of the cryostat. To cool down the sample liquid helium is pumped from the can into the helium tank of the cryostat while the interspace vacuum and the sample chamber are flooded with helium from the recirculation system. This offers a good thermal contact of the sample to the liquid helium and therefore cools it down rapidly. As the sample has the same temperature as the liquid helium (4.2 K) the connection to the helium recirculation is closed and interspace vacuum and sample chamber are evacuated. This reduction of pressure leads to even lower temperatures of about 3.8 K. The measurement program can be started as soon as the desired temperature is reached.
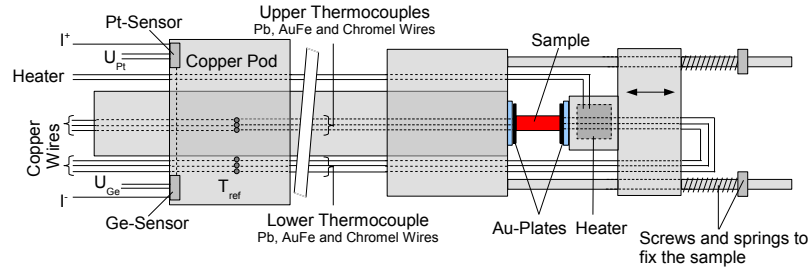
Figure 3.6: Sample holder for thermopower measurements at low temperatures. The sample is fixed between the two Au-plates. Temperature gradient and voltage are detected by the thermocouples fixed at the outer surfaces of the Au-plates. The lower part is movable in order to fix samples of different sizes.
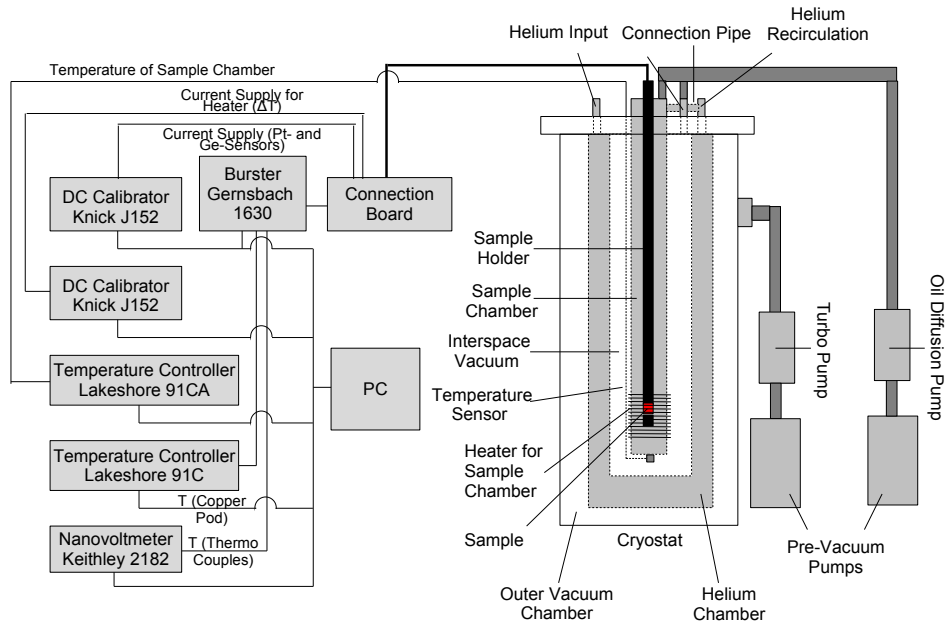
Figure 3.7: Measurement station for thermopower measurements at low temperatures.

3.2.2   High Temperatures

Measurement Setup

For thermopower measurements from 300 K up to 900 K thermocouples of type S (Pt-Pt10%Rh) are used to detect the termparatures and voltages at each end of the sample that is placed between two plates of platinum. This arrangement is similar to the low temperature setup, however, in this case the thermocouples are not connected to each other but are weld on the plates directly. The point where the temperarure is measured is then exactly where the PtRh-wire contacts the Pt-plate. Since this arrangement and the applied materials offer good thermal and electrical conductivity the difference between the measured temperature and that on the sample can be neglected in a first approximation. Like for resistivity measurements at high temperatures a thermo flask filled with ice water is used as reference temperature. The voltage drop along the sample is detected via the platinum wires. Consequently, the Seebeck coefficient is calculated by

$$S_{Sample} = S_{Pt} - \frac{U}{\Delta T}. \tag{3.8}$$

In contrast to the setup of the low temperature measurement it is the inner part of the upper sample holder that is movable and pushed by a spring downwards so that samples of different size and shape can be fixed between the two platinum plates. To switch between the voltages of the thermocouples a multi-plexer with gold coated mechanical contacts (*Buster 1630*) is used which sends each signal to a nanovoltmeter (*Keithley 181*). A power supply provides the heater with electrical current to apply the temperature gradient. The whole experiment is finally controlled by a PC. Figure 3.8 shows a sketch of the sample holder and Figure 3.9 gives an overview about how this measurement station looks like. More detailed information about how this measurement works can be found in the schematic diagram in the Appendix.

Work Flow

As for the other experiments the sample needs to be mounted first. In this case it has to be placed between the two platinum plates. After the sample holder is inserted into the steel pipe of the furnace (*Naber R70/9*) evacuation and heating procedure can be started. The vacuum should be sufficient before the furnace is turned on to prevent oxidation of the sample and the sample holder. Finally the measurement program can be started which controls all devices except of the furnace. This has to be programmed manually via its control board.
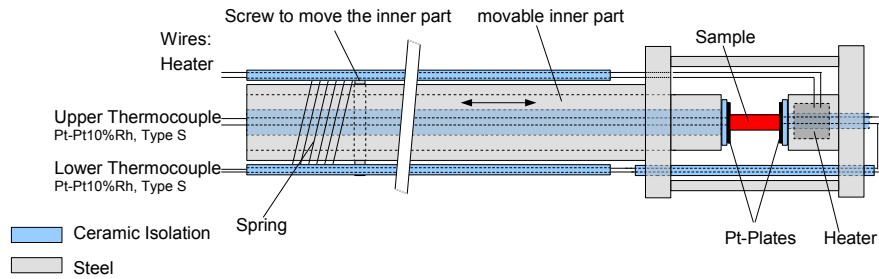
Figure 3.8: Sample holder for thermopower measurements at high temperatures. The sample is placed between the two Pt-plates and voltage as well as temperature are measured via the thermocouples on their back side. In contrast to the sample holder for low temperatures it is the upper part that is movable to fix samples of different sizes.
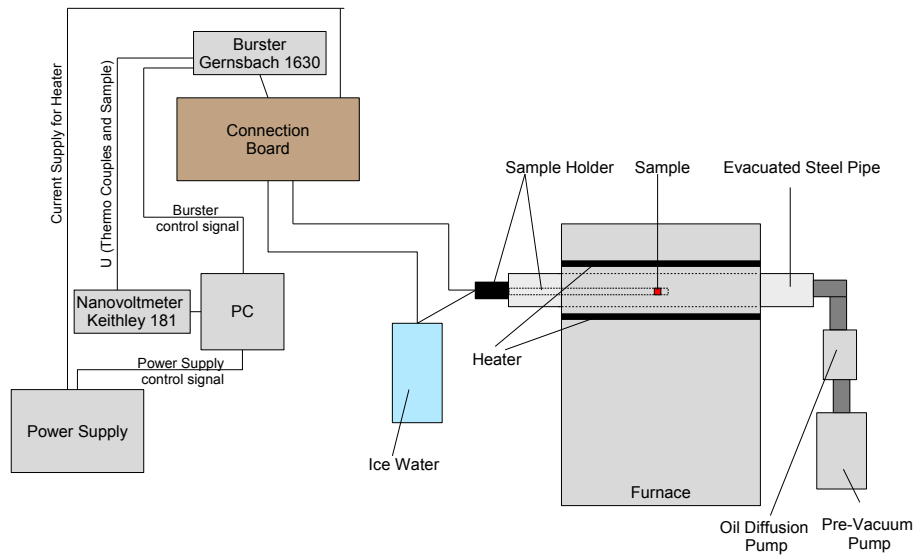
Figure 3.9: Sketch of the measurement station for thermopower measurements at high temperatures.

3.3   Thermal Conductivity

Measurements for thermal concuctivity at high temperatures are carried out using a Flash-Line devise. However, the setup requires cylindrical samples with a diameter of 6 mm and a thickness of a few mm. Since all sample pieces were used for the other thermoelectric measurements none was left to be prepared for this one. Therefore only the thermal conductivity at low temperatures could be measured.

In the following section the measurement equation is derived. The geometric factors of the sample are its tap length l and its cross section A. The basic principle of heat transport due to a temperature gradient is the *Fourier law*

$$\vec{q} = -\lambda \nabla T \tag{3.9}$$

where $\vec{q}$ is the heat flux density given by

$$\vec{q} = \frac{1}{A} \frac{dQ}{dt} = \frac{1}{A} \dot{Q}. \tag{3.10}$$

Q is the total amount of heat that can be transported. Because ∇T can be approximated by

$$\nabla T = \frac{dT}{dl} \approx \frac{T_2 - T_1}{l} = \frac{\Delta T}{l} \tag{3.11}$$

and $|\vec{q}| = \lambda |\nabla T|$ we finally get

$$\frac{1}{A} \dot{Q} = \lambda \frac{\Delta T}{l} \tag{3.12}$$

Hence, the measurement equation is

$$\lambda = \frac{l}{A} \frac{\dot{Q}}{\Delta T} \tag{3.13}$$

Thus, in order to measure the thermal conductivity one needs to know the sample's cross section A and to detect the heat quantity per time unit $\dot{Q}$ as well as the temperature difference ΔT along the tap length l. Consequently, the SI-unit of λ is $\frac{W}{cmK}$.

Measurement Setup

To measure the temperature gradient ΔT_S the sample is contacted to two Au0.07%Fe-Chromel thermocouples. One at its upper end and the second one at approximatley 2/3 of the sample length. Their voltages are detected by a *Keithley 181* nanovoltmeter. The sample is mounted onto a heat sink by

clamping its lower part (below the lower thermocouple) between a movable and a fixed panel of the heat sink. The former one can then be pushed towards the latter one by two screws. The area between these two parts is filled up with a conduction paste to provide good thermal contact between the sample and the heat sink. On the one hand this heat sink is necessary to keep one end of the sample at a stable temperature and on the other hand it provides the reference temperature for the thermocouples. Its temperature is measured by two sensors, a Pt-sensor and a Ge-sensor, both controlled by a temperature controller (*Lakeshore 91CA*). Due to their temperature dependent sensibility the Ge-sensor is used for the range up to 40 K while the Pt-Sensor is used for the range from 40 K up to 300 K (analog to the thermopower setup at low temperatures). In order to get a stable temperature gradient along the sample and to cool the shieldings (see below) the heat sink is cooled by a flux of liquid helium. This flux can be limited on the one hand by a needle valve on the sample holder and, on the other hand, by a computer controlled valve at the helium pump.

To apply the temperature gradient to the sample a strain gauge is mounted on its top. As the current I controlled by the constant DC calibrator (*Knick J152*) flows through the strain gauge it heats up the upper part of the sample. The voltage drop U at the strain gauge is measured by a voltmeter (*Prema 5000 Digital Multimeter*). Thus, if radiation losses of the strain gauge are neglected, the thermal flux Q can be set equal to the electrical performance P and calculated by $Q = P = U \cdot I$. For the calculation of the sample's average temperature T_S equation

$$T_S = T_0 + \Delta T_B + \frac{\Delta T_S}{2} \qquad (3.14)$$

is used where T_0 is the temperature of the heat sink, ΔT_S the difference between the two thermocouples and ΔT_B the difference between heat sink and lower thermocouple.

In order to protect the measurement against radiation three radiation shieldings surround the setup. While the outer ones are normal shieldings the purpose of the inner shielding is to establish radiation balance between the sample and its surrounding. Therefore, it should always have the same temperature as the sample which is enabled by a heater controlled by the *Lakeshore Temperature Controller 91C* and the thermal contact to the heat sink. While the temperature controller sends a current through a thermo coax wire that is spooled around the inner shielding to heat it up the heat sink and therefore the shielding is cooled by the flux of helium. This arrangement allows to control the temperature in the range of 4.2 K and room temperature and to keep it always at the same temperature as the sample.
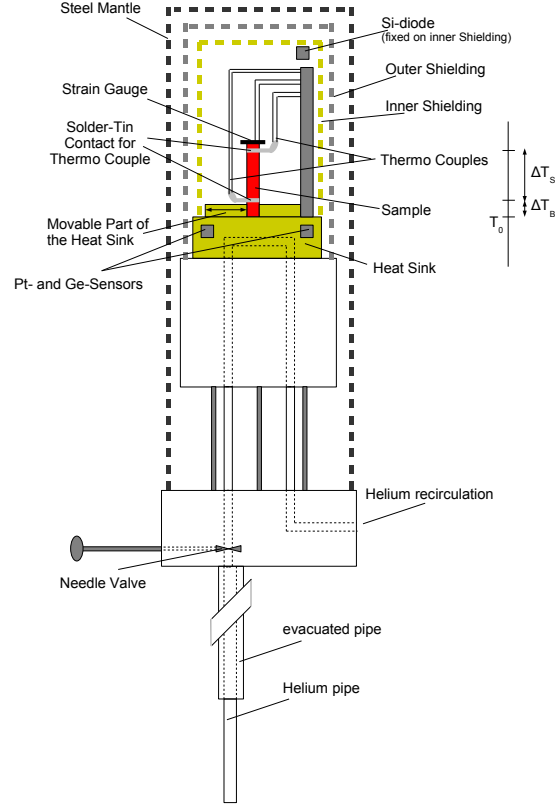
Figure 3.10: Sample holder for thermal conductivity measurements at low temperatures. The sample is fixed on the heat sink. On top of the sample the strain gauge is sticked up to apply the temperature gradient. ΔT is measured via the two thermocouples. Their temperature is ΔT_B and ΔT_S above that of the heat sink (T_0).

The measurement of the shielding's temperature is done by a *Si-diode Sensor* that is connected to the *Lakeshore 91C*. However, the results show that in practice there are still radiation losses at higher temperatures. This error has to be corrected afterwards as the measurement results are analysed. A futher explanation about this correction is given in Section 4.3.

Figure 3.10 gives an overview on how this measurement works. To evacuate the whole measuring fixture it is surrounded by a steel mantle (which also works as a shielding) that can be connected to the vacuum pump system. Figure 3.11 shows a sketch of the whole measurement station.
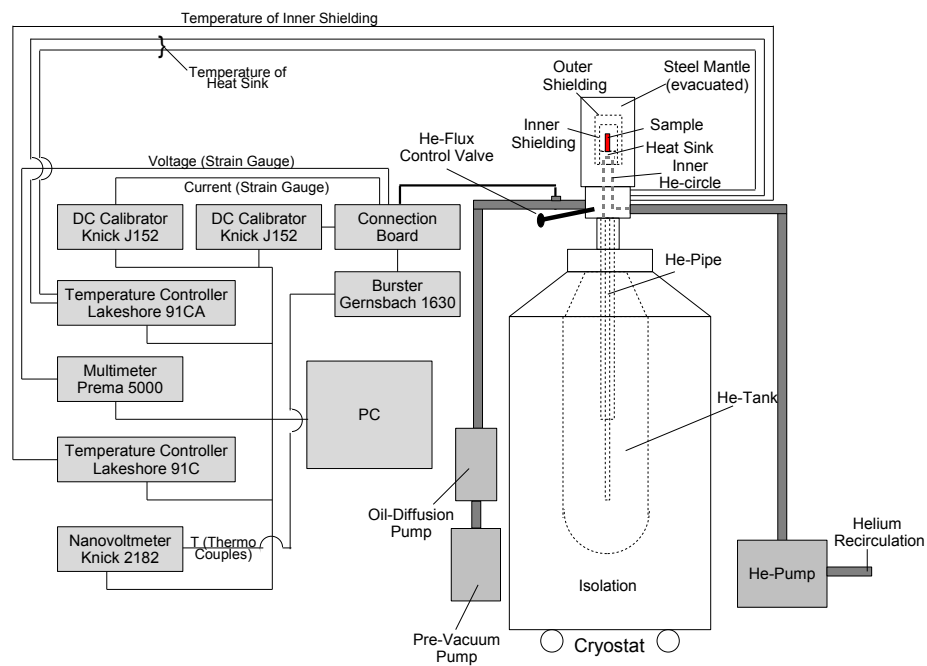
Figure 3.11: Sketch of the measurement station for thermal conductivity measurements at low temperatures.

Work Flow

In order to contact the thermocouples to the sample a copper wire is spooled
around it which is fixed with tin-solder. This arrangement provides good
thermal contact between the thermocouples and the sample. Afterwards,
a strain gauge is glued onto the sample's top. Subsequently, the sample is
mounted onto the heat sink and the tin-plated copper wires are soldered to
the thermocouples of the sample holder as well as the contacts of the strain
gauge are connected to the current supply. After the shieldings and the steel
cover are mounted the sample holder must be evacuated before it is inserted
into the helium can. Finally helium pump and measurement program are
started. It first opens the valve to cool down the measurement equipment
and then starts the measurement. The program controls the measurement
automatically and uses the formula above together with the detected values
to calculate the thermal conductivity λ.

Chapter 4

Measurement Results and Analysis

All measurements were taken on the devices described in Chapter 3. Based on their performance the measurement for ρ, S and λ were carried out from approximately 4 K up to room temperature and for ρ and S from room temperature to 700 K. In order to find materials offering excellent performance for thermoelectric applications the ternary clathrate phases $\mathrm{Ba_8M_xGe_{43-\frac{5}{8}x}\square_{3-\frac{3}{8}x}}$ with M = Cd, Cu and Zn were investigated. The respective chemical compositions are

- $\mathrm{Ba_8Cd_{2.4}Ge_{41.1}\square_{2.2}}$,

- $\mathrm{Ba_8Cd_{4.7}Ge_{40.3}\square_1}$,

- $\mathrm{Ba_8Cd_{6.5}Ge_{39.1}\square_{0.4}}$,

- $\mathrm{Ba_8Cd_{7.6}Ge_{38.4}}$,

- $\mathrm{Ba_8Cu_5Ge_{41}}$ and

- $\mathrm{Ba_8Zn_{7.7}Ge_{38.3}}$.

The physical data of these compositions such as the lattice parameter a, the atoms per unit cell and the resulting number of atoms per cubic meter are listed in Table 4.1.

Materials with large thermopower values are usually found in the proximity of a metal-to-insulator transition. To find an optimum between large thermopower but low electrical resistivity and thermal conductivity the included elements as well as their concentration are varied as described above. As the measurement data will show such kind of doping and substitution is a useful method to tune the charge carrier concentration [16, 17].

| | a | atoms/unit cell | n |
	[nm]		[1/m^3]
$Ba_8Cd_{2.4}Ge_{41.1}\square_{2.2}$	1.07571	51.8	4.16E28
$Ba_8Cd_{4.7}Ge_{40.3}\square_1$	1.08555	53.0	4.14E28
$Ba_8Cd_{6.5}Ge_{39.1}\square_{0.4}$	1.09149	53.6	4.12E28
$Ba_8Cd_{7.6}Ge_{38.4}$	1.09539	54.0	4.11E28
$Ba_8Cu_5Ge_{41}$	1.08555	53.0	4.14E28
$Ba_8Zn_{7.7}Ge_{38.3}$	1.07678	54.0	4.33E28

Table 4.1: Physical data of all compounds. a is the lattice parameter and n the number of atoms per cubic meter.

4.1   Resistivity

The interaction processes between electrons and defects as well as phonons cause a temperature dependent and independent contribution to electrical resistivity given by

$$\rho(T) = \rho_0 + \rho_{ph}(T). \tag{4.1}$$

The temperature dependent part of a simple metal follows from the *Bloch-Grüneisen* equation

$$\rho_{ph} = \mathcal{R}\left(\frac{T}{\theta_D}\right)^5 \int_0^{\frac{\theta_D}{T}} \frac{z^5}{(e^z - 1)(1 - e^{-z})} dz, \tag{4.2}$$

while ρ_0 represents the resistivity due to scattering processes on crystal imperfections.

From equations (2.40) and (2.41) a T^5-dependence for low temperatures ($T \ll \theta_D$) would be expected while at high temperatures ($T \gg \theta_D$) the dependence should be linear. Furthermore, the increasing cadmium content should lead to a more metallic like behaviour due to the larger charge carrier concentration. As expected from the Zintl concept, samples with larger cadmium content (7.6 and 6.5) show metallic like behaviour while that with lower cadmium content (4.7 and 2.4) show only at lower temperatures metallic behaviour. As the temperature increases their resistivity reaches a maximum value and decreases afterwards, thus, showing a resistivity behaviour of an semi-conductor. Since such an attitude belongs to semi-conductors these measurement data cannot be described by the Bloch-Grüneisen formula. Furthermore, the temperature dependence below 10 K is approximately $T^{2.5}$ and not T^5. Consequently, the electron-phonon scattering process (as described
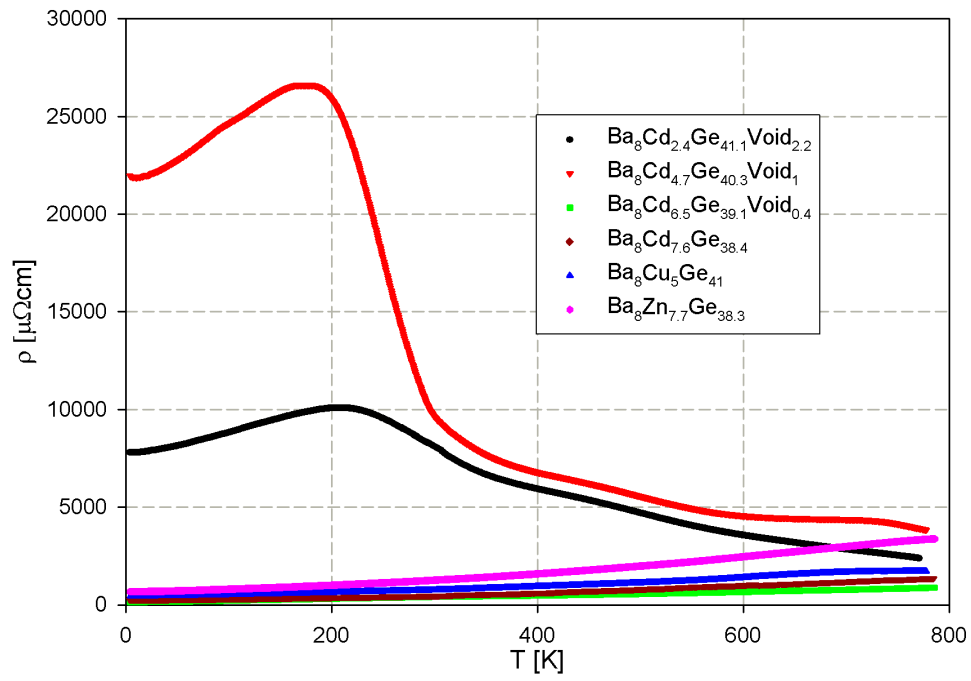
Figure 4.1: Overview on the resistivity measurements of all compounds. The compounds with lower cadmium content of $x = 2.4$ and 4.7 show semiconductor temperature dependence whereas as the compounds containing $x = 6.5$ and 7.6 cadmium atoms per unit cell show clearly metallic behaviour.

by the Bloch-Grüneisen formula) needs to be accounted for by an alternative model, which is a combination of the Bloch-Grüneisen law with a temperature dependent charge carrier density [18]. It includes a band gap in the density of states right above the Fermi energy. In order to simplify the calculations the band structure is assumed to be rectangular (see Figure 4.2). Within this model the charge carrier densities (n_n and n_p) as well as the width of the energy gap (E_g) can be calculated. According to the rectangular shape of the density of states and to the equations (2.8) and (2.9) n_n and n_p are given by

$$n_n(T) = -N_0 E_g + N_0 k_B T \ln \left(1 + e^{E_g/k_B T} \right) \tag{4.3}$$

and

$$n_p(T) = -N_0 k_B T \ln 2. \tag{4.4}$$

The total charge carrier density follows then from

$$n(T) = \sqrt{n_n(T) n_p(T)} + n_0 \tag{4.5}$$

where n_0 accounts for the residual resistivity[1]. The overall resistivity based on this model is therefore

$$\rho(T) = \frac{\rho_0 n_0 + \rho_{ph}}{n(T)}, \tag{4.6}$$

where ρ_0 is the residual resistivity due to crystal defects. Both measurements showing semi-conductor behaviour can be fitted by this model using the physical terms R, E_g, n_0, $N(E)$, ρ_0, θ_D and the difference in energy between the lower band edge and the Fermi energy as fit parameters. The measurement data and their corresponding least square fits are displayed in Figure 4.3. As a reason for the metallic temperature dependence the narrow distance between E_1 and E_F could be identified.

The measurements of the compounds showing metallic-like temperature dependence can be fitted by the Bloch-Grüneisen equation if the residual resistivity ρ_0 is added. The corresponding fit parameters are θ_D, ρ_0 and $\mathcal{R}$, respectively. Measurement data and fit curves are displayed in figure 4.4.

Program and functions used for these least square fits are explained in more detail in the Appendix, Section D.1. In Table 4.2 all relevant physical terms and their corresponding fit parameters and values are listed.

---

[1]$\rho(T = 0) = \rho_0 \neq 0$ due to crystal defects
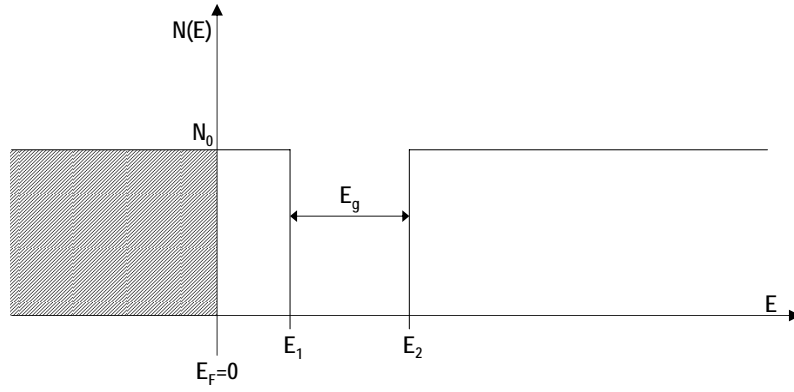
Figure 4.2: The model for the density of states as a function of energy.
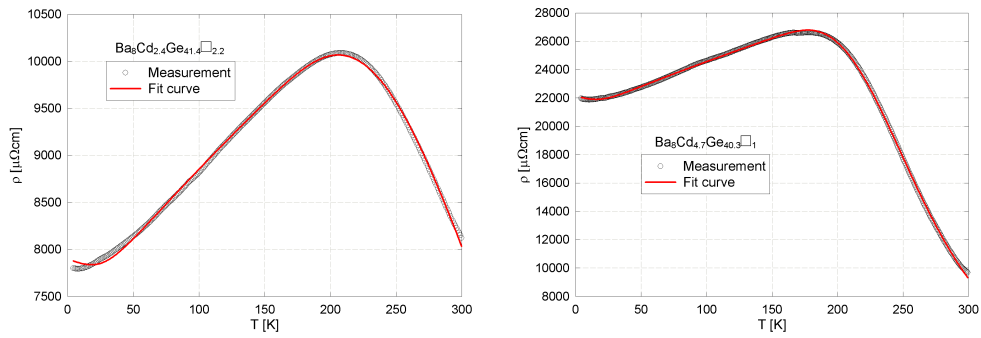
Figure 4.3: Measurement data and fit curves of the electrical resistivity of $Ba_8Cd_{2.4}Ge_{41.1}\square_{2.2}$ and $Ba_8Cd_{4.7}Ge_{40.3}\square_1$. Both samples show semiconductor temperature dependence, thus, the fit was performed by the model described in the text (equation (4.6)).

	$\mathcal{R}$ $[\mu\Omega\text{cm}]$	E_g [K]	n_0	$N(E)$ [1/J]	ρ_0 $[\mu\Omega\text{cm}]$	θ_D [K]	$E_1 - E_F$ [K]
$\text{Ba}_8\text{Cd}_{2.4}\text{Ge}_{41.1}\square_{2.2}$	2714	2459	0.24	2.23E21	7926	188	1.71E-3
$\text{Ba}_8\text{Cd}_{4.7}\text{Ge}_{40.3}\square_1$	1352	3134	0.06	9.34E21	22240	135	1.50E-5
$\text{Ba}_8\text{Cd}_{6.5}\text{Ge}_{39.1}\square_{0.4}$	1073	-	-	-	150	298	-
$\text{Ba}_8\text{Cd}_{7.6}\text{Ge}_{38.4}$	750	-	-	-	249	264	-
$\text{Ba}_8\text{Cu}_5\text{Ge}_{41}$	1513	-	-	-	456	376	-
$\text{Ba}_8\text{Zn}_{7.7}\text{Ge}_{38.3}$	3559	-	-	-	701	461	-

Table 4.2: List of fit parameters used for least square fits for electrical resistivity measurements. Due to their semiconduction temperature dependence the fits for $\text{Ba}_8\text{Cd}_{2.4}\text{Ge}_{41.1}\square_{2.2}$ and $\text{Ba}_8\text{Cd}_{4.7}\text{Ge}_{40.3}\square_1$ are based on the model including a temperature dependent charge carrier density (equation (4.6) [18]). All other fits are carried out using equation (4.1) and (4.2). For more details see D.1 in the Appendix.
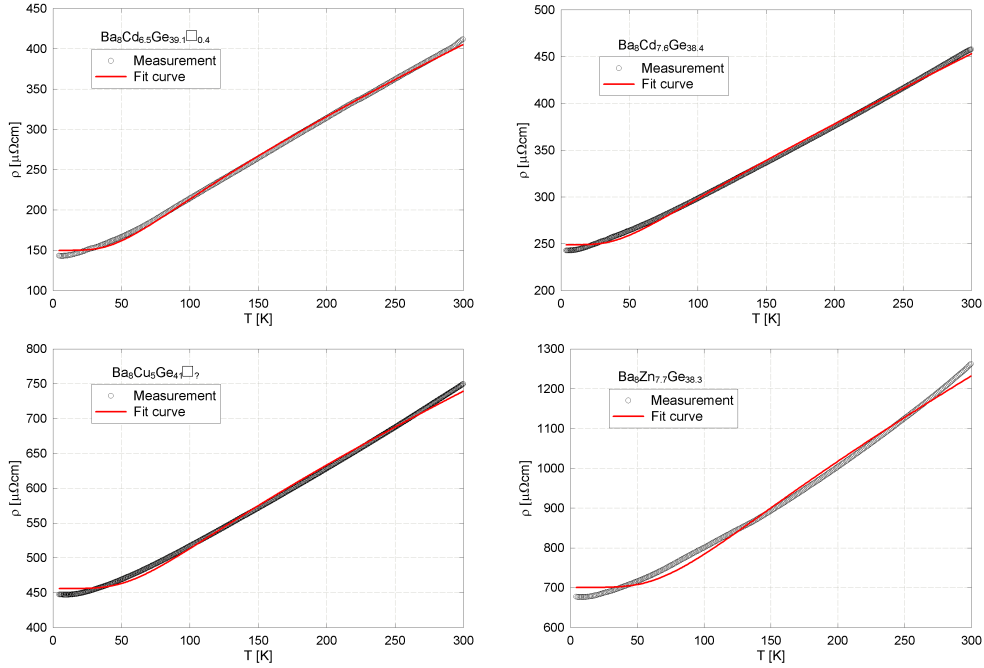
Figure 4.4: Measurement data and fit curves of the electrical resistivity of $\text{Ba}_8\text{Cd}_{6.5}\text{Ge}_{39.1}\square_{0.4}$, $\text{Ba}_8\text{Cd}_{7.6}\text{Ge}_{38.4}$, $\text{Ba}_8\text{Cu}_5\text{Ge}_{41}$ and $\text{Ba}_8\text{Zn}_{7.7}\text{Ge}_{38.3}$. The temperature dependences show metallic-like behaviour. Hence, the fits are carried out using equation (4.1) and (4.2).

4.2   Thermopower

Except of the low temperature range of the $Cd_{6.5}$-sample all thermopower values of the samples containing cadmium are below zero, showing that the main charge carriers are electrons. Only for $Ba_8Cd_{6.5}Ge_{39.1}\square_{0.4}$ below 200 K the charge transport consists obviously rather of holes than of electrons. In contrast to the electrical resistivity the temperature dependences of the Seebeck coefficients do not offer any special behaviour (except of the $Cd_{6.5}$-compound). Thus, the electronic transport can be assumed to be without any significant change in the temperature correlations. Furthermore, the small measurement values indicate a small energy dependence of the density of states next to the Fermi energy. However, the results also yield a more com-
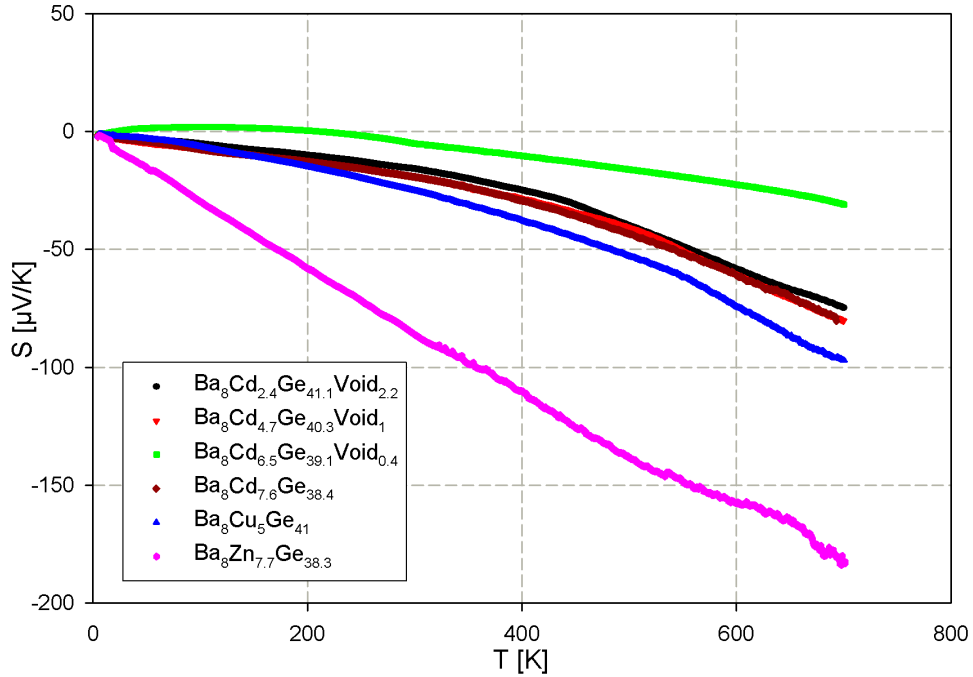
Figure 4.5: Overview on the thermopower measurements of all compounds.

plex behaviour concerning the change of the cadmium content. As Figure 4.5 shows the $Cd_{6.5}$-compound exhibits outstanding Seebeck values compared to the other Cd-compounds. The same holds for the resistivity measurements. $Cd_{2.4}$- and $Cd_{4.7}$-compounds show semi-conducting characteristics while the samples containing $Cd_{6.5}$ and $Cd_{7.6}$ offer metallic characteristics. Thus, as the cadmium content increases from below six atoms to an amount of more than six atoms per formula unit, the transport properties change signifi-
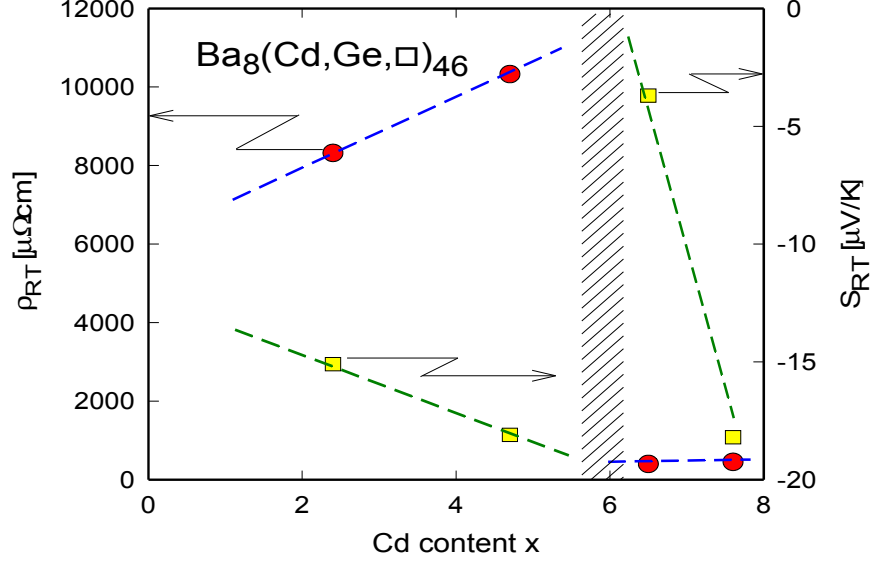
Figure 4.6: Dependency of electrical resistivity and thermopower on given concentrations of cadmium [16]. Each value is taken at room temperature.

cantly. Figure 4.6 compares the values for resistivity and thermopower at room temperature of compounds with different cadmium content. Like for the resistivity it is the increasing charge carrier density due to the increasing cadmium content that replaces the vacancies. The investigation becomes more interesting regarding the outstanding Seebeck value of $Ba_8Zn_{7.7}Ge_{38.3}$. It offers an almost constant slope of $-0.28\,\mu V/K$ until a thermopower of $-180\,\mu V/K$ at 700 K. This linearity can be explained by the free-electron model [19]. For $T > \theta_D$ the Seebeck effect due to the electron-phonon drag dominates leading to

$$S_d(T > \theta_D) = \frac{2\pi^2 k_B^2 m}{e\hbar^2 (3n\pi^2)^{2/3}} T.$$

(4.7)

Since for systems without significant electronic correlations at high temperatures m can be replaced by m_e. Thus, equation (4.7) allows an estimation of the charge carrier density n which is one of the most important parameters for thermoelectric properties. Based on the measurement data the charge carrier density is estimated to $n = 6 \cdot 10^{26}\ m^{-3}$.

4.3 Thermal Conductivity

The measurement data (Figure 4.7) show interesting temperature dependence of most compounds. Except of the $Cd_{2.4}$-compound all samples have a strong increasing thermal conductivity at lowest temperatures. After a maximum below 20 K the values decrease rapidly down to a minimum between 50 and 150 K. Beyond this temperature the values for λ seem to increase again. However, the slope is now much smaller than it was before. As it will be explained later on this rise of the values is not due to an increase of λ but to an measurement error caused by radiation losses. Since this error can be calculated the results can simply be corrected by subtracting this error from the measurement data(see Figure 4.8). The overall values for the thermal conductivity are small as it was expected for clathrates.

4.3.1 General Analysis of Thermal Conductivity

The overall values for λ are small as is was expected for clathrates. At lower temperatures (from 4 K up to the minimum) the lattice is responsible for heat transport. The strong increase at lowest temperatures refer to small contributions of phonon scattering on point defects and boundaries. As the temperature increases Umklapp-processes become dominant yielding lower thermal conductivity.

Additionally to the temperature dependence the elements included in the compounds and their concentration show a strong influence on this transport property. As described in Section 2.3 the atoms substituting the vacancies and the germanium atoms are placed in cages where they represent additional scattering centers for the phonons. The heavier this atom the stronger is the scattering process and the lower is the thermal conductivity. Therefore, the compound containing Zn_8 has larger values at low temperatures than the Cd_8-compound. However, as the electronic contribution becomes dominant this aspect cannot be observed anymore.

The difference between the values of the compounds containing different cadmium content can be explained on the one hand by phonon-electron scattering and on the other hand by interaction between phonons and crystal defects and boundaries. A larger cadmium content leads to higher charge carrier concentration that increases the probability for scattering of phonons by electrons. Thus, at medium temperatures, the thermal conductivity of the Cd_8- and Cd_6-compounds is lower than that of the Cd_4- and Cd_2-compounds. In contrast, the larger amount of vacancies inside the Cd_4- and Cd_2-compounds lead to more scattering processes of phonons on crystal defects than for the compounds with larger cadmium content. Thus, in the low temperature
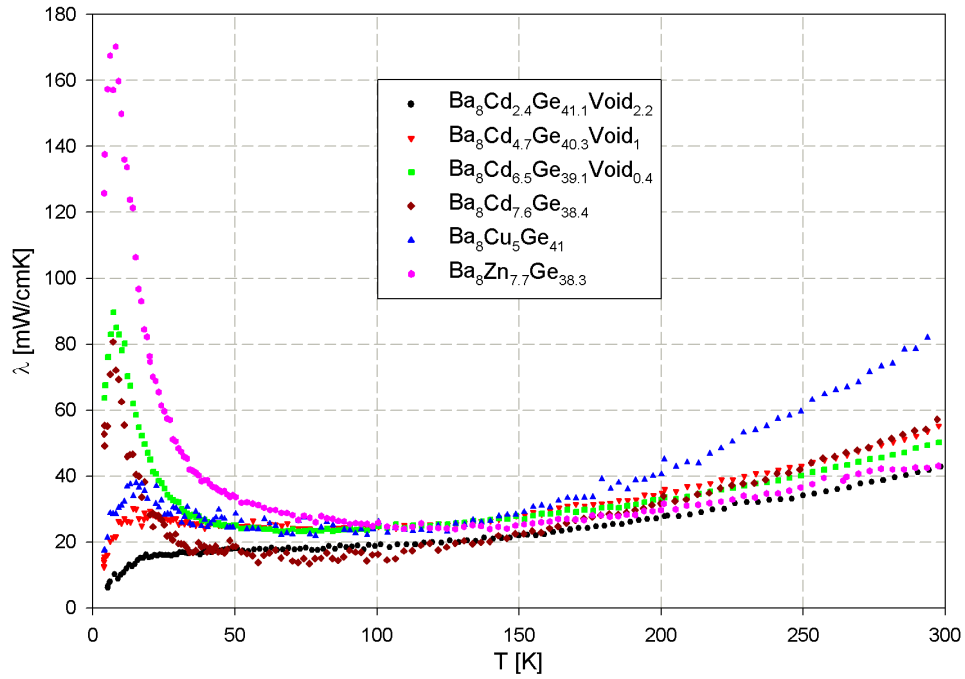
Figure 4.7: Overview on the thermal conductivity measurements of all compounds. The values increase rapidly at lowest temperatures governed by boundary- and point defect scattering. As the temperature increases Umklapp-processes become dominant leading to strong reductions of the thermal conductivity. At around 50 K the electron based conduction shows stronger influence for the compounds with larger Cd-content (x = 6.5 and 7.6). The rise of the values above 100 K is not due to λ_e but because of the measurement errors due to radiation losses.

range where the lattice contribution dominates, the thermal conductivity increases with increasing cadmium content.

Since it is difficult to separate the lattice and the electronic contribution, λ_l and λ_e the *Wiedemann-Franz law* is used in order to analyse the measured data. Thus, λ_l is calculated by

$$\lambda_l = \lambda - \lambda_e, \tag{4.8}$$

where the latter one is given by the Wiedemann-Franz law:

$$\lambda_e = \frac{L_0 T}{\rho}. \tag{4.9}$$

$L_0 = \frac{1}{3}\left(\frac{\pi k_B}{e}\right) = 2.45 \times 10^{-8} \ W\Omega K^{-2}$ is the *Lorenz number*. Figure 4.9 displays lattice and electronic contribution of all compounds.

As explained above radiation losses at elevated temperatures lead to an error of the measurement data. Since inner shielding and sample are not at the same temperature heat is lost due to radiation between the two measurement points. If T_S and A are temperature and surface of the sample, respetively, and T_0 is the temperature of the inner shielding the heat loss due to radiation is given by the *Stefan Boltzmann law*

$$Q = \varepsilon \sigma_{SB} A (T_S^4 - T_0^4)$$

In a first approximation this equation can be transformed to

$$Q = 2\varepsilon \sigma_{SB} A T_S^3 \Delta T_S$$

which explains why radiation effects show a T^3-dependence of $\lambda(T)$ at elevated temperatures. ε is the emission coefficient of the sample and $\sigma_{SB} = 5.67 \times 10^{-8} \ Wm^{-2}K^{-4}$ is the Stefan-Boltzmann constant. In order to get rid of these losses one has to subtract a T^3-term from the measurement data. The corrected values for thermal conductivity are plotted in Figure 4.8 while Figure 4.7 shows the values as they were measured. Thus, analyses of each sample contain the measurement data and the separation in an electronic as well as a lattice part based on the Wiedemann-Franz law. Furthermore, one curve fit of the lattice contribution using the Callaway model including the correction due to radiation losses and one fit of the electronic contribution using the Wilson equation were carried out. The least square fits were performed in *Table Curve 2D 5.01* using *user defined functions*. For more details see Chapter D.2 in the Appendix.
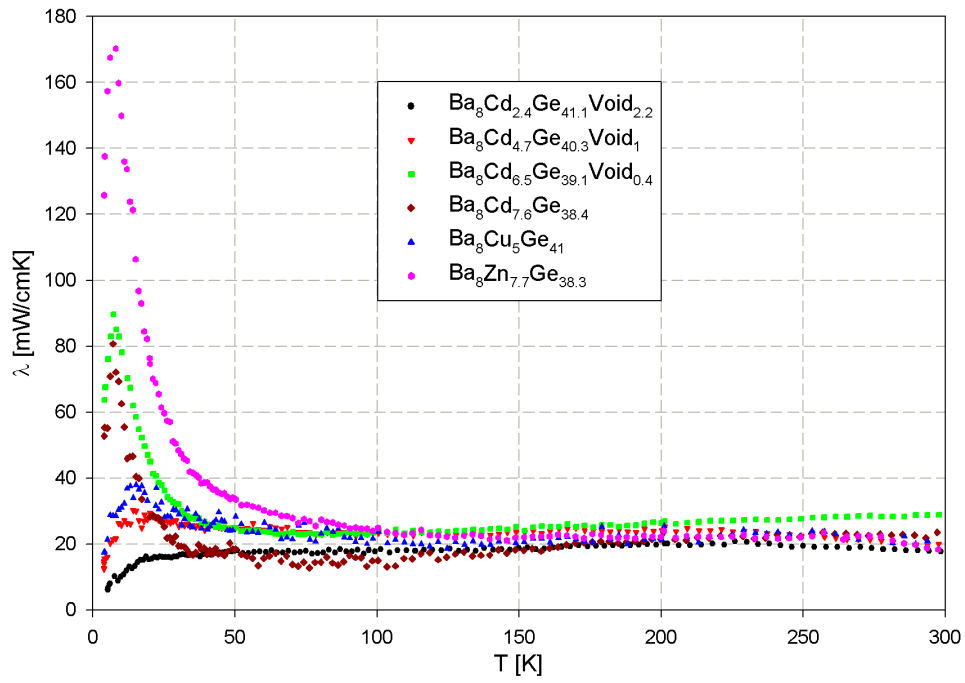
Figure 4.8: Overview on the thermal conductivity measurements of all compounds. In contrast to Figure 4.7 the values are corrected for radiation losses.
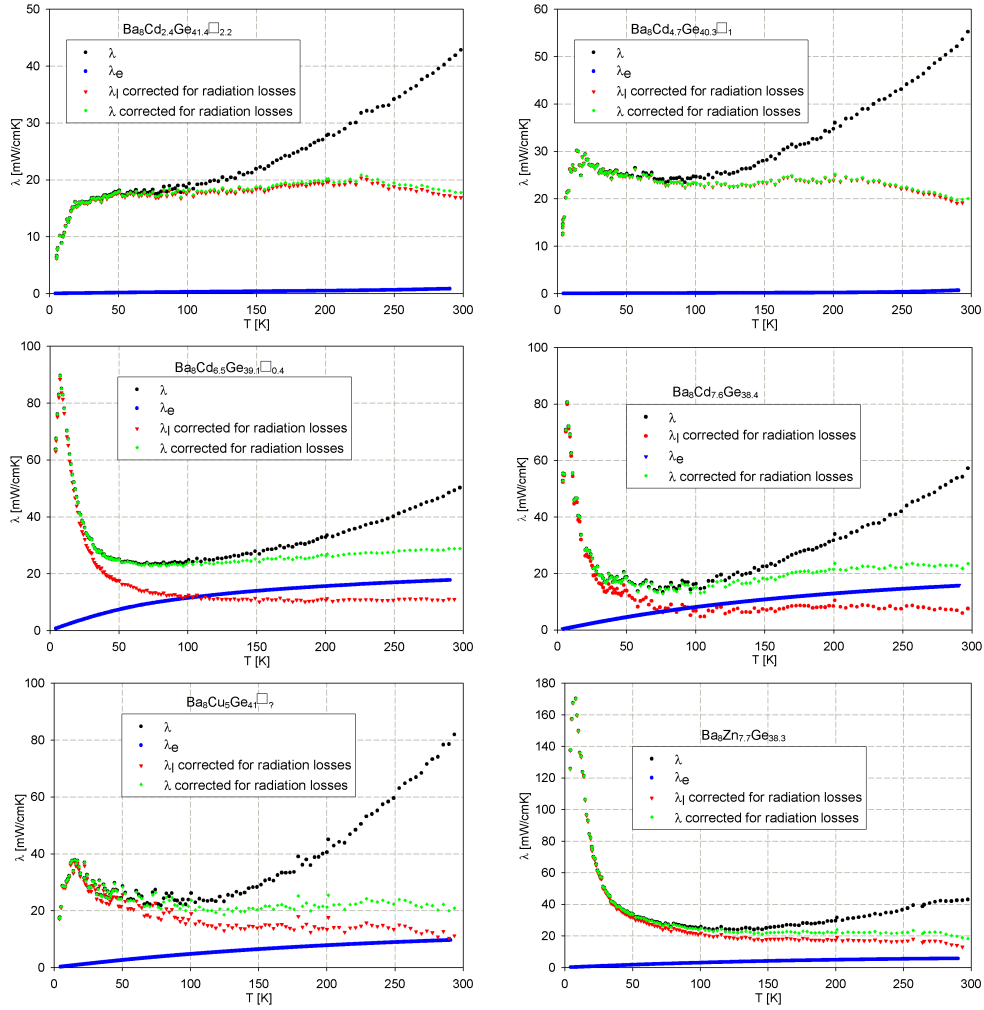
Figure 4.9: Lattice and electronic contribution to thermal conductivity of all compounds. The correction for radiation losses are based on the considerations explained in Section 4.3.1. Their calculation was carried out by least square fits using the Callaway model.

4.3.2   Fits and Analysis of the Lattice Contribution to Thermal Conductivity

Analyses and fits of the lattice thermal conductivity can be performed using *Callaway's model* (Section 2.1.5):

$$\lambda_l = G\frac{T^3}{\theta_D}\int_0^{\frac{\theta_D}{T}}\tau_l\frac{x^4e^x}{\left(e^x-1\right)^2}dx + FT^3 \tag{4.10}$$

FT^3 is the temperature dependent correction due to radiation losses and τ_l is the total relaxation time derived by

$$\frac{1}{\tau_l} = \frac{1}{\tau_{l,0}} + \frac{1}{\tau_U} + \frac{1}{\tau_{l,e}} + \frac{1}{\tau_{l,b}}. \tag{4.11}$$

τ_U represents the relaxation time due to Umklapp-processes and $\tau_{l,0}$, $\tau_{l,e}$ as well as $\tau_{l,b}$ stand for phonon-defect, phonon-electron and phonon-boundary interaction processes, respectively. These contributions are calculated by

$$\frac{1}{\tau_{l,0}} = Dx^4T^4, \tag{4.12}$$

$$\frac{1}{\tau_U} = AT^3x^2e^{\frac{-\theta_D}{aT}}, \tag{4.13}$$

$$\frac{1}{\tau_{l,e}} = CTx \qquad \text{and} \tag{4.14}$$

$$\frac{1}{\tau_{l,b}} = B \tag{4.15}$$

$$\tag{4.16}$$

where $x = \frac{\hbar\omega}{k_BT}$. The pre-factors A, B, C and D, the Debye temperature θ_D, the exponent a in equation (4.14) and F are used as fit parameters while G is calculated from the sample data (see Table 4.1) based on equation

$$G = \frac{k_B^3(6\pi^2n)^{\frac{1}{3}}}{2\pi^2\hbar^2} \tag{4.17}$$

In order to simplify this fit Normal-processes are neglected. The corresponding values of all samples are listed in Table 4.3. Measurement data (resulting from the split due to Wiedemann-Franz law) and fit curves are displayed in figure 4.11 while figure 4.10 compares the lattice thermal conductivity of all compounds.

Table 4.3 shows the influence of each parameter and, therefore, of each physical process of the lattice contribution to thermal conductivity. For example parameter B represents the probability for Umklapp-processes that
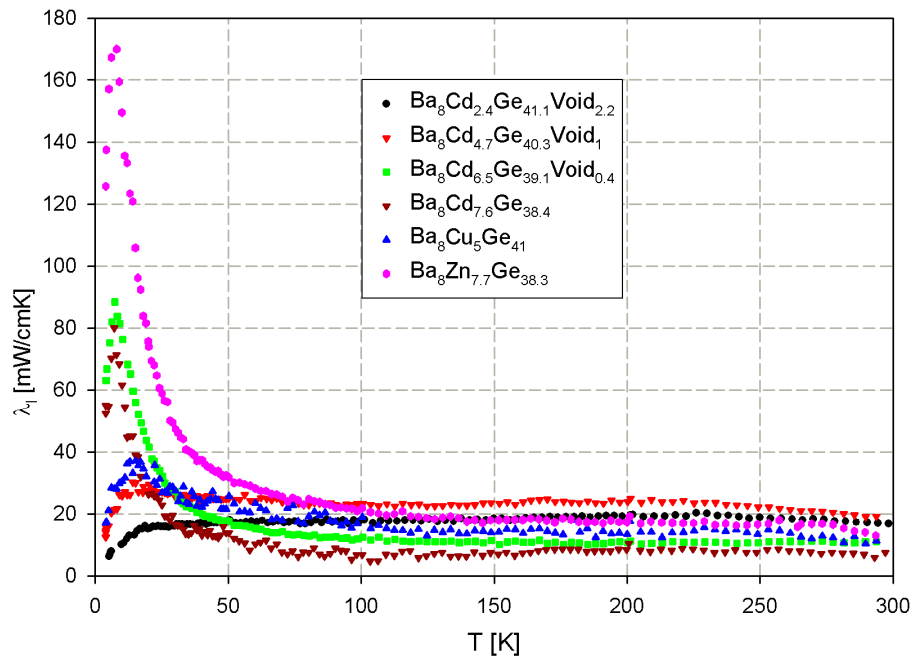
Figure 4.10: Comparison of lattice thermal conductivity of all samples. At lowest temperatures the compositions containing less unoccupied points in the crystal ($Zn_{7.7}$, $Cd_{7.6}$ and $Cd_{6.5}$) have larger values for λ_l than such with more unoccupied sites due to scattering processes of phonons on crystal defects. These data are corrected for radiation losses.
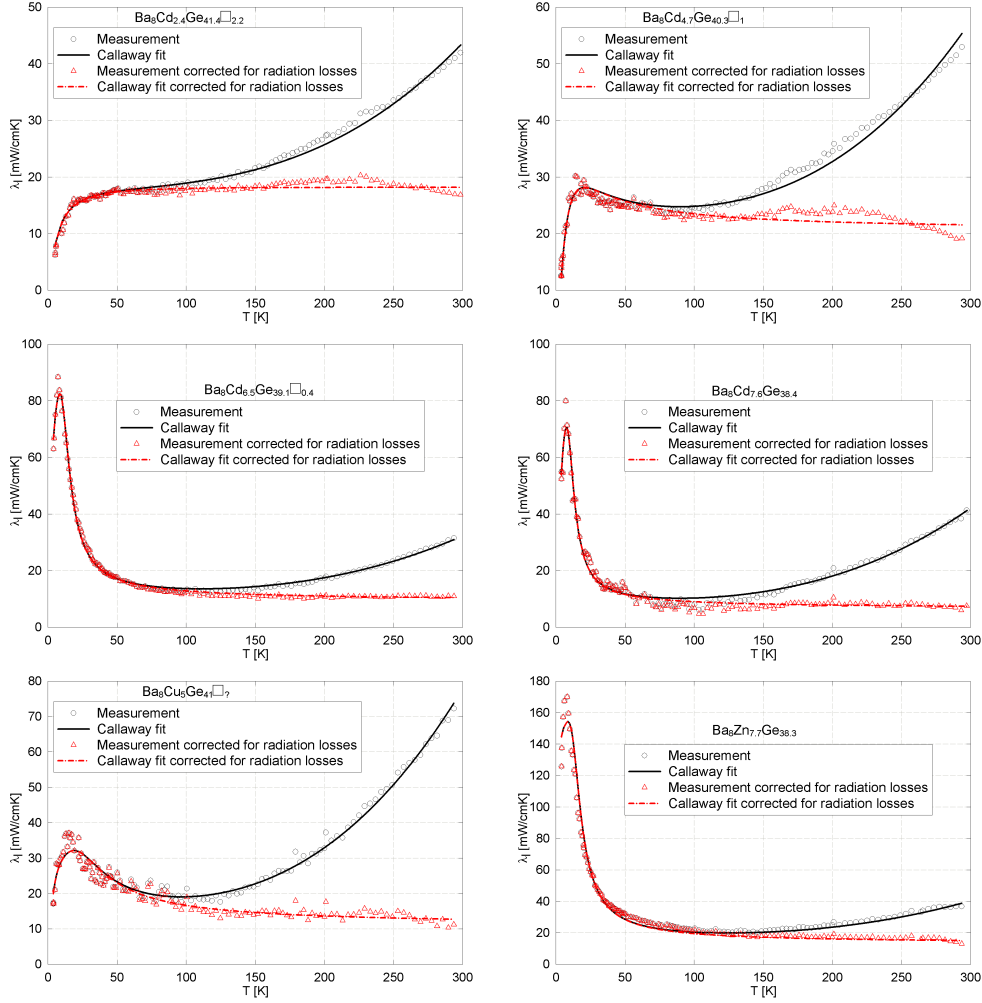
Figure 4.11: Measurement data and fit curves of the lattice contribution to thermal conductivity including the correction for radiation losses. Fit parameters are summarised in Table 4.3.

	A [1/K^{4}s]	B [1/K^{3}s]	C [1/s]	D [1/Ks]
Ba$_8$Cd$_{2.4}$Ge$_{41.1}\square_{2.2}$	149300	5467	987.90E6	87.66E6
Ba$_8$Cd$_{4.7}$Ge$_{40.3}\square_1$	99841	46.78E6	591.25E6	78.18E6
Ba$_8$Cd$_{6.5}$Ge$_{39.1}\square_{0.4}$	57799	79.79E6	16.42E6	11414
Ba$_8$Cd$_{7.6}$Ge$_{38.4}$	49481	393.28E6	39.32E6	1.40E6
Ba$_8$Cu$_5$Ge$_{41}$	91923	52.94E6	59.62E6	4.42E6
Ba$_8$Zn$_{7.7}$Ge$_{38.3}$	91577	36.94E6	146329	29993

	θ_D [K]	$\#F$ [mW/cmK^4]	a	G [mW/cmK^{3}s]
Ba$_8$Cd$_{2.4}$Ge$_{41.1}\square_{2.2}$	189	9.4420E-7	3.0	5.08726E9
Ba$_8$Cd$_{4.7}$Ge$_{40.3}\square_1$	130	1.3338E-6	3.0	5.07978E9
Ba$_8$Cd$_{6.5}$Ge$_{39.1}\square_{0.4}$	224	8.1071E-7	3.5	5.07113E9
Ba$_8$Cd$_{7.6}$Ge$_{38.4}$	200	1.2865E-6	3.5	5.06361E9
Ba$_8$Cu$_5$Ge$_{41}$	300	2.4123E-6	3.0	5.07978E9
Ba$_8$Zn$_{7.7}$Ge$_{38.3}$	321	9.3695E-7	4.0	5.15316E9

Table 4.3: List of fit parameters used for least square fits for the lattice contribution to thermal conductivity measurements.

increases the more cadmium atoms a unit cell contains. Since Umklapp-processes become dominant as the temperature increases above 20 K the influence of other parameters decreases as the values show. Because the added cadmium atoms replace the vacancies in the crystal lattice scattering of phonons on crystal defects such as unoccupied places become less important. Parameter A denotes for phonon scattering on defects. Thus, it decreases with increasing cadmium content. Electron-phonon scattering processes are represented by the parameter D. Since the probability for this kind of interaction increases with increasing electron concentration, the value of D is larger for the compounds containing less cadmium. Parameter C gives an idea, how the grain size changes as the cadmium content increases.

The values of the Debye temperature do not correspond to those calculated by the fit for electrical resistivity because θ_D is temperature dependent. For the Callaway-fit the low temperature range is more important. Thus θ_D was optimised in this range in order to improve the quality of the fit. However, the fits based on the Bloch-Grüneisen model were optimised for higher temperatures (up to 300 K). Consequently, the Debye temperature resulting from the lattice thermal conductivity fits is lower than that resulting from the fits for electrical resistivity.

4.3.3 Fits and Analysis of the Electronic Contribution to Thermal Conductivity
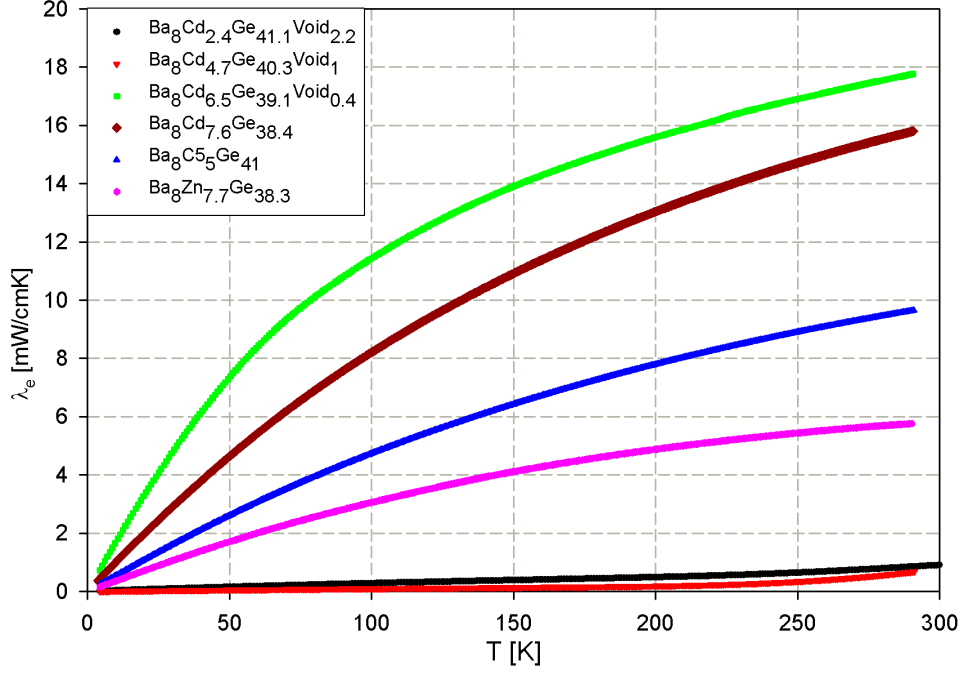
Figure 4.12: Temperature dependence of the electronic contribution to thermal conductivity of all compounds. The values were calculated from electrical resistivity measurements using the Wiedemann-Franz law. Thus, λ_e is nothing else, but a different way to display the electrical resistivity.

The values for the electronic thermal conductivity were derived from the measurements of electrical resistivity using the *Wiedemann-Franz* law. Hence, the values for λ_e of $Ba_8Cd_{2.4}Ge_{41.1}\square_{2.2}$ and $Ba_8Cd_{4.7}Ge_{40.3}\square_1$ are small compared to the other compounds. The overall thermal conductivity of these samples is therefore almost solely determined by the lattice contribution. Figure 4.12 displays the temperature dependence of λ_e of all compounds.

Further analyses were carried out using

$$\frac{1}{\lambda_e} = W_{e,0} + W_{e,ph} \tag{4.18}$$

with (*Wilson equation*)

$$W_{e,ph} = \frac{4R}{L_0 T}\left(\frac{T}{\theta_D}\right)^5\left[\left(1 + \frac{3}{4\pi^2}\left(\frac{\theta_D}{T}\right)\right)J_5(z) - \frac{1}{2\pi^2}J_7(z)\right] \tag{4.19}$$

	θ_D [K]	α [cmK^2/mW]	$4R/L_0$ [cmK^2/mW]	R [$\mu\Omega$cm]
$\mathrm{Ba_8Cd_{2.4}Ge_{41.1}\square_{2.2}}$	190	303.83	447.83	2743
$\mathrm{Ba_8Cd_{4.7}Ge_{40.3}\square_1}$	140	863.33	783.62	4799
$\mathrm{Ba_8Cd_{6.5}Ge_{39.1}\square_{0.4}}$	305	5.54	45.47	278
$\mathrm{Ba_8Cd_{7.6}Ge_{38.4}}$	260	9.48	31.49	192
$\mathrm{Ba_8Cu_5Ge_{41}}$	380	17.57	65.56	401
$\mathrm{Ba_8Zn_{7.7}Ge_{38.3}}$	465	26	151.51	928

Table 4.4: List of fit parameters used for least square fits for the electronic contribution to thermal conductivity. Since the values for λ_e are based on that of the electrical resistivity the values of the fit parameters are associated with that of table 4.2.

and

$$W_{e,0} = \frac{\alpha}{T} \tag{4.20}$$

to fit the measurement curves. The Debye temperature θ_D, the factor α in equation (4.20) and the pre-factor $4R/L_0$ in Wilson's equation were used as fit parameters. Because the calculation of W_e is based on the electrical resistivity, α is related to ρ_0 via the Lorenz number L_0.

The values for λ_e and the corresponding Fits are plotted in Figure 4.13 while in Table 4.4 the parameters resulting from these fits are listed. Comparing the values for θ_D to that derived in the fit for the lattice thermal conductivity large differences can be observed. As explained for the lattice thermal conductivity θ_D depend on the temperature range the fit is optimised for. Since the calculation of the values for λ_e are based on the corresponding values for electrical resistivity using the Wiedemann-Franz law the values for θ_D listed in Table 4.4 correspond better to that listed in Table 4.2 than with the values calculated for λ_l.

The factor α represent the influence of electron-defect interaction processes to the total thermal resistivity. Because the number of defects decreases with increasing cadmium content $W_{e,0}$ and, thus, the values for α are much larger for $\mathrm{Ba_8Cd_{2.4}Ge_{41.1}\square_{2.2}}$ and $\mathrm{Ba_8Cd_{4.7}Ge_{40.3}\square_1}$ than for the compounds containing more cadmium. Furthermore, also the values of R depend on the cadmium concentration. The values of the electron thermal conductivity are based on the electric resistivity and R has the dimension of ρ. Thus, the change of its values as the cadmium content changes correspond to that of ρ for all compounds.

Based on the fit-curves the electronic contribution to the thermal resistivity as described by (4.18) was split into its parts, namely the resistivity due
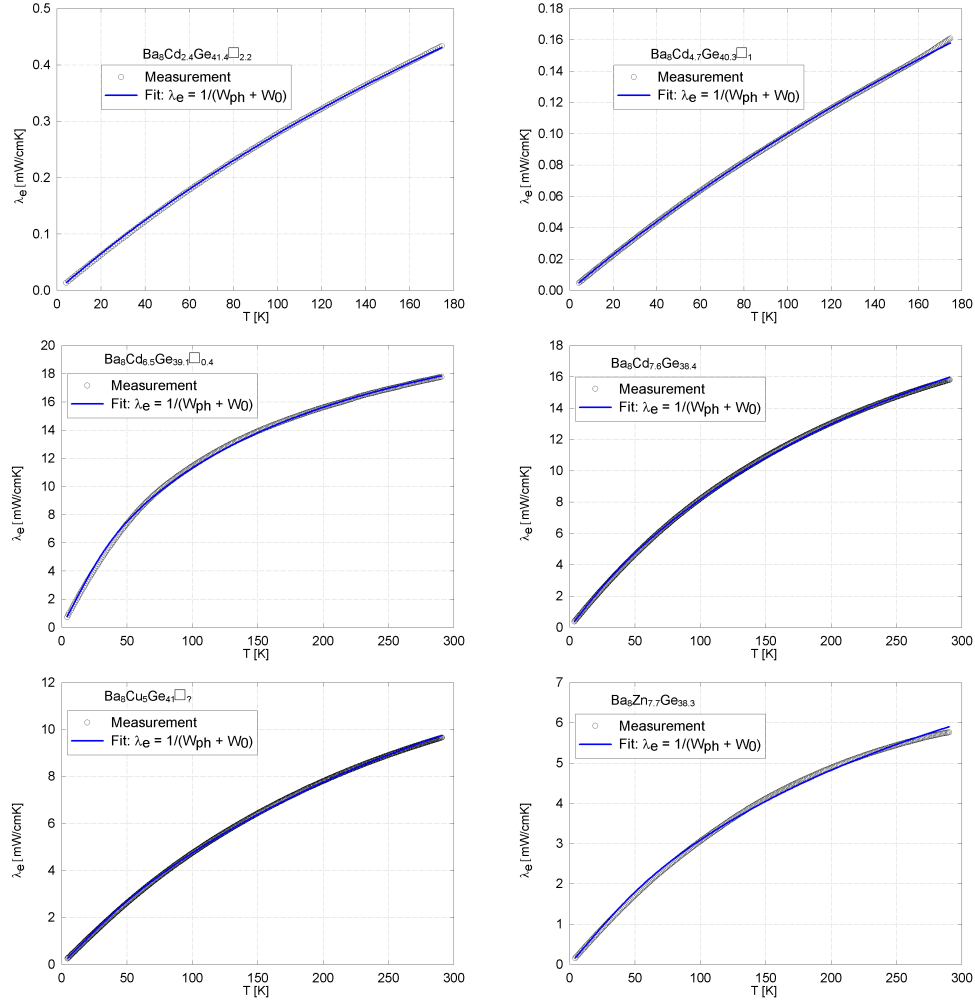
Figure 4.13: Measurement data and fit curves of the electronic contribution to thermal conductivity. The measurement and fit curves for the $Cd_{2.4}$– and $Cd_{4.7}$–sample were abandoned at 180 K since the fit by Wilson's equation requires a metallic temperature dependence. Thus, no fit can be performed as soon as the second derivation of λ_e becomes positive.

to electron-phonon interaction processes as described by the Wilson equation and that because of the crystal defects (see (4.20)). Figure 4.14 and 4.15 compare these contribution for all compounds. Because of the increasing phonon density at elevated temperatures the probability for electron-phonon interaction increases as well as leads to larger values for $W_{e,ph}$. Consequently, the influence of scattering processes of electrons on crystal defects decreases causing lower values for $W_{e,0}$. The reason for the larger $W_{e,0}$-value for $Ba_8Cd_{2.4}Ge_{41.1}\square_{2.2}$ and $Ba_8Cd_{4.7}Ge_{40.3}\square_1$ is their larger number of vacancies compared to the other compounds. The same two compounds offer also larger values for $W_{e,ph}$. However, the number of electrons do not increase the probability of electron-phonon interactions. Thus, the thermal resistivity should be in the same range for all compounds. The reason for this contradiction is situated in the way the electronic thermal conductivity is calculated. As explained in Section 2.1.6 the simplification of using L_0 instead of $L_e(T)$ within the Wiedemann-Franz law is only correct for metals. The electrical resistivity of $Ba_8Cd_{2.4}Ge_{41.1}\square_{2.2}$ and $Ba_8Cd_{4.7}Ge_{40.3}\square_1$ show, however, semiconductor temperature dependence. Thus, their values for λ_e probably do not represent the true values.
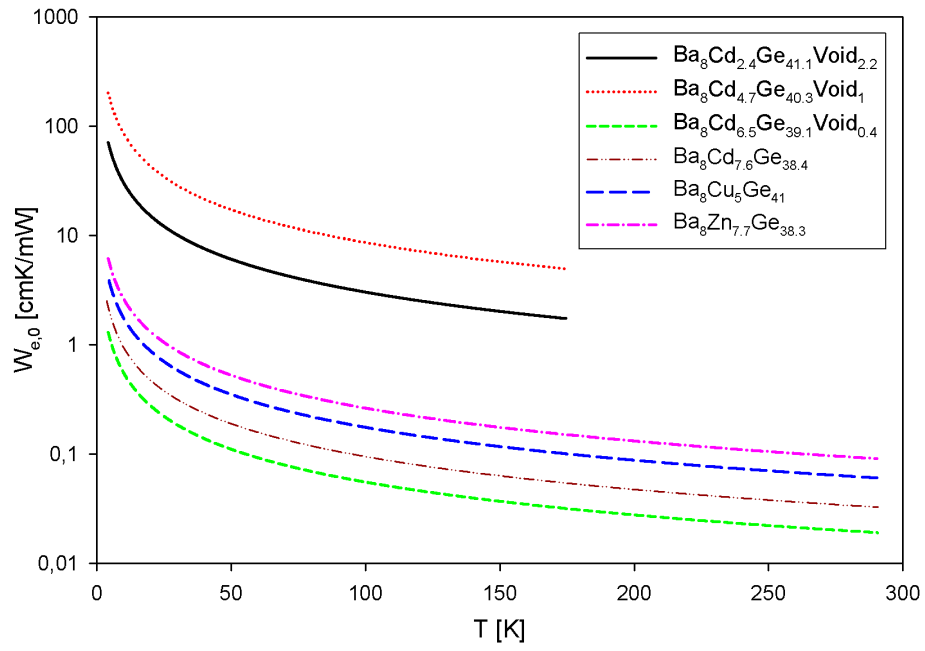
Figure 4.14: Overview on the contribution of electron-crystal defect interaction processes to thermal resistivity of all compounds. For the compounds with lower cadmium content $W_{e,0}$ is much larger than for that with more cadmium atoms per unit cell due to the larger probability for electron-defect scattering.
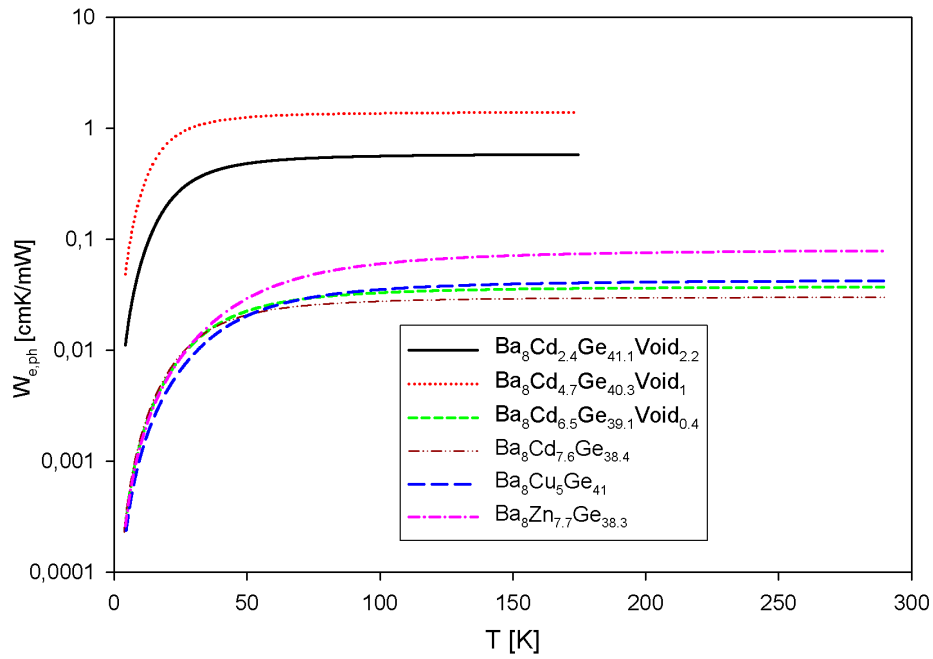
Figure 4.15: Overview on the contribution of electron-phonon interaction processes to thermal resistivity of all compounds. The difference between the λ_e-values of $Ba_8Cd_{2.4}Ge_{41.1}\square_{2.2}$ and $Ba_8Cd_{4.7}Ge_{40.3}\square_1$ do not represent the truth. The reason for this discrepancy is within the way the values for λ_e are calculated. Since $\rho(T)$ of these two samples show semi-conductor behaviour the calculation via the Wiedemann-Franz law (only correct for metallic samples) might lead to wrong results. Nevertheless, in literature the Wiedemann-Franz law is used in most cases.
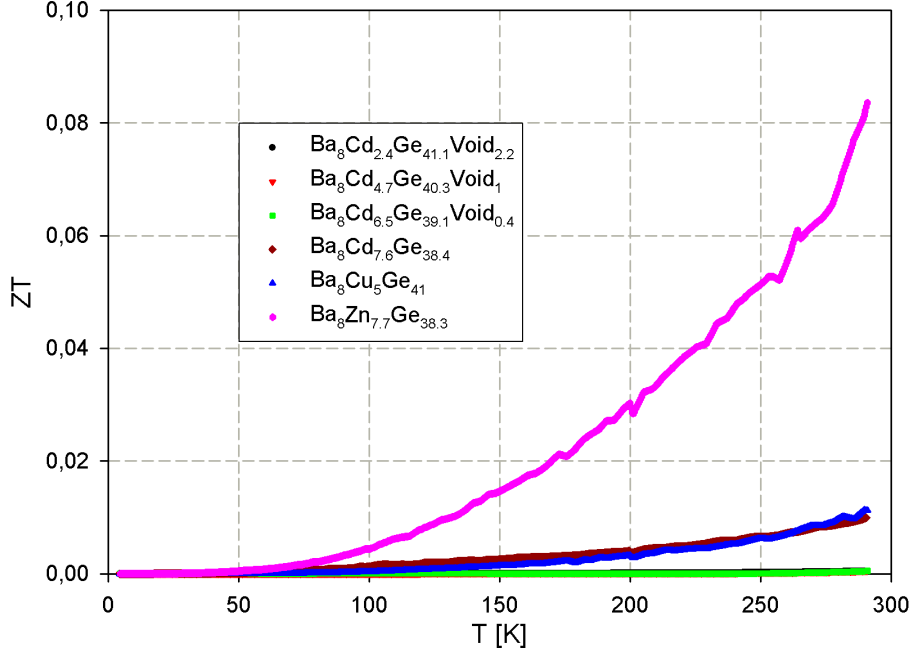
Figure 4.16: Figure of merit of all compounds. The values are calculated using $Z = S^2/\lambda\rho$ where the values for λ are corrected for radiation losses. The most interesting compound for thermoelectric application is $Ba_8Zn_{7.7}Ge_{38.3}$ due to its enhanced values for thermopower.

4.4 Thermoelectric Performance and Figure of Merit

The thermoelectric performance for each material is given by its figure of merit calculated by

$$ZT = \frac{S^2}{\lambda\rho}. \tag{4.21}$$

In Figure 4.16 the temperature dependence of the values for ZT are plotted up to room temperature[2]. Above that no values for λ are available since no bulks of the samples were left for this measurement. However, Figure 4.16 shows clearly the basic temperature dependences. The compound consisting of $Ba_8Zn_{7.7}Ge_{38.3}$ shows excellent values as the temperature increases. This performance is based on outstanding thermopower values of this sample. Furthermore, the Cu_5- and $Cd_{7.6}$-samples show interesting values for thermoelectric applications. The thermoelectric performances of the other

---

[2]For the calculation of ZT values of λ corrected for radiation losses are used.
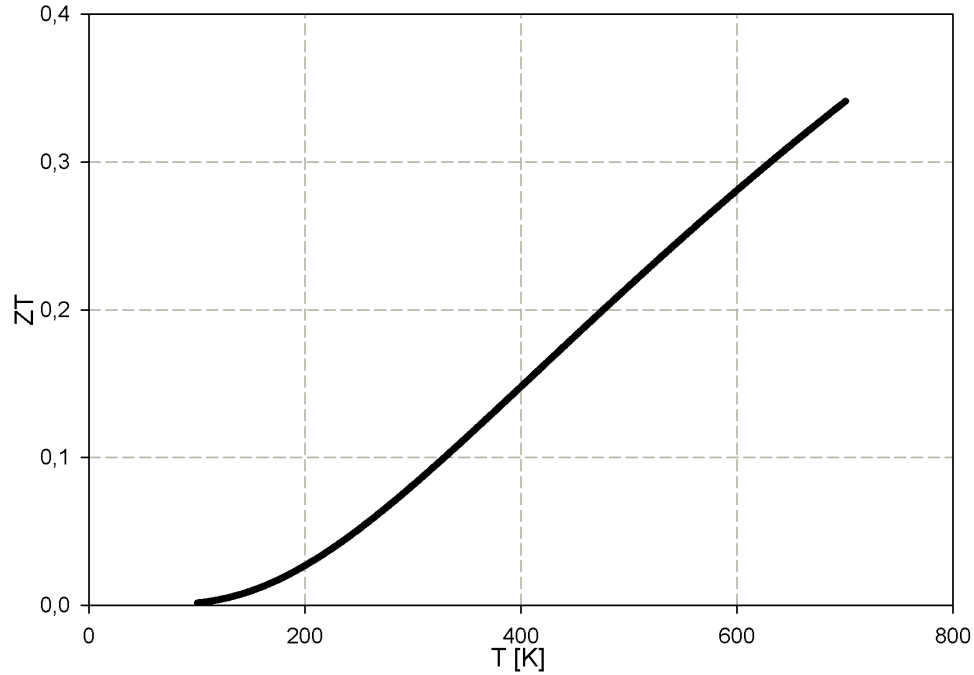
Figure 4.17: Extrapolation of the figure of merit of $Ba_8Zn_{7.7}Ge_{38.3}$ based on a rough least square fit of the data for thermal conductivity. The fit data were then extrapolated up to 700 K.

compounds are too small to be useful. For $Ba_8Cd_{6.5}Ge_{39.1}\square_{0.4}$ the thermopower is too small while for $Ba_8Cd_{2.4}Ge_{41.1}\square_{2.2}$ and $Ba_8Cd_{4.7}Ge_{40.3}\square_1$ it is the large electrical resistivity that is responsible for the small values of ZT.

Within this selection of compounds $Ba_8Zn_{7.7}Ge_{38.3}$ seems to be the most promising composition for thermoelectric applications. Since most applications are used in temperature ranges above 300 K a careful estimation up to 700 K was carried out. For thermal conductivity no data above room temperature are available. Thus, the low temperature data were first fitted by a rough least square fit. Subsequently, these fit data were extrapolated up to 700 K. Finally, the extrapolated data for λ together with the measured data for ρ and S were used to estimate the figure of merit at elevated temperatures for this compound. Figure 4.17 shows the extrapolated values. The estimated value for $ZT(700 \text{ K})$ of the $Zn_{7.7}$-sample is approximately 0.35.

Chapter 5

Conclusion

Based on the parent compound Ba_8Ge_{43} various d-elements such as cadmium, copper and zinc were added in order to investigate clathrates with interesting thermoelectric properties. While the basic crystal structure is made of germanium atoms barium atoms are used as electropositive element to fill up the cages. Cadmium, zinc or copper atoms fill up the voids of this structure and, susequently, replace the germanium atoms. This change of elements and their concentration in clathrates by substitution and doping has a strong influence on their charge carrier concentration and thermoelectric properties. For thermoelectric applications compounds with large zinc content turned out to be the most interesting ones. The figure of merit ZT for $Ba_8Zn_{7.7}Ge_{38.3}$ is derived as 0.09 at 300 K and extrapolated to 0.35 at 700 K. Furthermore, $Ba_8Cd_{7.6}Ge_{38.4}$ and $Ba_8Cu_5Ge_{41}$ show interesting behaviour at elevated temperatures. However, their figure of merit is much lower than for the $Zn_{7.7}$-compound. The ZT-values for the other compounds are much too low to be of any interest.

In addition to the change of the thermoelectric performance, a metal-to-insulator transition can be observed as the cadmium content increases. Compounds containing a lower number of cadmium atoms ($Cd_{2.4}$ and $Cd_{4.7}$) show semiconductor temperature dependence concerning their electrical resistivity whereas the $Cd_{6.5}$ and $Cd_{7.6}$-compounds show metallic behaviour.

Further analyses were carried out using theoretical models to fit the measurement data. For the samples with semiconductor behaviour in their electrical resistivity a model was developed including a gap of rectangular shape in the density of states right above the Fermi energy [18]. Measurements of compounds with metallic temperature dependence were fitted using the Bloch-Grüneisen equation. The lattice contribution to thermal conductivity is fitted by the Callaway-model while for the electronic contribution the Wilson-model is used. The parameters calculated by these fits show how the

change of the elements and their concentrations influence the charge carrier concentration and therefore the thermoelectric properties.

For further study of this topic fine-tuning of the charge carrier concentration based on substitution and doping needs to be carried out.

Appendix A

Measurement Results - Detailed View

In this section the data as they were measured are displayed without any fits or corrections. Only the curves of the figure of merit are based on calculations.

	ρ [$\mu\Omega$cm]	λ [mW/cmK]	S [μV/cmK]	ZT
$Ba_8Cd_{2.4}Ge_{41.1}\square_{2.2}$	8400	41	-15.3	4.5E-4
$Ba_8Cd_{4.7}Ge_{40.3}\square_1$	10700	52	-18.4	4.6E-4
$Ba_8Cd_{6.5}Ge_{39.1}\square_{0.4}$	400	49	-4.3	4.7E-4
$Ba_8Cd_{7.6}Ge_{38.4}$	450	54	-18.5	9.8E-3
$Ba_8Cu_5Ge_{41}$	740	79	-24.0	11.3E-3
$Ba_8Zn_{7.7}Ge_{38.3}$	1230	42	-82.8	82.0E-3

Table A.1: Values of the transport coefficients for electrical resistivity, thermal conductivity, thermopower and figure of merit at room temperature for all compounds.

A.1   Resistivity
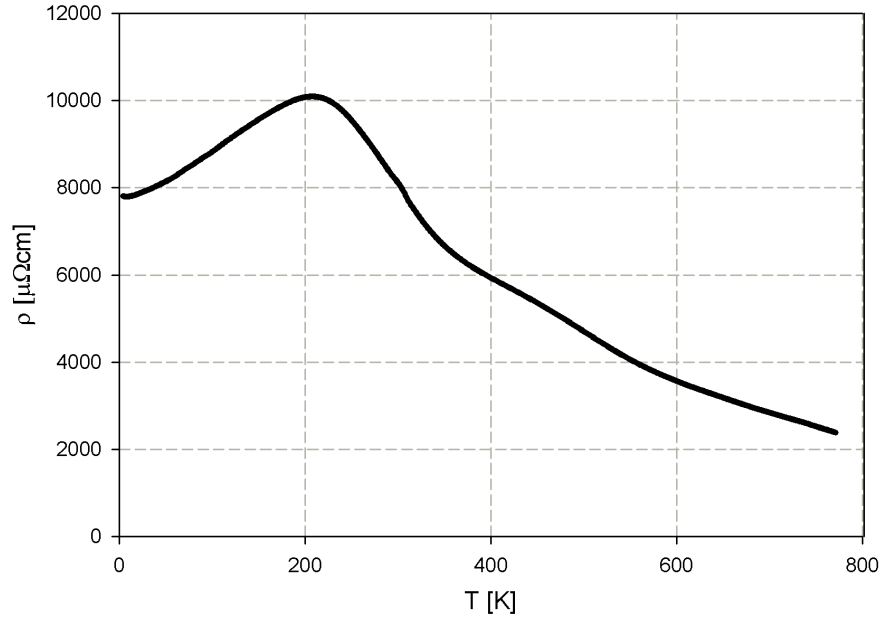
Figure A.1: Resistivity of $Ba_8Cd_{2.4}Ge_{41.1}\square_{2.2}$
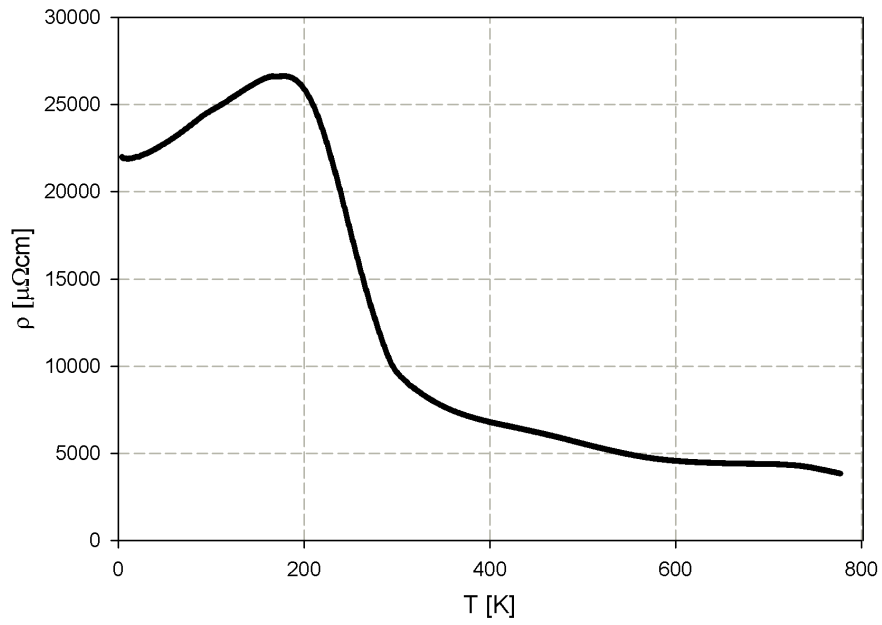
Figure A.2: Resistivity of $Ba_8Cd_{4.7}Ge_{40.3}\square_1$
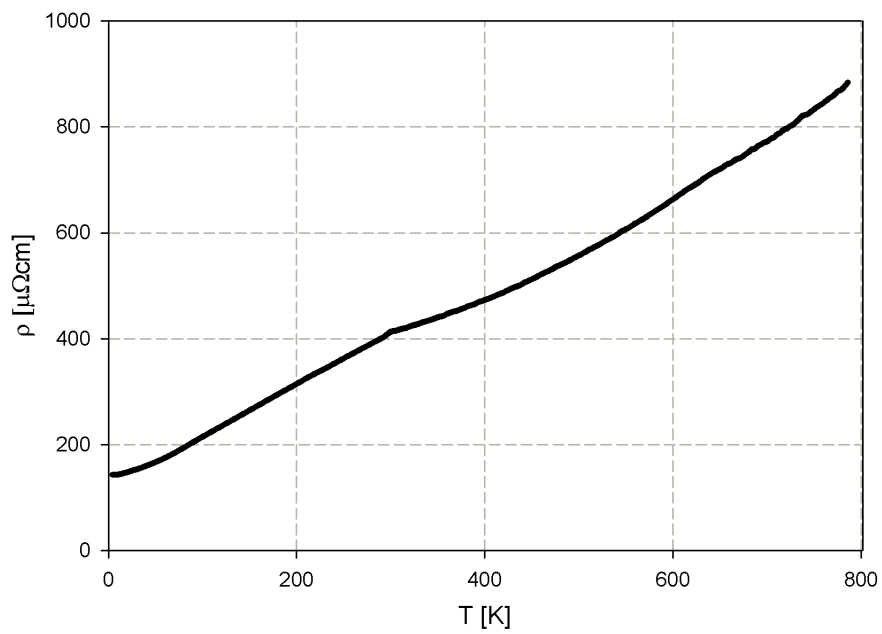
Figure A.3: Resistivity of $Ba_8Cd_{6.5}Ge_{39.1}\square_{0.4}$
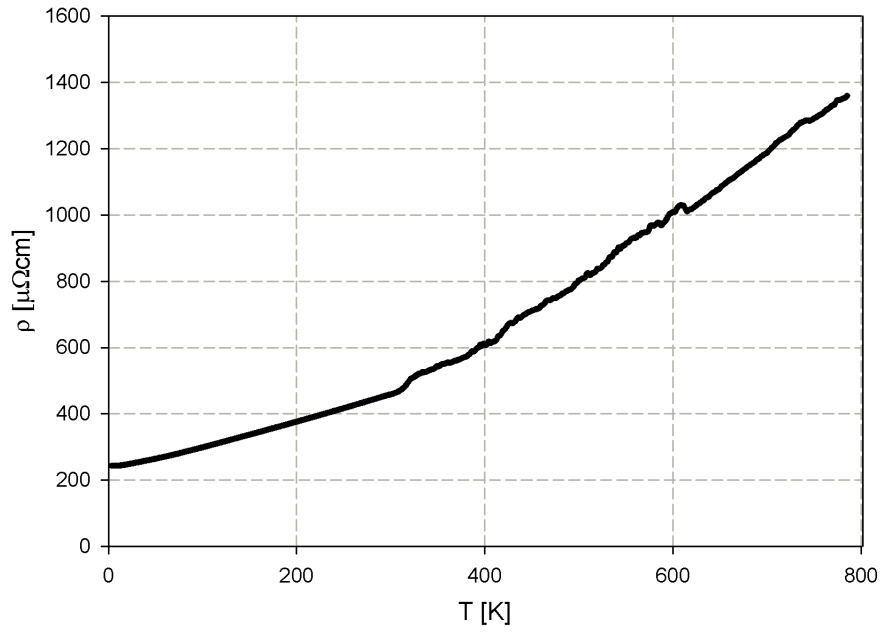
Figure A.4: Resistivity of $Ba_8Cd_{7.6}Ge_{38.4}$
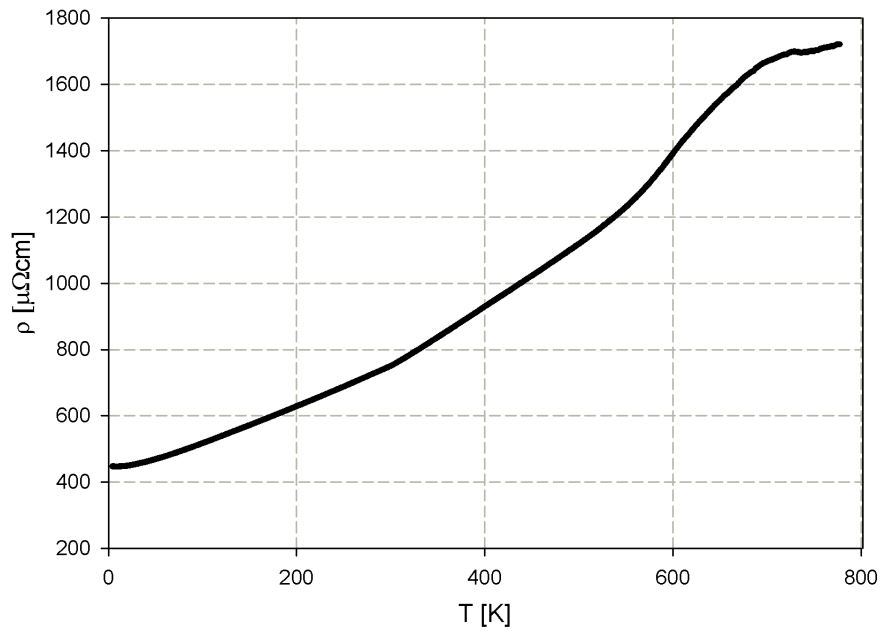
Figure A.5: Resistivity of $Ba_8Cu_5Ge_{41}$
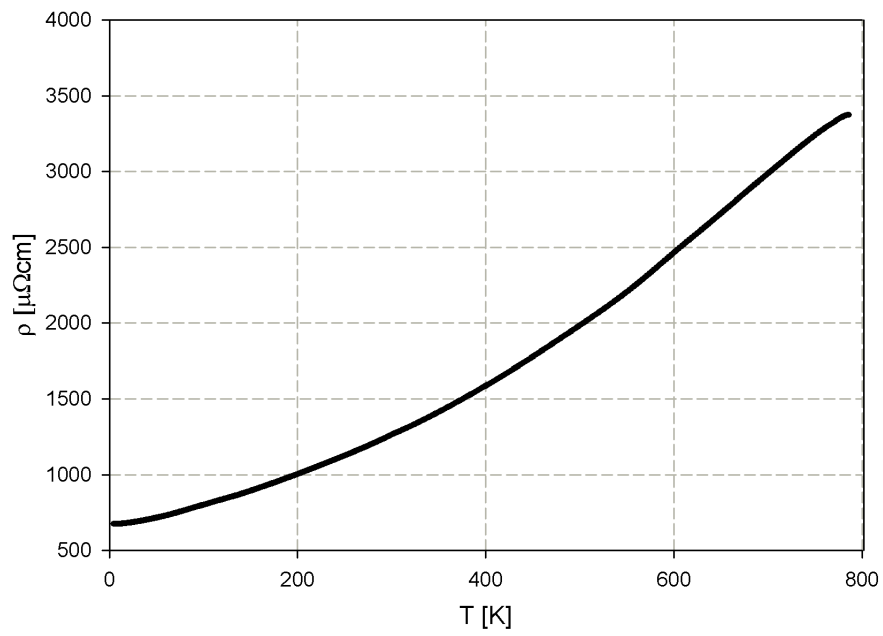
Figure A.6: Resistivity of $Ba_8Zn_{7.7}Ge_{38.3}$

A.2   Thermopower
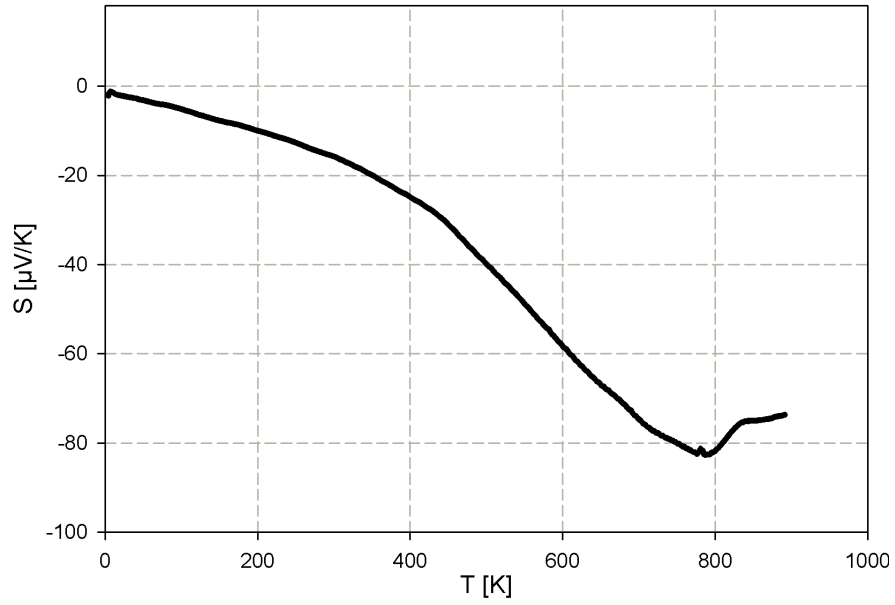
Figure A.7: Thermopower of $Ba_8Cd_{2.4}Ge_{41.1}\square_{2.2}$
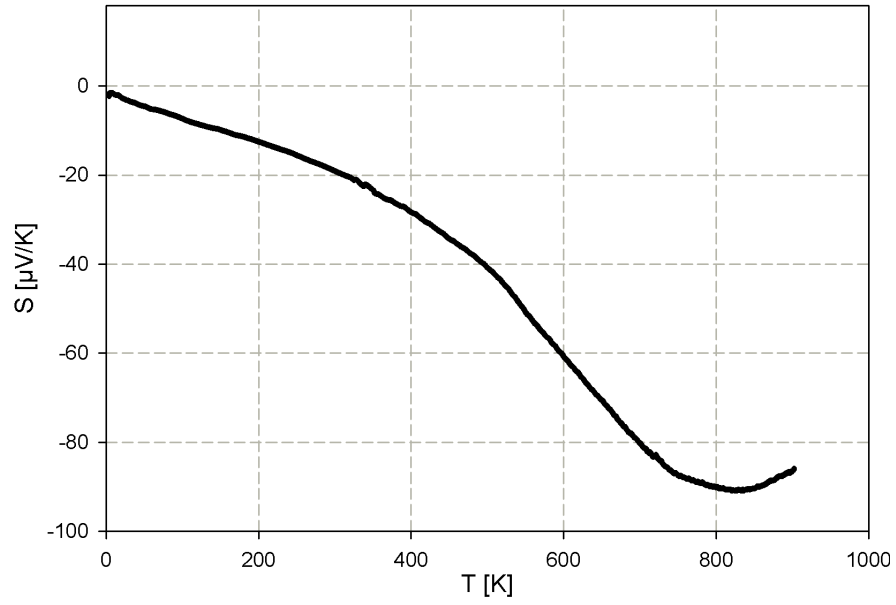
Figure A.8: Thermopower of $Ba_8Cd_{4.7}Ge_{40.3}\square_1$
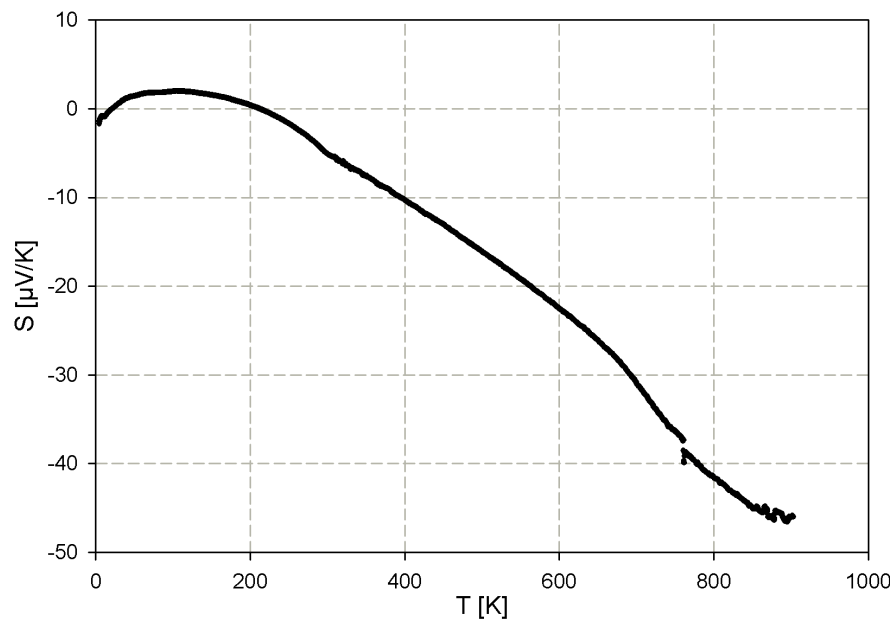
Figure A.9: Thermopower of $Ba_8Cd_{6.5}Ge_{39.1}\square_{0.4}$
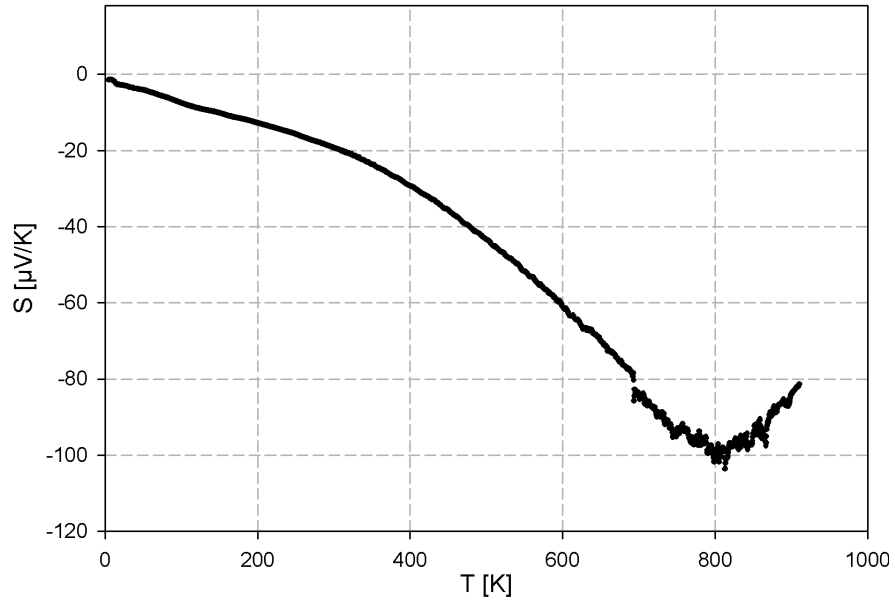
Figure A.10: Thermopower of $Ba_8Cd_{7.6}Ge_{38.4}$
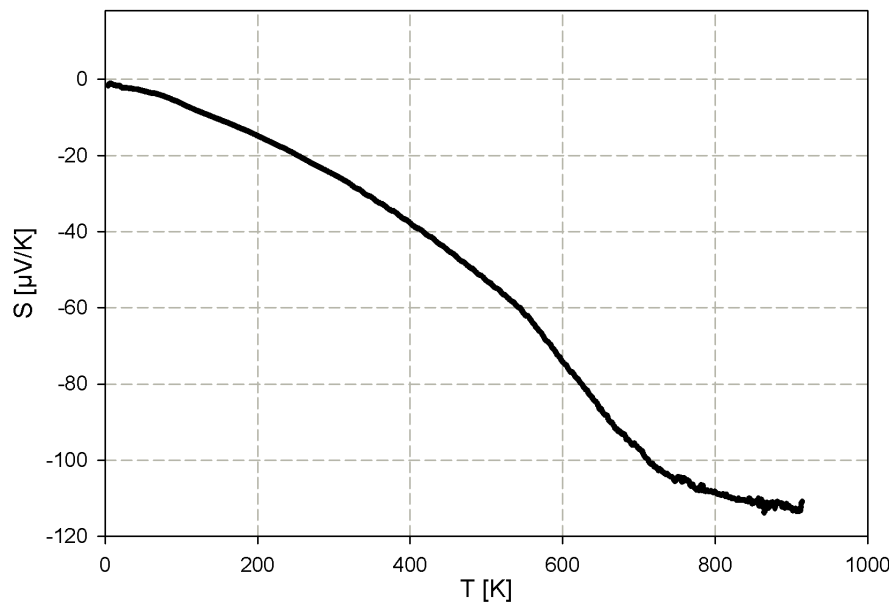
Figure A.11: Thermopower of $Ba_8Cu_5Ge_{41}$
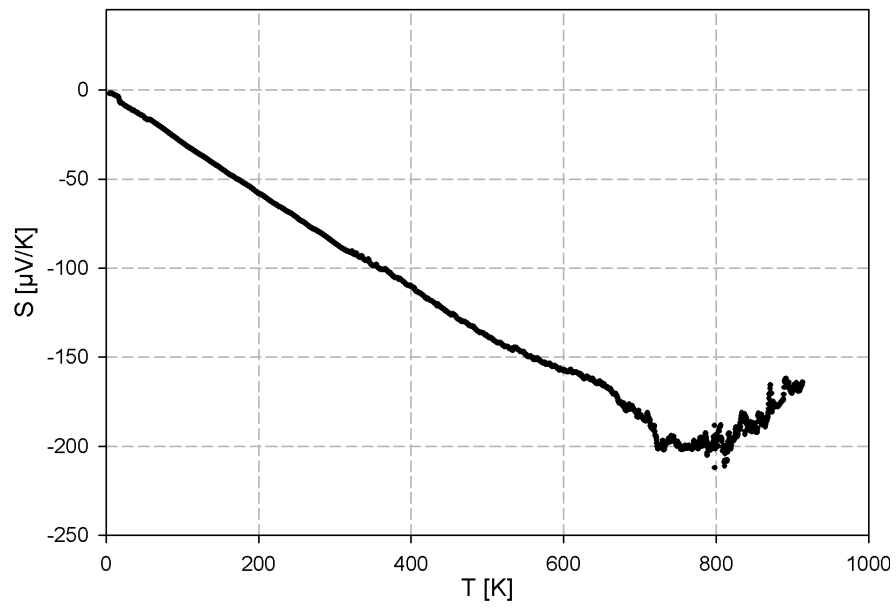
Figure A.12: Thermopower of $Ba_8Zn_{7.7}Ge_{38.3}$

A.3 Thermal Conductivity
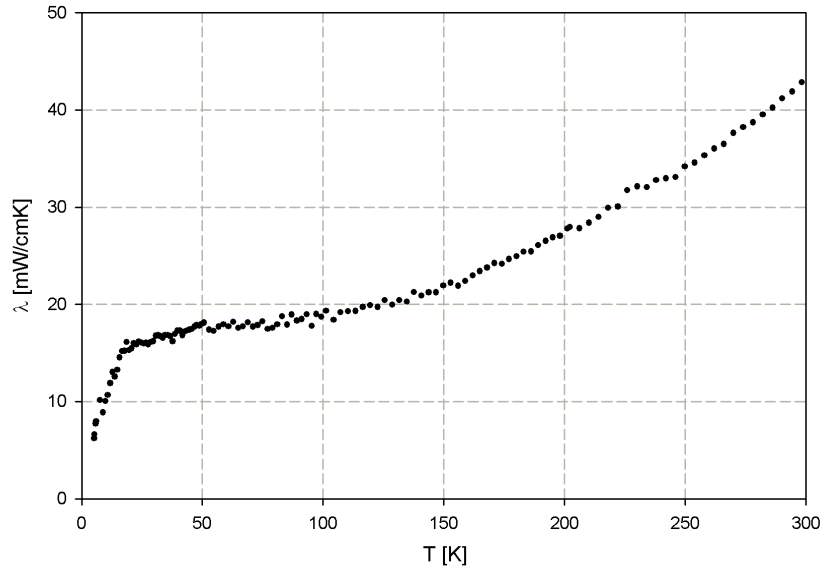
Figure A.13: Thermal conductivity of $Ba_8Cd_{2.4}Ge_{41.1}\square_{2.2}$
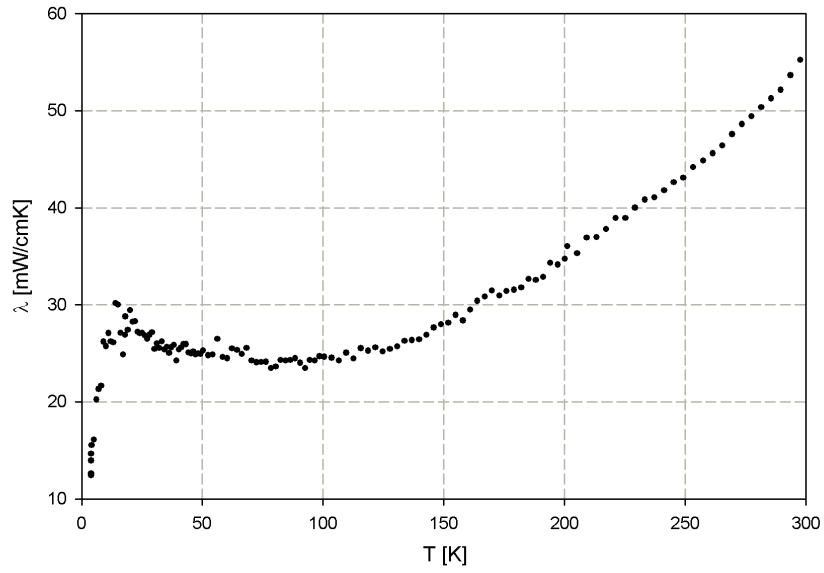
Figure A.14: Thermal conductivity of $Ba_8Cd_{4.7}Ge_{40.3}\square_1$
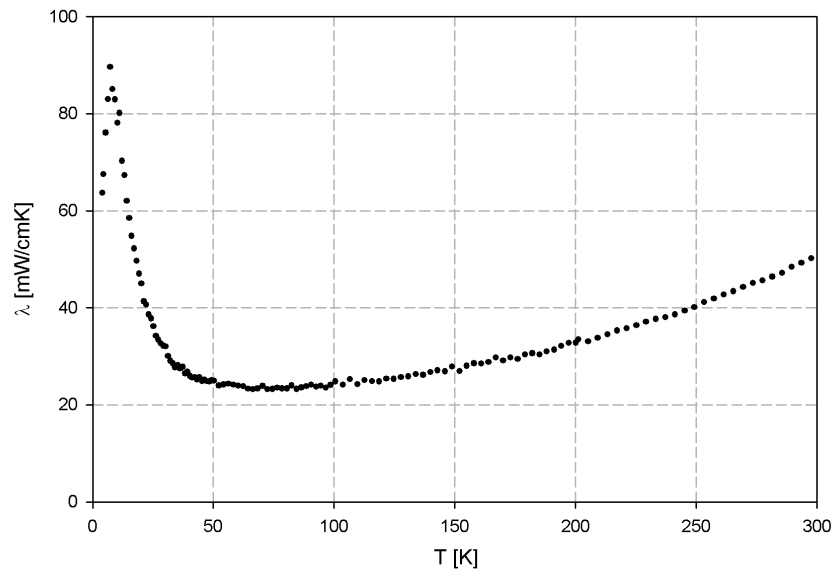
Figure A.15: Thermal conductivity of $Ba_8Cd_{6.5}Ge_{39.1}\square_{0.4}$
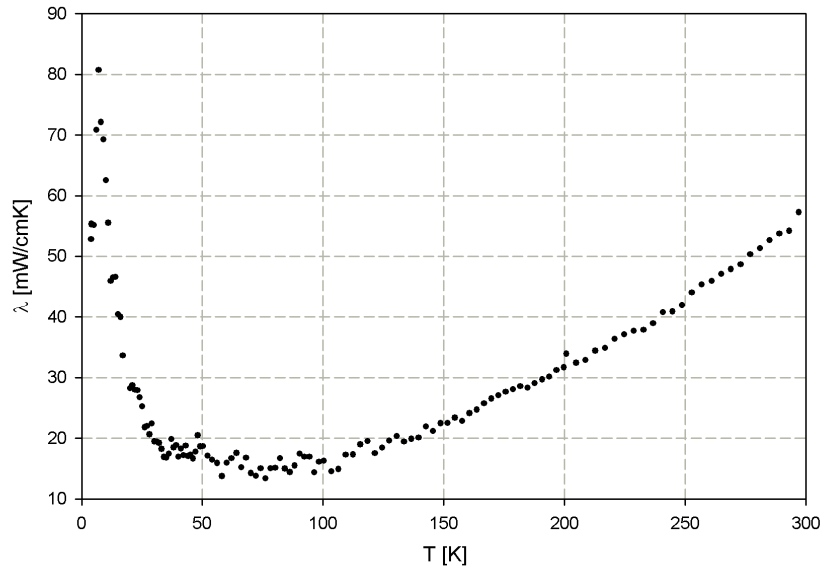
Figure A.16: Thermal conductivity of $Ba_8Cd_{7.6}Ge_{38.4}$
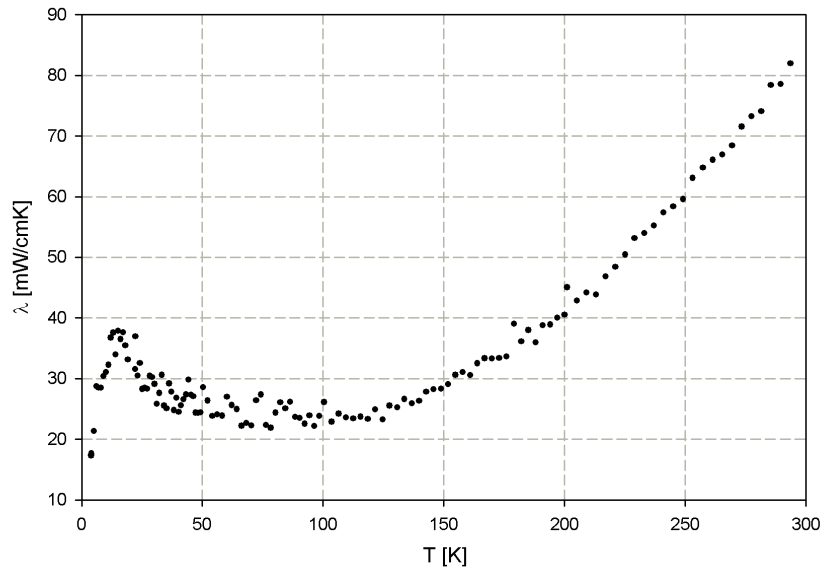
Figure A.17: Thermal conductivity of $Ba_8Cu_5Ge_{41}$
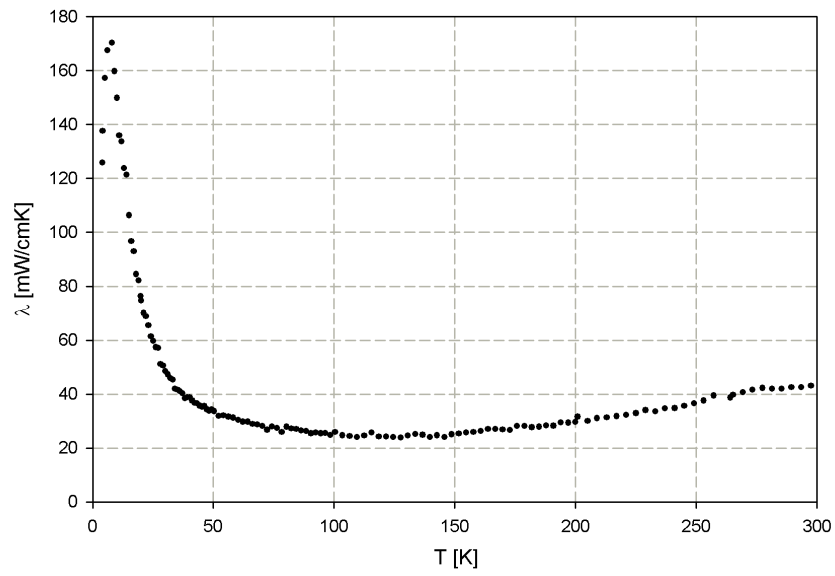
Figure A.18: Thermal conductivity of $Ba_8Zn_{7.7}Ge_{38.3}$

A.4   Figure of Merit
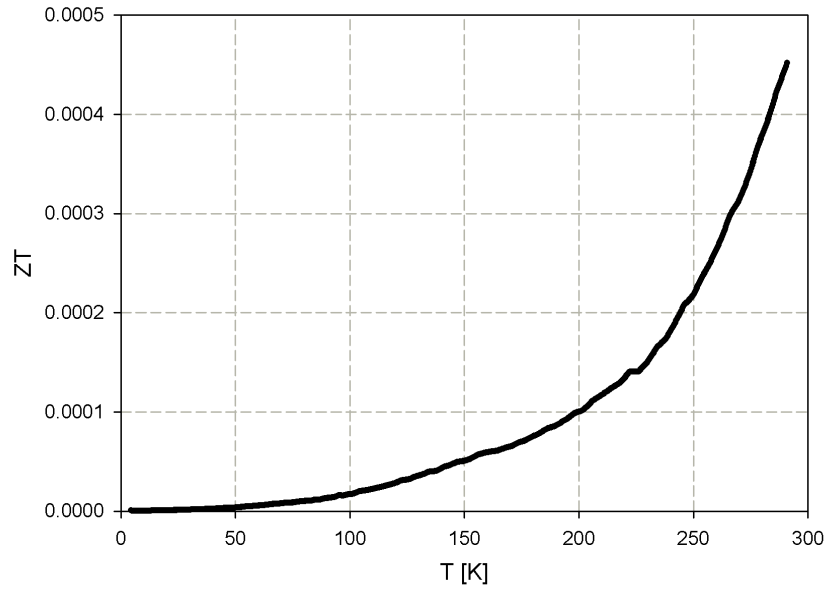
Figure A.19: Figure of Merit of $Ba_8Cd_{2.4}Ge_{41.1}\square_{2.2}$
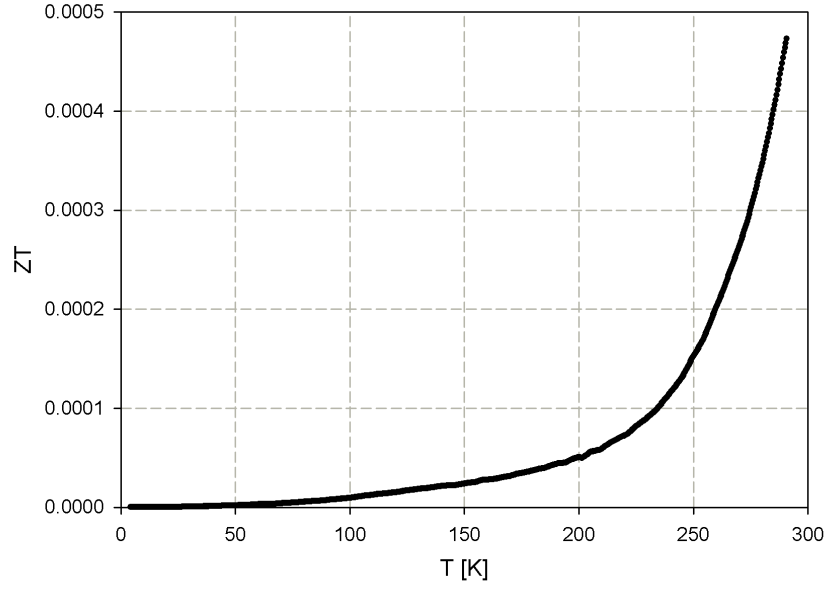
Figure A.20: Figure of Merit of $Ba_8Cd_{4.7}Ge_{40.3}\square_1$
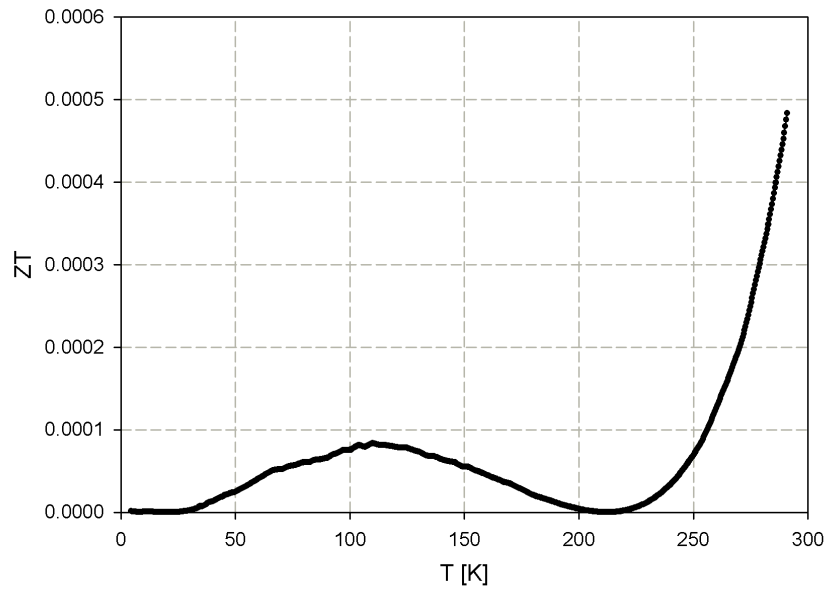
Figure A.21: Figure of Merit of $Ba_8Cd_{6.5}Ge_{39.1}\square_{0.4}$
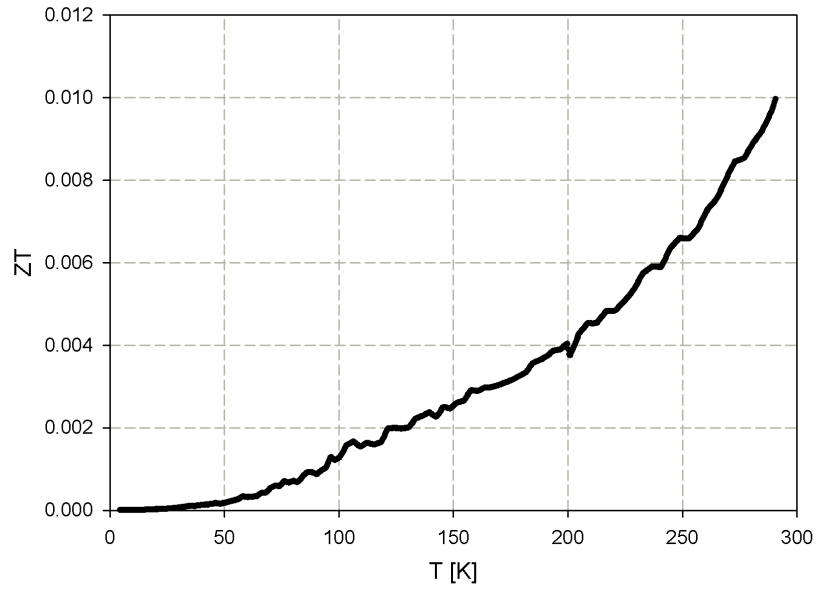
Figure A.22: Figure of Merit of $Ba_8Cd_{7.6}Ge_{38.4}$
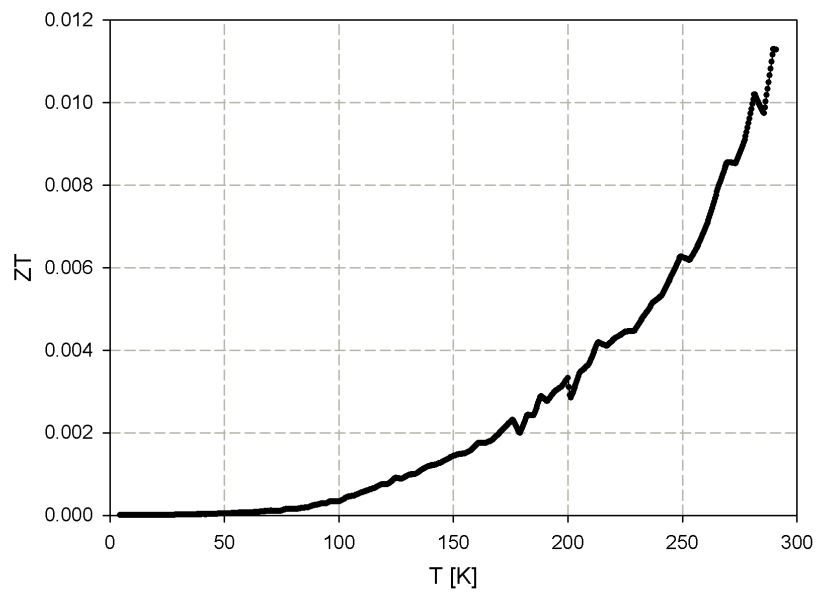
Figure A.23: Figure of Merit of $Ba_8Cu_5Ge_{41}$
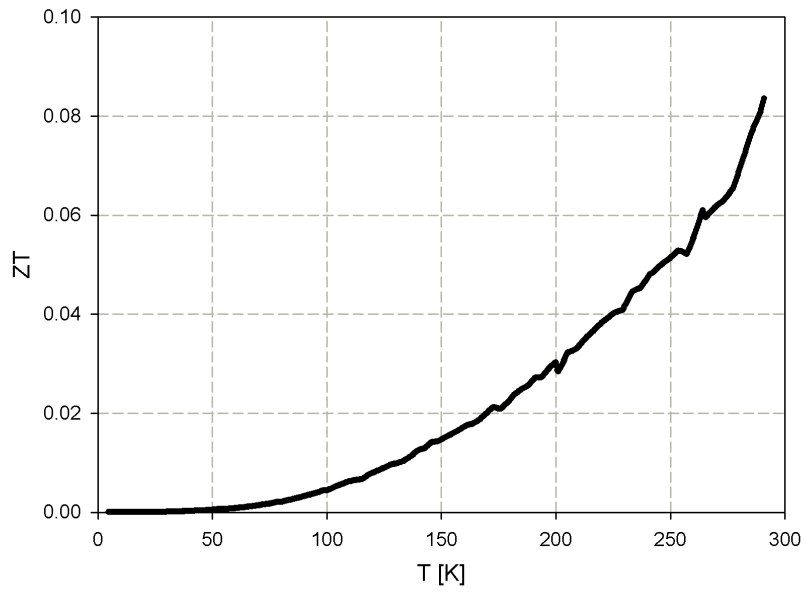
Figure A.24: Figure of Merit of $Ba_8Zn_{7.7}Ge_{38.3}$

Appendix B

Schematic Diagrams
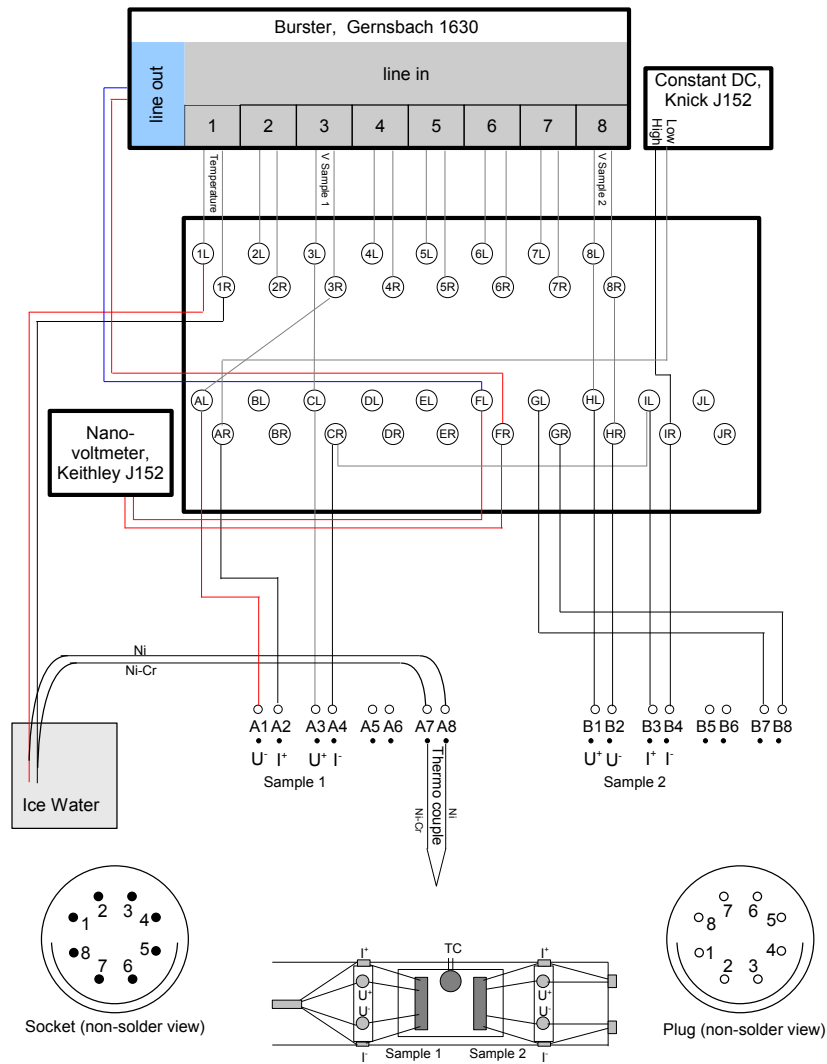
Figure B.1: Schematic diagram of the setup for resistivity measurements at high temperatures
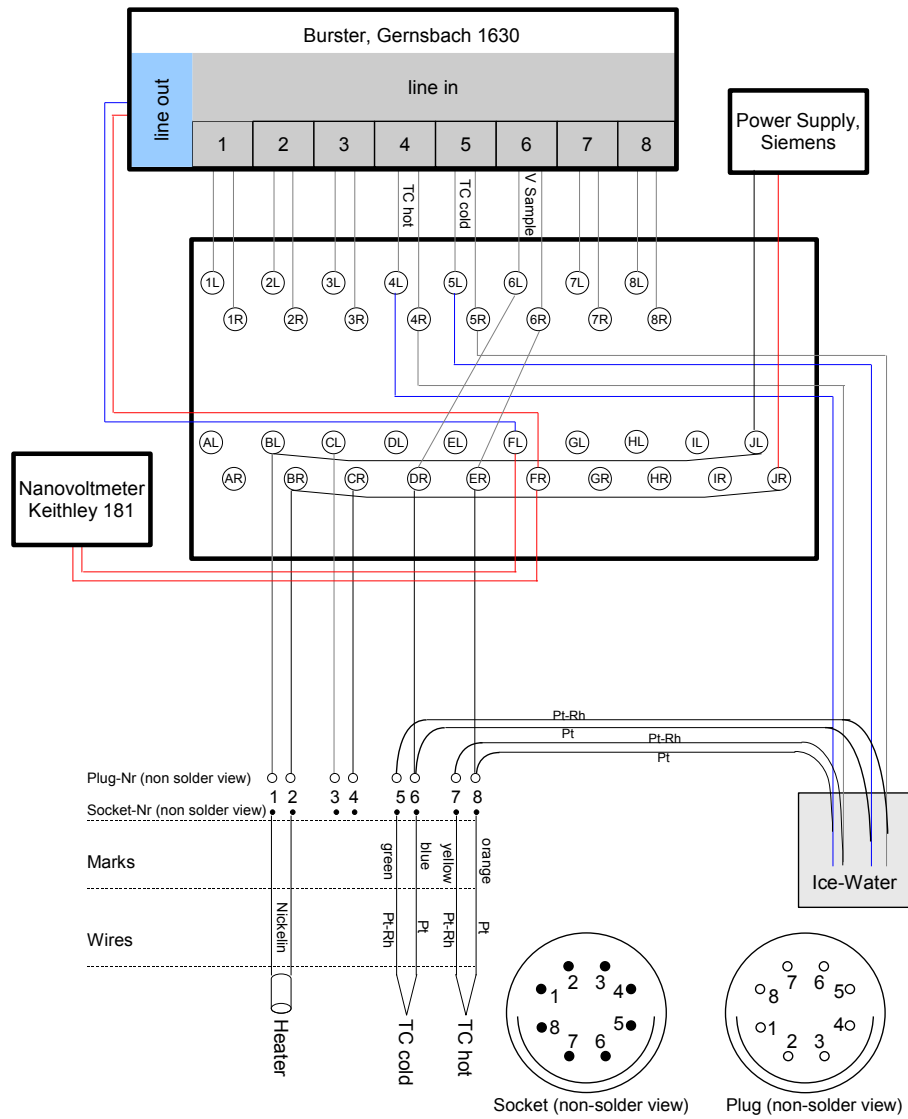
Figure B.2: Schematic diagram of the setup for thermopower measurements at high temperatures

Appendix C

How a Thermo-Couple Works

As explained in Section 2.1.4 a voltage results inside a material if a temperature gradient is applied. The relation between this voltage and the gradient is given by the *Seebeck coefficient* of the material (see equation (2.45)). This effect can be used to measure temperatures. The setup requires two thermo-wires with known Seebeck coefficient, a known reference temperature (e.g. ice bath), measurement wires (e.g. lead or copper wires) and a voltmeter. Figure C.1 describes the principle of measuring the temperature by using thermo-couples. Based on equation (2.45) the measurement equation can be derived as follows:

$$U_{meas} = \int_{meas}^{ref} S_{Pb}(T)\frac{dT}{dx}dx + \int_{ref}^{tip} S_A(T)\frac{dT}{dx}dx +$$

$$+ \int_{tip}^{ref} S_B(T)\frac{dT}{dx}dx + \int_{ref}^{meas} S_{Pb}(T)\frac{dT}{dx}dx \qquad \text{(C.1)}$$

The first and the last integral sum up to zero. Since this measurement is not influenced by its geometry but only by the differences in temperature we can replace $\int dx$ by $\int dT$. Assuming a perfect thermal contact between the tip of the thermo-couple and the sample we get

$$U_{meas} = \int_{T_{ref}}^{T_{sample}} S_A(T)dT - \int_{T_{ref}}^{T_{sample}} S_B(T)dT \equiv \int_{T_{ref}}^{T_{sample}} S_{AB}(T)dT \quad \text{(C.2)}$$

In case S_{AB} has a constant slope for $T \in (T_{ref}, T_{sample})$ the integral can be replaced by a difference.

$$U_{meas} = S_{AB}(T) \cdot (T_{sample} - T_{ref}). \qquad \text{(C.3)}$$

Consequently, the sample temperature can be measured by

$$T_{sample} = T_{ref} + \frac{U_{meas}}{S_{AB}}. \qquad \text{(C.4)}$$

Thermocouple

Lead wire   *Gage*

Tip

+   A

+

V_{out}

-                B

-

Target
surface

Ice bath
(known constant
temperature
for reference)

Ref.

Reference junctions
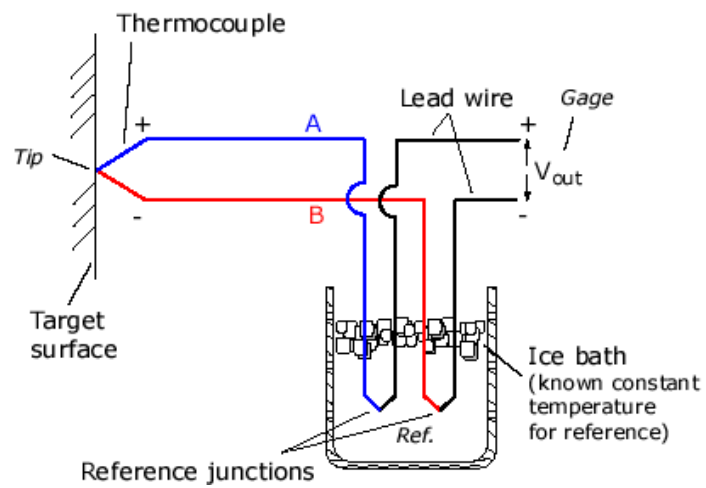
Figure C.1: Sketch of the principle how a measurement of temperature with thermo-couples works.

Appendix D

User Defined Functions

For analyses performed in Chapter 4 least square fits to the data were carried out using the program *TableCurve 2D 5.01.*

D.1 Electrical resistivity

In order to fit the low temperature ranges (4 K up to room temperature) of the resistivity measurements for all samples two fit functions were used.

D.1.1 Semi-Conductor Behaviour

For $Ba_8Cd_{2.4}Ge_{41.1}\square_{2.2}$ and $Ba_8Cd_{4.7}Ge_{40.3}\square_1$ the model explained in Section 4.1 [18] was used with $\mathcal{R}$, E_g, n_0, $N(E)$, ρ_0, θ_D and the width above E_F as fit parameters (see Table 4.2):

$$\rho(T) = \frac{\rho_0 n_0 + \rho_{ph}}{n(T)}. \tag{D.1}$$

ρ_0 is the residual resistivity while ρ_{ph} describes the electron-phonon interaction given by the *Bloch-Grüneisen* equation:

$$\rho_{ph}(T) = \mathcal{R} \left(\frac{T}{\theta_{\mathrm{D}}} \right)^5 \int_0^{\theta_{\mathrm{D}}/T} \frac{z^5}{(e^z - 1)(1 - e^{-z})} dz. \tag{D.2}$$

User defined function:

```
F7=1.381*10^(-23)
F1=$^5/(EXP($)-1)/(1-EXP(-$))
F2=#A*(X/#F)^5*AI(1,1E-10,#F/X)
F3=F7*(-#B+X*LN(2)-X*LN(1+EXP(#G/X))+X*LN(1+EXP((#G+#B)/X)))
```

```
F4=#D*SQRT(F3*X*F7*LN(2))+#C
Y=(#C*#E/F4)+(F2)/F4
```

Variables and Fit Parameters:

- F7 ... Boltzmann's constant k_B

- F1 ... integrand of Bloch-Grüneisen

- F2 ... ρ_{ph} (Bloch-Grüneisen)

- F3 ... density of electrons as charge carriers $n_n(T)$

- F4 ... total charge carrier density $n(T)$

- X ... temperature

- #A ... $\mathcal{R}$ (electron-phonon interaction constant)

- #B ... energy gap E_g

- #C ... residual density n_0

- #D ... DOS $N(E)$

- #E ... residual resistivity ρ_0

- #F ... Debye temperature θ_D

- #G ... energy difference between E_F and the lower band edge

D.1.2   Metallic Behaviour

Due to their more metallic like behaviour the measurement data of the other samples were fitted using the Bloch-Grüneisen equation adding a constant for the residual resistivity:

$$\rho(T) = \rho_{ph} + \rho_0 \tag{D.3}$$

User defined function:

```
F1=$^5/(EXP($)-1)/(1-EXP(-$))
Y=#C*(X/#A)^5*AI(1,1E-10,#A/X)+#B
```

Variables and Fit Parameters:

- F1 ... integrand for Bloch-Grüneisen

- X ... temperature

- #A ... Debye temperature θ_D

- #B ... residual resistivity ρ_0

- #C ... $\mathcal{R}$ (electron-phonon interaction constant)

The values of these fit parameters can be found in Table 4.2.

D.2 Thermal Conductivity

D.2.1 Lattice Contribution

Based on the model of Callaway [7, 8, 9] introduced in Section 4.3 the lattice thermal conductivity λ_l (in units of [mW/cmK]) is given by

$$\lambda_l = G\frac{T^3}{\theta_D}\int_0^{\theta_D/T} \tau_l \frac{x^4 e^x}{(e^x - 1)^2}dx + \#FT^3 \tag{D.4}$$

where the pre-factor G is derived by

$$G = \frac{k_B^3(6\pi^2 n)^{\frac{1}{3}}}{2\pi^2\hbar^2} \tag{D.5}$$

x in equation (D.4) is equal to $\hbar\omega/k_B T$ and n in equation (D.5) is the number of atoms per unit volume. $\frac{1}{\tau}$ is the sum of the reciprocal relaxation times for Umklapp processes, point defect scattering, boundary scattering and scattering of phonons by electrons, respectively:

$$\frac{1}{\tau_l} = \frac{1}{\tau_{l,0}} + \frac{1}{\tau_U} + \frac{1}{\tau_{l,e}} + \frac{1}{\tau_{l,b}} \tag{D.6}$$

$$\frac{1}{\tau_{l,0}} = Ax^4 T^4, \tag{D.7}$$

$$\frac{1}{\tau_U} = BT^2 x^2 e^{\frac{-\theta_D}{3T}}, \tag{D.8}$$

$$\frac{1}{\tau_{l,b}} = C, \tag{D.9}$$

$$\frac{1}{\tau_{l,e}} = DTx \tag{D.10}$$

User defined function:

```
G= see table 4.3
F1=#A*$^4*X^4
F2=#B*$^2*X^2*EXP(-#E/(a*X))
F3=#C
F4=#D*X*$
F5=F1+F2+F3+F4
F6=($^4*EXP($)/(EXP($)-1)^2)*(1/F5)
Y=F*X^3#E*AI(6, 0, (#E/X)) + #F*T^3
```

Variables and Fit Parameters:

- F1 ... $\frac{1}{\tau_{l,0}}$

- F2 ... $\frac{1}{\tau_U}$

- F3 ... $\frac{1}{\tau_{l,b}}$

- F4 ... $\frac{1}{\tau_{l,e}}$

- F5 ... $\frac{1}{\tau_l}$

- F6 ... integrand of Callaway equation

- X ... temperature

- #A ... parameter for scattering processes on defects

- #B ... parameter for Umklapp-processes

- #C ... parameter for scattering processes at boundaries

- #D ... parameter for scattering processes on electrons

- #E ... Debye temperature θ_D

- #F ... correction parameter for radiation losses

The values of the fit-parameters #A − #F, of the pre-factor G and that of the factor a in the exponent of $\tau_{l,ph}$ are listed in table 4.3.

D.2.2 Electronic Contribution

The fits for the electronic contribution to thermal conductivity were carried out using Wilson's equation and the formula for the residual thermal resistivity:

$$\frac{1}{\lambda_e} \equiv W_e = W_{e,0} + W_{e,ph} \tag{D.11}$$

where

$$W_{e,0} = \frac{\alpha}{T} \tag{D.12}$$

and

$$W_{e,ph} = \frac{4R}{L_0 T}\left(\frac{T}{\theta_D}\right)^5 \left[\left(1 + \frac{3}{4\pi^2}\left(\frac{\theta_D}{T}\right)\right)J_5(z) - \frac{1}{2\pi^2}J_7(z)\right]. \tag{D.13}$$

User defined function:

```
F1=#A/X
F2=#B/X
F3=#C/X
F4=$^5/(EXP(-$)+EXP($)-2)
F5=$^7/(EXP(-$)+EXP($)-2)
F6=F3*F1^-5*((1+(3*F1^2/(4*PI^2)))*AI(4,0,F1)-AI(5,0,F1)/(2*PI^2))
Y=1/(F2+F6)
```

Variables and Fit Parameters:

- F1 ... $\frac{\theta_D}{T}$

- F2 ... $W_{e,0}$

- F3 ... $\frac{4R}{L_0 T}$

- F4 ... J_5

- F5 ... J_7

- F6 ... $W_{e,ph}$ (Wilson's equation)

- X ... temperature

- #A ... θ_D

- #B ... α

- #C ... $\frac{4R}{L_0}$

The values of the fit parameters are listed in Table 4.4.

List of Figures

List of Tables

Bibliography

[1] T. J. Seebeck. Über den Magnetismus der galvanischen Kette. In *Abhandlungen der Königlichen Akademie der Wissenschaften zu Berlin*, page 289. 1821.

[2] D. M. Rowe, editor. *CRC Handbook of Thermoelectrics*. CRC Press, 1995.

[3] G.S.Nolas, J.Sharp, and H.H.Goldsmid. *Thermoelectrics–Basic Principles and New Materials Developments*. Springer-Verlag Berlin-Heidelberg, 2001.

[4] P. Debye. Zur Theorie der spezifischen Wärme. *Ann.Phys.*, 39:789, 1912.

[5] A. Eucken. Concerning the dependence on temperature of heat conduction in solid non-metals. *Ann.Phys.*, 34:185, 1911.

[6] R.Peierls. Zur kinetischen Theorie der Wärmeleitung in Kristallen. *Ann.Phys.*, 3:1055, 1929.

[7] J. Callaway. Model for lattice thermal conductivity at low temperatures. *Phys.Rev.*, 113:1046, 1959.

[8] J. Callaway and H. von Baeyer. Effect of point imperfections on lattice thermal conductivity. *Phys.Rev.*, 120:1149, 1960.

[9] J. Callaway. d bands in cubic lattices III. *Phys.Rev.*, 121:1351, 1961.

[10] E. Grüneisen. *Ann. Phys.*, 16:530, 1933.

[11] E.Bauer and S.Bühler-Paschen. *Highly Correlated Electron Systems*. Institute for Solid State Physics, Vienna University of Technology, 2006.

[12] G. Wiedemann and R. Franz. Über die Wärme–Leitungsfähigkeit der Metalle. *Ann. Phys.*, 89:497, 1853.

[13] G.S.Nolas, G.A.Slack, D.T.Morelli, T.M.Tritt, and A.C.Ehrlich. The effect of rare–earth filling on the lattice thermal conductivity of skutterudites. *J.Appl.Phys.*, 79:4002, 1996.

[14] W.Carillo-Cabrera, J.Curda, K.Petters, M.Baenitz, Y.Grin, and von Schnering H. ???? *Zeitschrift für Kristallographie – New Crystal Structures*, 215: 321, 2000.

[15] W.Carillo-Cabrera, S.Budnyk, Y.Prots, and Y.Grin. Ba_8Ge_{43} revisited: a 2a' x2a' x2a' superstructure of the clathrate-I type with full vacancy ordering. *Zeitschrift für Anorganische und Allgemeine Chemie*, 630:2267, 2004.

[16] N.Melnychenko-Koblyuk, A.Grytsiv, St.Berger, H.Kalderar, H.Michor, F.Röhrbacher, E.Royanian, E.Bauer, P.Rogl, H.Schmid, and G.Giester. Ternary clathrates Ba-Cd-Ge, phase equilibria, crystal chemistry and physical properties. *J.Phys.:Cond.Matter*, 19:23, 2007.

[17] N.Melnychenko-Koblyuk, A.Grytsiv, L.Fornasari, H.Kalderar, H.Michor, F.Röhrbacher, M.Koza, E.Royanian, E.Bauer, P.Rogl, M.Rotter, H.Schmid, F.Marabelli, A.Devishvili, M.Doerr, and G.Giester. Ternary clathrates Ba-Zn-Ge, phase equilibria, crystal chemistry and physical properties. *J.Phys.:Cond.Matter*, submitted.

[18] Stefan Berger. *Novel thermoelectric materials.* PhD thesis, Institute for Solid State Physics, Vienna University of Technology, 2003.

[19] S.Paschen, V.H.Tran, M.Baenitz, W.Carrillo-Cabrera, Y.Grin, and F.Steglich. Clathrate Ba_6Ge_{25}: Thermodynamic, magnetic and transport properties. *Phys.Rev.*, B65:134435, 2002.